

**CHARACTERIZATION OF URANIUM
MINERALIZATION AND DEVELOPMENT OF GENETIC
MODEL FOR SABRAOLI OCCURRENCE, ALWAR
GROUP, ALWAR DISTRICT, RAJASTHAN, INDIA**

by

MANOJ KUMAR ROUTRAY

ENGG1G201801010

Bhabha Atomic Research Centre, Mumbai

*A thesis submitted to the
Board of Studies in Engineering Sciences*

In partial fulfillment of requirements

for the Degree of

MASTER OF TECHNOLOGY

of

HOMI BHABHA NATIONAL INSTITUTE

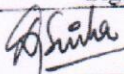
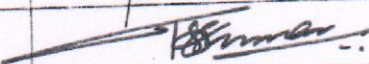
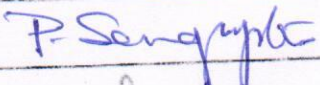
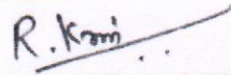
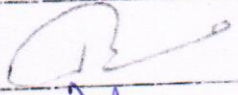
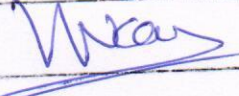


February, 2021

Homi Bhabha National Institute

Recommendations of the Thesis Examining Committee

As members of the Thesis examining Committee, we recommend that the thesis prepared by **Manoj Kumar Routray** entitled "**Characterization of uranium mineralization and development of genetic model for Sabraoli occurrence, Alwar Group, Alwar district, Rajasthan, India**" be accepted as fulfilling the thesis requirement for the Degree of Master of Technology.

	Name	Signature
Member-1	Dr. D. K. Sinha	
Member-2	Dr. T. S. Sunil Kumar	
Member-3	Dr. Navin Goyal	
Member-4	Dr. Pranesh Sengupta §	
Member-5	Dr. A. Rama Raju	
Technical Advisor	Shri Pawan Misra	
Examiner	Prof. R. Krishnamurthi §	
Guide & Convener	Dr. Rajeev Bidwai	
Chairman	Prof. Vivekanand Kain §	

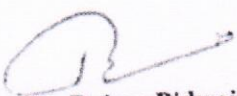
§ participated through video conferencing

Final approval and acceptance of this thesis is contingent upon the candidate's submission of the final copies of the thesis to HBNI.

I hereby certify that I have read this thesis prepared under my direction and recommend that it may be accepted as fulfilling the thesis requirement.

Date: 11-02-2021

Place: Hyderabad


(Dr. Rajeev Bidwai)
Guide

DECLARATION

I, hereby declare that the investigation presented in the thesis has been carried out by me. The work is original and has not been submitted earlier as a whole or in part for a degree / diploma at this or any other Institution / University.

Manoj Kumar Routray

(Manoj Kumar Routray)

*Dedicated
To
My Family*

ACKNOWLEDGEMENTS

I would like to give my heartfelt gratitude to my guide Dr. Rajeev Bidwai, Deputy Regional Director, Western Region and Technical Advisor Shri Pawan Misra, Scientific Officer-F for their invaluable guidance, support and encouragement in all perspectives throughout this project. It was only possible to complete this project for their precious remarks and valuable input.

I am extremely thankful to the competent authorities of HBNI, Mumbai for providing me an opportunity to pursue M.Tech. I am deeply thankful to Dr. D. K. Sinha, Director, AMD for kind permission and providing necessary facilities to carry out this project. I sincerely wish to acknowledge Shri Sandeep Hamilton, Additional Director, Op-I, AMD, Dr. B.S. Bisht, Regional Director, AMD/WR, Shri S. K. Sharma, Incharge, NDF-2 Investigation, AMD/WR, Jaipur, Dr. A. Rama Raju, Incharge, BARC Training School, AMD Campus, Hyderabad, Dr. S.K. Srivastava, former Head, BARC Training School, AMD Campus, Hyderabad for their constant advice and support.

I would also like to thank officers and staffs of different laboratories, AMD for providing analytical support and data. I would like to thank Mrs. Anubhooti Saxena, SO/E and Shri Kuldeep Nautiyal, SO-G for their help in petrographical studies.

I also acknowledge and thank the members of the M. Tech Monitoring Committee for their valuable suggestions throughout the M. Tech. project.

I am grateful to my senior officers of AMD/WR and my batchmates of BARC Training School who were always helpful to me with their critical suggestions while preparing manuscript.

Finally, I thank my family for their love, support and encouragement at all times.

Manoj Kumar Routray
(Manoj Kumar Routray)

CONTENTS

	Page No.
SYNOPSIS	iii
LIST OF FIGURES	v
LIST OF TABLES	x
CHAPTER 1 INTRODUCTION	1
1.1 Objectives of the study	3
1.2 Location and accessibility	3
1.3 Physiography, drainage and climate	4
1.4 Flora and fauna	5
1.5 Previous work in Alwar sub-basin by AMD	6
CHAPTER 2 REGIONAL GEOLOGY	9
2.1 Geology of Alwar sub-basin	14
2.2 The Raialo Controversy	20
2.3 Evolution of Alwar sub-basin	21
CHAPTER 3 LOCAL GEOLOGY	25
3.1 Detailed Geological Mapping around Sabraoli	25
3.2 Lithostratigraphy of study area	29
3.3 Structure	30
3.4 Geological sections across Sabraoli occurrence	35
3.5 Subsurface investigation from core samples	37
3.6 Delineation of lineaments and other structural features over satellite imagery	39
CHAPTER 4 METHODOLOGY	41
4.1 Petrology Laboratory	41
4.2 Wavelength Dispersive X-Rays Fluorescence (WDXRF) Laboratory	42
4.2.1 Sample preparation	42
4.3 Chemical Laboratory	42
CHAPTER 5 RESULTS	45
5.1 Petrography	45
5.1.1 Basement granite-gneiss	45
5.1.2 Xenoliths	45
5.1.3 Quartz muscovite/sericite schist	47

5.1.4 Quartzite (Serrate Formation)	47
5.1.5 Meta-basic rock (Quartz-hornblende schist)	47
5.1.6 Quartzite (Tehla Formation)	48
5.1.7 Quartz-biotite-sericite schist	49
5.1.8 Gritty Feldspathic Quartzite (Rajgarh Formation)	49
5.1.9 Radioactive samples (basal part of Rajgarh Formation)	51
5.2 XRD Laboratory	56
5.3 Radiometric assay of representative rock samples	57
5.4 Geochemistry	59
5.4.1 Major oxides of basement granite	59
5.4.2 Trace elements and rare earth elements of basement granite	60
5.4.3 Major oxides of xenoliths within basement granite	61
5.4.4 Trace elements and rare earth elements of xenoliths within basement granite	67
5.4.5 Major oxides of quartz-muscovite/sericite schist	68
5.4.6 Trace elements and rare earth elements of quartz-muscovite/sericite schist	69
5.4.7 Major oxides of quartzite (Serrate Formation)	69
5.4.8 Trace elements and rare earth elements of quartzite (Serrate Formation)	69
5.4.9 Major oxides of quartz-hornblende schist	71
5.4.10 Trace elements and rare earth elements of quartz-hornblende schist	72
5.4.11 Major oxides of quartzite (Tehla Formation)	73
5.4.12 Trace elements and rare earth elements of quartzite (Tehla Formation)	73
5.4.13 Major oxides of quartz-biotite-sericite schist	74
5.4.14 Trace elements and rare earth elements of quartz-biotite-sericite schist	75
5.4.15 Major oxides of gritty quartzite (Rajgarh Formation)	75
5.4.16 Trace elements and rare earth elements of gritty quartzite (Rajgarh Formation)	75
5.4.17 Trace elements and rare earth elements of quartzo-feldspathic veins	76
5.4.18 Major oxides of radioactive samples (basal part of Rajgarh Formation)	76
5.4.19 Trace elements and rare earth elements of radioactive samples (basal part of Rajgarh Formation)	77
CHAPTER 6 DISCUSSION	85
6.1 Proposed Genetic Model	92
CHAPTER 7 CONCLUSION	95
REFERENCES	97

SYNOPSIS

The Alwar sub-basin is the largest among the three sedimentary sub-basins of North Delhi Fold Belt in Aravalli craton. The area comprises of basement rocks of Mangalwar Complex (Bhilwara Supergroup) unconformably overlain by meta-volcano sedimentary sequences of Delhi Supergroup, which is further divided into three groups namely the Raialo, the Alwar and the Ajabgarh. The three groups are separated from each other by prominent unconformity surfaces. The Raialo Group consists of dominantly carbonate litho-unit along with quartzite and meta-basic rocks followed by arenaceous units of Alwar Group. The Ajabgarh Group comprises alternate sequence of arenaceous, argillaceous and carbonaceous sequences. The Alwar sub-basin known for its base metal deposits has opened new avenues for uranium exploration due to its suitable geo-tectonic set up for uranium mineralisation.

Sabraoli uranium mineralization is situated at the south-eastern part of the Alwar sub-basin. The area exposes the Raialo and the Alwar Group of rocks overlying basement granite gneiss. The surface mineralisation is located at the hinge zone of regional syncline and is confined to the basal part of Rajgarh Formation (Alwar Group). The area has undergone several phases of deformation and low grade metamorphism and is characterised by NE-SW striking foliation with steeply dip towards NW corresponding to axial planar cleavage of regional fold. Two prominent unconformity surfaces viz. between basement granite-gneiss (Mangalwar Complex) with Raialo Group and Raialo-Alwar Group are exposed in the area. Uranium mineralisation occurs within gritty quartzite/meta-conglomerate proximal to unconformity surface between Rajgarh Formation (Alwar Group) and quartz-biotite-sericite schist of Raialo Group. The radioactive meta-conglomerate is composed of quartz, muscovite/sericite, magnetite, apatite, biotite, and tourmaline. Presence of S-C fabric, polycrystalline quartz fish, grain boundary bulging and grain boundary migration represent high strain conditions in the area.

The radioactivity is assayed from 0.014% to 0.096% eU_3O_8 and $<0.010 ThO_2$ (n=11). The samples analyzed uranium (T) from 51ppm to 814ppm with leachability (L) from 34ppm to 644ppm. Other litho-units exposed in the area are either thoriferous in nature or have negligible radio-elements except few samples of quartz-biotite-sericite schist and quartzo-feldspathic veins which have comparatively higher uranium content.

The basement granite-gneiss is characterized as monzogranite, peraluminous nature, magnesian, alkali-calcic to calc-alkalic and is depleted in HREE compared to LREE with negative Eu anomaly. The quartzites of Serrate Formation and Tehla Formation (Raialo Group) are of sub-litharenite and litharenite type, derived from felsic igneous rocks under a semi-humid palaeoclimatic condition.

Quartzite of Rajgarh Formation (Alwar Group) is of sub-arkose to arkose, sub-litharenite to litharenite type, derived mostly from felsic and to some extent intermediate igneous rocks under semi-humid to semi-arid conditions. However, the radioactive samples from the basal part of Rajgarh Formation represent derivation mostly from intermediate to felsic and mafic igneous rocks under humid to semi-humid conditions. The quartz-biotite-sericite schist of Raialo Group underlying the Rajgarh quartzite is derived from intermediate igneous rocks.

Uranothorite, allanite and metanatroautunite (traces) are the major radioactive phases identified from petrographic and x-ray diffraction studies. Besides, inclusions of uraninite and U-Ti-Si-Fe complexes within sphene have also been reported from the area. Uranothorite is the primary or proto-ore for uranium mineralization. Uraninite and U-Ti-Si-Fe complexes and allanite are the second phase of uranium minerals associated with sphene. The Sabraoli uranium mineralization is spatially related to unconformity between Raialo and Alwar Group of meta-sediments. The mineralization depicts unconformity proximal type of mineralization and provides scope for potential target of uranium exploration in Alwar sub-basin.

LIST OF FIGURES

Figure No.	Description	Page. No.
1.1	Location map of study area.	4
1.2	Part of toposheet no. 54A/12 showing topographic feature in and around Sabraoli, Dausa District, Rajasthan.	5
2.1	Geological map of the Aravalli Mobile Belt (after Singh et al., 2010).	10
2.2	Generalized geological map of part of Alwar sub-basin, northeastern Rajasthan showing location of study area (after Khanam et al. 2020).	16
2.3	Map showing location, syn-sedimentary dislocation and various tectonic blocks of the eastern part of the Alwar sub-basin. Evolutionary trend of Alwar sub-basin (mainly eastern part): A. Development of main Alwar sub-basin (I); B. Down warping and reactivated block faulting, birth of Baswa horst (II) and Surer graben (III); C. Eruption of basic flows; D. Wider down warping and origin of Thatra graben (IV); E. Major down warping and marine transgression submerging all the barriers between different basins (after Khanam et al. 2020 & Singh, 1982a).	23
3.1	Geological map around Sabraoli-Uprera area.	25
3.2	(a) Contact of basement granite with gritty quartzite of Rajgarh Formation, (b) Contact of basement granite with serrate quartzite, (c), (d) Juxtaposition of quartzite of Rajgarh Formation and Serrate Formation, (e) Megascopic view of granite gneiss showing phenocryst of feldspar, (f) Lensoidal xenolith within basement granite-gneiss.	27
3.3	(a) Sharp contact of quartz-sericite schist with serrate quartzite, (b) Serrate quartzite, (c) Quartz-hornblende schist, (d) Oligomictic conglomerate within quartzite of Tehla Formation, (e) Quartz-biotite-sericite schist (QBSS), (f) Quartzo-feldspathic vein within quartz-biotite-sericite schist.	31

3.4	(a) Polymictic boulder conglomerate at Kalesan, representing basal part of the Rajgarh Formation, (b) Gritty quartzite of Rajgarh Formation, (c) Highly stretched, elongated quartz pebbles/cobbles of Rajgarh Formation, (d) Flattened cobble along foliation plane, (e) Cliff face exposing meta-conglomerate, basal part of Rajgarh quartzite, (f) Meta-conglomerate.	32
3.5	(a) Stereonet plot of foliation data and poles to the foliation (n=12) for Serrate quartzite (Raialo Group). (b) Rose diagram of the foliation planes (arrow points in the average direction and bulls eye represents pole to the average foliation plane) Average strike of the foliation plane is N46°E with dip 83° towards N44°W.	33
3.6	(a) Stereonet plot of foliation data and poles to the foliation (n=46) for gritty feldspathic quartzite of Rajgarh Formation (Alwar Group). (b) Rose diagram of the foliation planes (arrow points in the average direction and bulls eye represents pole to the average foliation plane). Average strike of the foliation plane is N46°E with dip 77° towards N44°W.	33
3.7	Rose diagrams for 1(a), 2(a), 3(a) strike of joint planes, 1(b), 2(b), 3(b) poles to joint planes. The plots show joint planes around Sabraoli-Uprera area have average strike of NW-SE with moderate to high dip either towards NE or SW.	34
3.8	(a), (b) Kink folds developed within quartzite of Rajgarh Formation around Sabraoli.	35
3.9	Hypothetical geologic cross section along AB line.	36
3.10	Hypothetical geologic cross section along CD line.	36
3.11	(a) Gritty feldspathic quartzite of Rajgarh Formation, (b) Metaconglomerate composed of pebbles/cobbles of quartz embedded in matrix of quartz, feldspar, tourmaline, magnetite, sericite/muscovite (c) Contact between met-conglomerate and quartz-biotite-sericite schist, (d) Lensoidal quartzo-feldspathic material within quartz-biotite-sericite schist.	38

3.12	Transverse section through borehole SBR-2, Sabraoli area, Dausa district, Rajasthan.	38
3.13	Cartosat satellite image with interpreted structural elements around Sabraoli area, Dausa district, Rajasthan.	39
5.1	(a) Textural view of basement granite-gneiss showing gneissosity defined by alignment of flaky minerals (TL, 2N, MA-216), (b) Warping of muscovite/sericite around phenocryst of plagioclase enclosing quartz grain (TL, 2N, MA-216), (c) Hematitization of magnetite within granite samples (RL, 1N, MA-259), (d) Textural view of xenolith within basement granite (TL, 1N, MA-219), (e) Occasionally larger laths of biotite occur with groundmass of quartz, feldspar, biotite, muscovite/sericite (TL, 2N, MA-219) (f) Sericitization of plagioclase feldspar within xenoliths of basement granite (TL, 2N, MA-218). Bt = biotite, Fsp = feldspar, Hem = hematite, Ms = muscovite, Mt = magnetite, Pl = plagioclase, Qtz = quartz.	46
5.2	Shear lenses of polycrystalline quartz (Qtz) with muscovite (Ms)/sericite warping and few opaque mineral grains (TL, 2N, MA-264).	47
5.3	(a) Highly stretched quartz (Qtz) clasts with minor flakes of sericite (Ser) aligned parallel to the foliation (TL, 2N, MA-221), (b) Tourmaline (Tur) clast within Serrate quartzite (TL, 2N, MA-221).	48
5.4	(a) Alignment of prismatic hornblende (Hbl) with quartz (Qtz) grains filling the interstices, (b) Very minor plagioclase (Pl) within qtz-hornblende schist.	48
5.5	(a) Polygonal mosaic of quartz clasts (TL, 2N, MA-269), (b) Tourmaline (Tur) clasts within quartzite of Tehla Formation (TL, 2N, MA-269).	49
5.6	(a) Fine grained quartz (Qtz)-biotite (Bt)-sericite (Ser) schist with highly elongated quartz clasts and opaque minerals (TL, 2N, MA-254), (b) Polycrystalline quartz lens with polygonal mosaic of sub-grains (TL, 2N, MA-254), (c) Kinks within qtz-	50

- bt-sericite schist with development of shear lenses (TL, 2N, MA-280), (d) Polycrystalline quartz shear lens (TL, 2N, MA-280).
- 5.7 (a) Prismatic tourmaline (Tur) clast showing high order interference colour (TL, 2N, MA-273); Mc = microcline, Qtz = quartz, Ser = sericite. Note higher content of feldspars (mostly microcline), (b) Plagioclase (Pl) with stretched quartz (Qtz) clast aligned along the schistosity plane (TL, 2N, MA-223). 51
- 5.8 (a) Quartz (Qtz) augen wrapped by muscovite (Ms), TL, 1N, (b) Microcline (Mc) clast in the groundmass of quartz (Qtz), apatite (Ap), muscovite (Ms), (c) Granular apatite (Ap) aggregate in groundmass, (d) Grain boundary bulging (GBL)/migration of quartz (Qtz) clasts. 52
- 5.9 (a) Martitised magnetite with hydrated iron oxides/goethite, E-665, (b) High density alpha tracks corresponding to hydrated iron oxide/goethitised patch in fig. 5.8a, (c) Suspected inclusion of uranothorite grain within quartz surrounded by chloritic rims, corresponding alpha track shown inset, (d) Fine grained radioactive phase with iron masking and corresponding alpha track showing alignment. Chl = chlorite, FeOH = hydrated iron oxide, Gth = goethite, Hmt = hematite, Mt = magnetite, Qtz = quartz, Ser = sericite, UTh = uranothorite. 53
- 5.10 (a) General texture of quartz (Qz)-biotite (Bt)-muscovite (Ms)/sericite (Seri) schist (QBMS), (b) Quartz with mica beard in QBMS, (c) Allanite (Alln) grains (brown core) having epidote (Epi) overgrowth (clear rim). (d) Longitudinal zircons (Zr) in QBMS, (e) Suspected cubic grain of uranothorite (Uth) and corresponding alpha tracks shown in inset, QBMS, TL,1N,E-914, (f) Uranothorite (UTh?) is making strong pleochroic haloes in host biotite, QBMS, TL,1N,E-914. 55
- 5.11 (a) Q-A-P normative plot after Le Maitre et al. (2002) and (b) TAS diagram (Middlemost, 1994) showing granitic composition for the samples, (c) AFM diagram showing calc- 64

	alkaline trend of the samples (d) A/CNK [Alumina Saturation Index, ASI, molar $\text{Al}_2\text{O}_3/(\text{CaO}+\text{Na}_2\text{O}+\text{K}_2\text{O})$] vs. A/NK (molar $\text{Al}_2\text{O}_3/(\text{Na}_2\text{O}+\text{K}_2\text{O})$) (e) Fe^* [$\text{FeO}^t/(\text{FeO}^t + \text{MgO})$] vs. SiO_2 , and (f) MALI-index ($\text{Na}_2\text{O}+\text{K}_2\text{O}-\text{CaO}$) vs. SiO_2 diagrams after Frost et al. (2001).	
5.12	Harker's variation diagram (Harker, 1909) of SiO_2 vs. major oxides for the granite from southern part of study area.	65
5.13	Harker's variation diagram (Harker, 1909) of SiO_2 vs. trace elements for the granite from southern part of study area.	66
5.14	Chondrite-Normalised REE pattern (Boynton, 1984) of basement granite gneiss (n=3).	67
5.15	Sandstone classification diagram using $\log(\text{Na}_2\text{O}/\text{K}_2\text{O})$ vs. $\log(\text{SiO}_2/\text{Al}_2\text{O}_3)$ (after Pettijohn et al. 1987).	78
6.1	Inferred source rocks for quartzites and quartz-biotite-sericite schist of Raialo Group as revealed in Zr vs. TiO_2 plot (after Hayashi et al., 1997)	90
6.2	Inferred source rocks for quartzites/conglomerates (Rajgarh Formation) of Alwar Group as revealed in Zr vs. TiO_2 plot (after Hayashi et al., 1997).	90
6.3	Influence of climatic conditions on the chemical maturity of quartzites of Serrate, Tehla Formations expressed as a function of SiO_2 and $(\text{Al}_2\text{O}_3+\text{K}_2\text{O}+\text{Na}_2\text{O})$ (after Suttner and Dutta, 1986).	91
6.4	Influence of climatic conditions on the chemical maturity of quartzite of Rajgarh Formation expressed as a function of SiO_2 and $(\text{Al}_2\text{O}_3+\text{K}_2\text{O}+\text{Na}_2\text{O})$ (after Suttner and Dutta, 1986).	91
6.5	(a) Back scattered image of uranothorite surrounded by chloritic rim (b) Back scattered image of patches of U-Ti-Si-Fe complex rimmed by allanite. Note fine inclusion of uraninite within sphene (after Saxena, 2020).	94

LIST OF TABLES

Table No.	Description	Page. No.
2.1	Lithostratigraphic classification of Rajasthan and Northern Gujarat (Gupta et al., 1980).	13
2.2	Stratigraphy of Delhi System (after Heron, 1917).	14
2.3	Stratigraphic sequence of the Delhi Super Group of northeastern Rajasthan (after Banerjee, 1980; Singh, 1988a, 1988b).	17
5.1	X-ray diffraction analysis of radioactive samples from Sabraoli area, Dausa district, Rajasthan.	56
5.2	Physical assay results of radioactive samples, Sabraoli area, Dausa district, Rajasthan.	57
5.3	Physical assay results of non-radioactive samples, Sabraoli area, Dausa district, Rajasthan.	58
5.4	Major oxides (wt %) and trace elements (ppm) of basement granite-gneiss from southern part of the study area.	62
5.5	Major oxides (wt %) and trace elements (ppm) of xenoliths within basement granite.	68
5.6	Major oxides (wt %) and trace elements (ppm) of quartz-muscovite/sericite schist.	70
5.7	Major oxides (wt %) and trace elements (ppm) of quartzite (Serrate Formation).	71
5.8	Major oxides (wt %) and trace elements (ppm) of quartz-amphibole schist.	72
5.9	Major oxides (wt %) and trace elements (ppm) of quartzite (Tehla Formation).	74
5.10	Major oxides (wt %) of quartz-biotite-sericite schist.	78
5.11	Trace elements (ppm) of quartz-biotite-sericite schist.	79
5.12	Major oxides (wt %) and trace elements (ppm) of gritty quartzite (Rajgarh Formation).	79
5.13	Rare Earth Elements (REE) of different non-radioactive litho-units.	80
5.14	Trace elements concentration of quartzo-feldspathic veins.	81

5.15	Rare Earth Elements (REE) concentration of quartzo-feldspathic veins.	81
5.16	Major oxides (wt %) composition of radioactive samples, Sabraoli, Dausa district, Rajasthan.	82
5.17	Trace elements concentration of radioactive samples from Sabraoli area, Dausa district, Rajasthan.	82
5.18	Rare Earth Elements (REE) concentration in radioactive samples from Sabraoli area, Dausa district, Rajasthan.	83
5.19	Correlation matrix of major oxides and trace elements composition of radioactive samples, Sabraoli area, Dausa district, Rajasthan.	84

CHAPTER 1

INTRODUCTION

Alwar sub-basin of North Delhi Fold Belt exposed in the north eastern part of Rajasthan comprises meta-volcano sedimentary sequences and is divided into three distinct groups namely Raialo, Alwar and Ajabgarh (Banerjee et al., 2011; GSI, 2011; Ahmad, 2015; Mukhopadhyay et al., 2018). It is postulated that initiation of Delhi sedimentation in the basin started with Raialo Group at two independent depocentres around Dogeta and Makrana over the basement rocks of Mangalwar Complex. Carbonate sediments of Dogeta Formation accumulated in shallow basins under stable conditions. This was followed by block faulting and upliftment (Dausa uplift) initiating rudaceous and arenaceous sedimentation of Serrate Quartzite and Nithar Formation in a transgressive beach environment. The end-phase of Raialo sedimentation was marked by rejuvenation of faults and development of intra basinal faults with intrusion of volcanics of Tehla Formation (Sinha-Roy et al., 2013; Ramakrishnan and Vaidyanadhan, 2008). The Alwar Group consists dominantly of quartzites and conglomerates deposited in a sub - tidal to tidal flat environments with an unconformity over the Raialo Group as well as over pre-Delhi rocks. The sedimentation of Ajabgarh Group overlying the Alwar Group started with carbonates and interlayered with basic volcanics. It was followed by alternate sequence of arenaceous (quartzite), argillaceous (carbon phyllite, mica schist) and carbonaceous sequences. The sedimentary features suggest an environment of braided stream or alluvial fan followed by tidal flat to lagoonal (Sinha-Roy et al., 2013). In addition, the basin is intruded by several granitic bodies such as Bairat, Ajitgarh, Barodia and Harsora granites (Ramakrishnan and Vaidyanadhan, 2008). The rocks of the Alwar sub-basin have undergone three phases of deformation with early isoclinal NNE-SSW trending folds, overprinted by folds with large interlimb angle and steep axial planes, and finally followed by last phase of open folds (Ramakrishnan and Vaidyanadhan, 2008). The map pattern is

controlled by interference of these folds, resulting in hook-shaped to dome and basin structure.

The Alwar sub-basin is well known for base metals deposits (Khan et al., 2013). Uranium mineralization has been reported along fracture/shear zones cutting across different lithologies in Kho-Dariba area (Shaji et al., 2009). The basin forms a potential uranium province because of suitable geo-tectonic set up. The basement shears contain a number of occurrences of uranium bearing zones which are indicative of remobilization and enrichment of the metal in a fertile terrain. Existence of suitable pelitic rocks with carbonaceous and carbonate units in basement with manifestation of uranium mineralization at places, associated with middle Proterozoic cover rocks, shear zones affecting basement and cover sequences, granitic and pegmatitic activity and presence of numerous uranium anomalies reflect suitability of the basin for uranium exploration (Padhi et al., 2016).

Atomic Minerals Directorate for Exploration and Research (AMD) is engaged in uranium exploration over seven decades in various favourable geo-environments especially in Raialo meta-sediments, at the contact of Raialo and Alwar meta-sediments, and in Ajabgarh meta-sediments. In Field Season 2018-19, significant radioactivity due to uranium has been reported at the basal part of quartzite of Rajgarh Formation (Alwar Group) at Sabraoli, Dausa district, Rajasthan. This geological setting hosting uranium anomaly opened scope for further subsurface uranium exploration in the Alwar sub-basin and also subject for keen research to understand the mineralisation and its genesis. Keeping in view the significance and importance of the geological environment, the current study has been undertaken with an emphasis on detailed litho-structural, geochemical characterisation of the mineralisation and develop a genetic model. Thus, an area of 2 sq. km. around Sabraoli-Uprera, Dausa district has been selected for the geological understanding.

1.1 Objectives of the study

- (i) To study meta volcano-sedimentary sequence of Raialo & Alwar Groups near Sabraoli over an area of 2 sq. km on 1:2000 scale.
- (ii) To study the uranium mineralization and its characteristics in meta volcano-sedimentary sequence.
- (iii) To understand its structural history and emplacement of quartzo-feldspathic veins containing uranium.
- (iv) To interpret the geotectonic environment of deposition of volcano-sedimentary sequence.
- (v) To propose genetic model for uranium mineralization with reference to above objectives.

1.2 Location and accessibility

The study area is bounded by latitude N27°06' to N27°09' and longitude E76°33' to E76°39' and is a part of Toposheet No. 54A/12. The present area, located about 120 km northeast of Jaipur, forms the southern part of Alwar district and northern part of Dausa district and is well connected by both road and rail (fig. 1.1). The nearby railway stations are Rajgarh, Bandikui, Alwar and Dausa. Further, Jaipur-Delhi broad gauge Railway line (Western Railway) passes through Dausa-Bandikui-Rajgarh-Alwar area. The area is accessible via National highway NH-11 (Jaipur-Agra) which connects State highway SH25 through Sikandra and passes via Bandikui-Baswa-Rajgarh-Alwar road. The area is also connected by road via Dausa-Sainthal-Tehla, and Tehla-Rajgarh road. The interiors are approachable by fair jeepable roads.

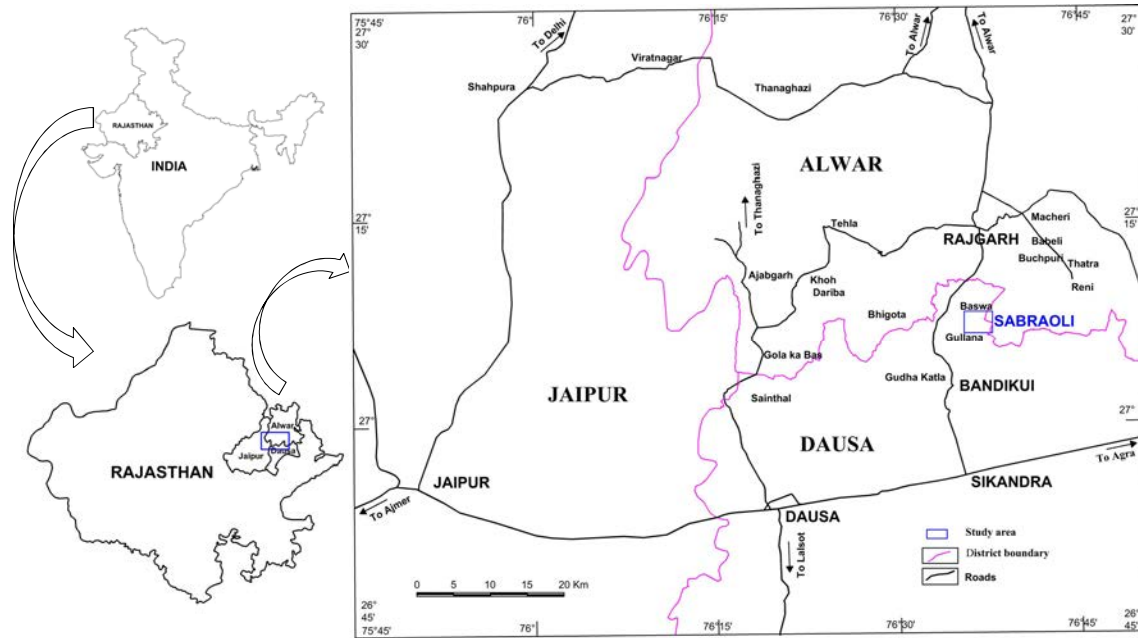


Figure 1.1 Location map of study area.

1.3 Physiography, drainage and climate

Geomorphology of the area is characterised by N-S to NE-SW trending moderate to high linear ridges as well as isolated hillocks and peneplain area (fig. 1.2). In Rajgarh-Baswa area, the highest peak is 525m above MSL. The average ground level is 300m above MSL. The relief is around 225m. The isolated hills in the peneplained area form contrasting topography. The drainage of Baswa-Rajgarh area is controlled by the Palasan Nadi, on the other hand drainage in Bhigota area (west of Sabraoli) is controlled by Sanwan Nadi.

In addition to these, there are several smaller nalas which get water from seasonal rain and either join these rivers or bigger nalas or merge with some bundh. The climate of the area is semi-arid to dry and is characterized by hot summer, moderately cold winter and a short monsoon. The average temperature in Alwar is 25.4°C. During the summer season the temperature often touches a maximum of 48°C. Winter season is between November and March and records temperature up to 0°C. Rainfall and pleasant weather is experienced from mid July. The average annual rainfall of the area is 577.7mm.

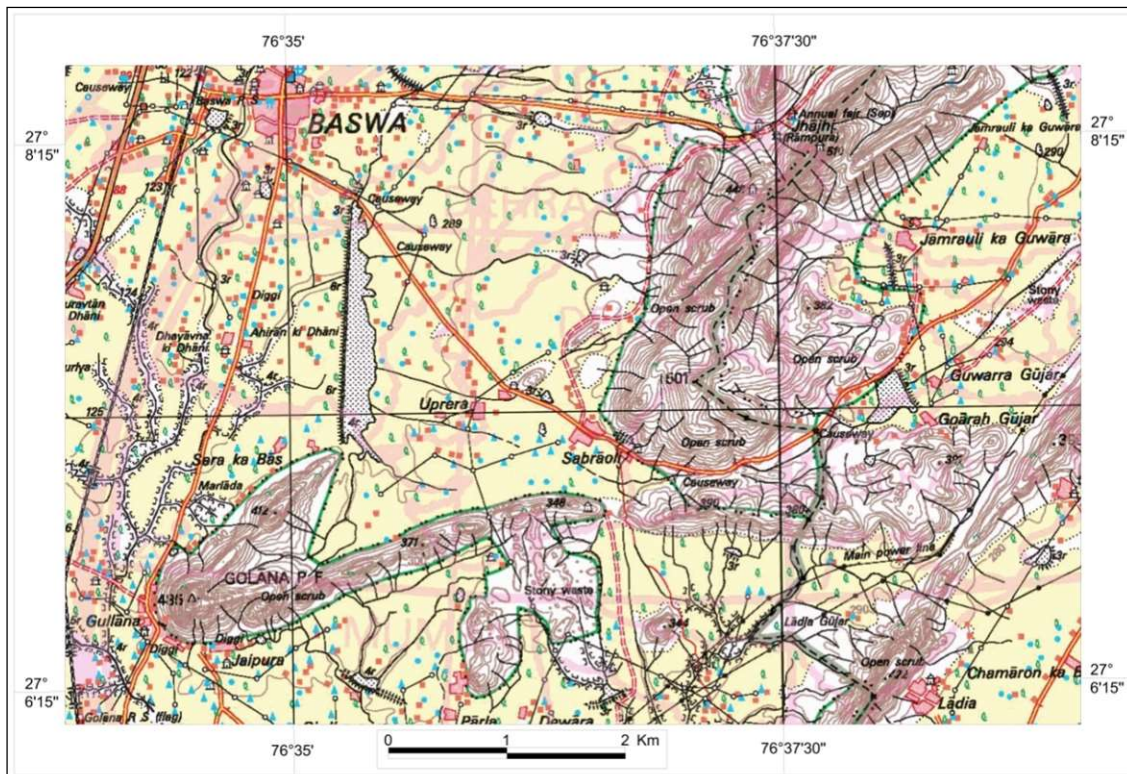


Figure 1.2 Part of toposheet no. 54A/12 showing topographic feature in and around Sabraoli, Dausa District, Rajasthan.

1.4 Flora and fauna

The hilly part of the mapped area, around Sabraoli, Parla, Kesupura, Gullana, Jamrauli ka Guwara, Jhajhi Rampura comes under reserved forest. These forests exhibit extensive varieties of trees and scrubs. The vegetation includes trees like babool (*Acacia nilotica*), ronjh (*Acacia leucophloea*), khair (*Acaia catechu*), keekar (*Prosopis juliflora*), neem (*Azadirachta indica*), maharukh (*Ailanthus excelsa*), shisham (*Dalbergia sissoo*) pipal (*Ficus religiosa*), dhak (*Butea monosperma*), dhok (*Anogeissus pendula*), ber (*Ziziphus mauritiana*), banyan (*Ficus benghalensis*), mango (*Mangifera indica*), etc. and many more which grows mainly in the hill slope and valley portion. Scrubs like hingot (*Balanites roxburghii*), arusha (*Justicia adhatoda*) are also very common. These forest areas are the natural habitat of numerous carnivores including leopard, wild dog, jungle cat, and other wild

animals like rabbit, neelgai, jackal, snake, wild lizard, scorpion etc. and also for different type of birds.

1.5 Previous work in Alwar sub-basin by AMD

High order radioactivity was located in conglomerates and phyllites of Kho-Dariba in the F.S. 1953-54 by Shri N. K. Duggal. Subsequently during the F.S. 1955-56, Shri D. B. Ghosh and A. C. Saraswat examined the old underground workings and six bore holes (2 surfaces and 4 underground) were drilled by AMD. These investigations brought to light about the sporadic uranium mineralisation in the form of stringers and veinlets of uraninite along shears and faults. Uranium values upto 6.78% U_3O_8 (chemical) in pegmatites of Khairtal; 0.027% eU_3O_8 in granites of Khairtal; 0.04% U_3O_8 (chemical) in granites of Hajipur; 0.022% eU_3O_8 in amphibolites of Mandawar-Pahel; 14.26% U_3O_8 (chemical) in pegmatites and granites of Samda and 0.095% (chemical) in granites and pegmatites of Harsora were reported (Rode, 1961).

Shri Ravi Kaul during the F.S. 1960-61, located Radioactivity mainly due to thorium in Raialo conglomerates of Barsia Devi. He also reported values up to 0.021% U_3O_8 (chemical) in brecciated carbonaceous phyllites near Ajabgarh and 0.018% U_3O_8 (chemical) in brecciated ferruginous limestone in an old copper working SSE of Burja. During the F.S. 1982-83, Shri G.V.G. Sharma, reported radioactivity mainly due to thorium in the conglomerates of Mangalasar-Malana area and uranium mineralisation in the Ajabgarh carbonaceous phyllites of Dholan analyzing up to 0.029% U_3O_8 . During the F.S. 1983-84, ground checking of the aerial survey anomalies by Shri B.N. Khazanchi led to the discovery of hydrothermal uranium vein type mineralisation in Ajabgarh carbonaceous/calcareous phyllites at Narwas with grab samples analyzing up to 0.219% eU_3O_8 , 0.26% U_3O_8 and 0.03% ThO_2 . Subsequent detailed extensional geological survey resulted in extended this anomaly area to 170m × 40m (Sharma, 1985).

Presence of high grade radioactive samples measuring up to 6.6% U₃O₈ within the mine dumps of Kho-Dariba area were reported (Chopra et al., 2001). Subsequently, hydro-uranium anomalous zone proximal to unconformable contact between BGC and Delhi along Derah-Kelpurakhera-Dagadaga tract, SW of Reni were delineated and few low order uraniferous surface anomalies hosted by carbon phyllite at Soti, southwest of Kho were located (Khandelwal et al., 2002). Significant shear controlled uranium mineralisation occurring intermittently over 1.3km associated with Raialo quartzites near Dariba has been located and grab samples assayed up to 0.30% U₃O₈ with <0.005% ThO₂ (Shaji and Panigrahi, 2008).

Heliborne TDEM, magnetic and gamma-ray spectrometric survey during 2016-19 over Alwar sub basin, North Delhi Fold Belt, Jaipur, Sikar, Alwar, Dausa, Karauli and Bharatpur districts, Rajasthan and Rewari and Gurugram districts, Haryana were carried out by ASRS Group, AMD, Hyderabad.

Significant uraniferous radioactivity at Sabraoli area at contact of Raialo/Alwar Group of rocks over 30m x 2m associated with meta-conglomerates was located. Physical assay of samples from the surface anomaly of Sabraoli are 0.015-0.029% eU₃O₈, <0.010-0.043U₃O₈ and <0.010% ThO₂ (n=3). Chemical analysis showed 113-604ppm U (T), 88-495ppm U(L), 42-436ppm Cu (n=3). XRF analysis of one of the sample resulted 58.91% SiO₂, 0.67% TiO₂, 17.29% Al₂O₃, 12.49% Fe₂O₃ (t), 2.84% MgO, 1.51% Na₂O, 4.18% K₂O, 262ppm Cu. Radioactivity associated with carbonaceous phyllite (Ajabgarh Group) assayed 0.015-0.029% eU₃O₈, 0.010-0.032% U₃O₈ and <0.010% ThO₂ (n=3) at Sehra- Sonari area. Chemical analysis of samples has been assayed 60-244ppm U(T), 52-99ppm U(L), 152-180ppm Ni, 294-804ppm Zn (n=2) (Pawan Misra, F.S. 2018-19).

CHAPTER 2

REGIONAL GEOLOGY

The NE-SW trending Aravalli Mobile Belt in north-western India characterized by the Aravalli mountain ranges encompasses the state of Rajasthan, parts of Gujarat and Madhya Pradesh and fringes of Delhi and Haryana. It is flanked by the Mewar and Marwar cratons in the east and west, respectively (fig. 2.1). It curves around the Mewar craton, which forms a promontory structure along the western edge of the Bundelkhand Proto-continent, forming a westerly closing flexure as a result of indentation tectonics, a process comparable to that which formed the Himalaya along the northern edge of the Indian Peninsula (Singh et. al., 2010). The composite Aravalli craton is bound to the east by the Great Boundary Fault (GBF) and Vindhyan basin that separate the Aravalli from the Bundelkhand craton. It is separated by the SONATA (Son-Narmada-Tapti) lineament from the Central Indian Tectonic Zone in the south. The Mewar craton comprises of Mesoarchaean Tonalite-Trondhjemite-Granodiorite (TTG) gneisses and sporadic greenstone belts. The age of Mewar gneisses is referred as 2.45–3.50 Ga (Sivaraman and Odom, 1982; MacDougall et al., 1983; Wiedenbeck and Goswami, 1994; Roy and Kröner, 1996). The Marwar craton is extensively intruded by the Erinpura and Malani granites, and at several places has been covered by younger volcano-sedimentary sequences belonging to the Sindreth, Punagarh, and Marwar groups. Isolated outcrops of the basement rocks are exposed only at few places (near Bar, Heron, 1953). The Aravalli- Delhi mobile belts of north-western India depicts a juxtaposition of several terranes along NE-SW trending shear zones represented as lineaments on the map (fig.2.1). The terranes are namely the Aravalli, Hindoli-Jahajpur, Sandmata-Mangalwar, Delhi and Sirohi. Each individual terrane is characterized by distinct depositional history and deformational metamorphism, and comprises thick sequences of Proterozoic metasedimentary and meta-igneous rocks unconformably overlying the basement gneisses.

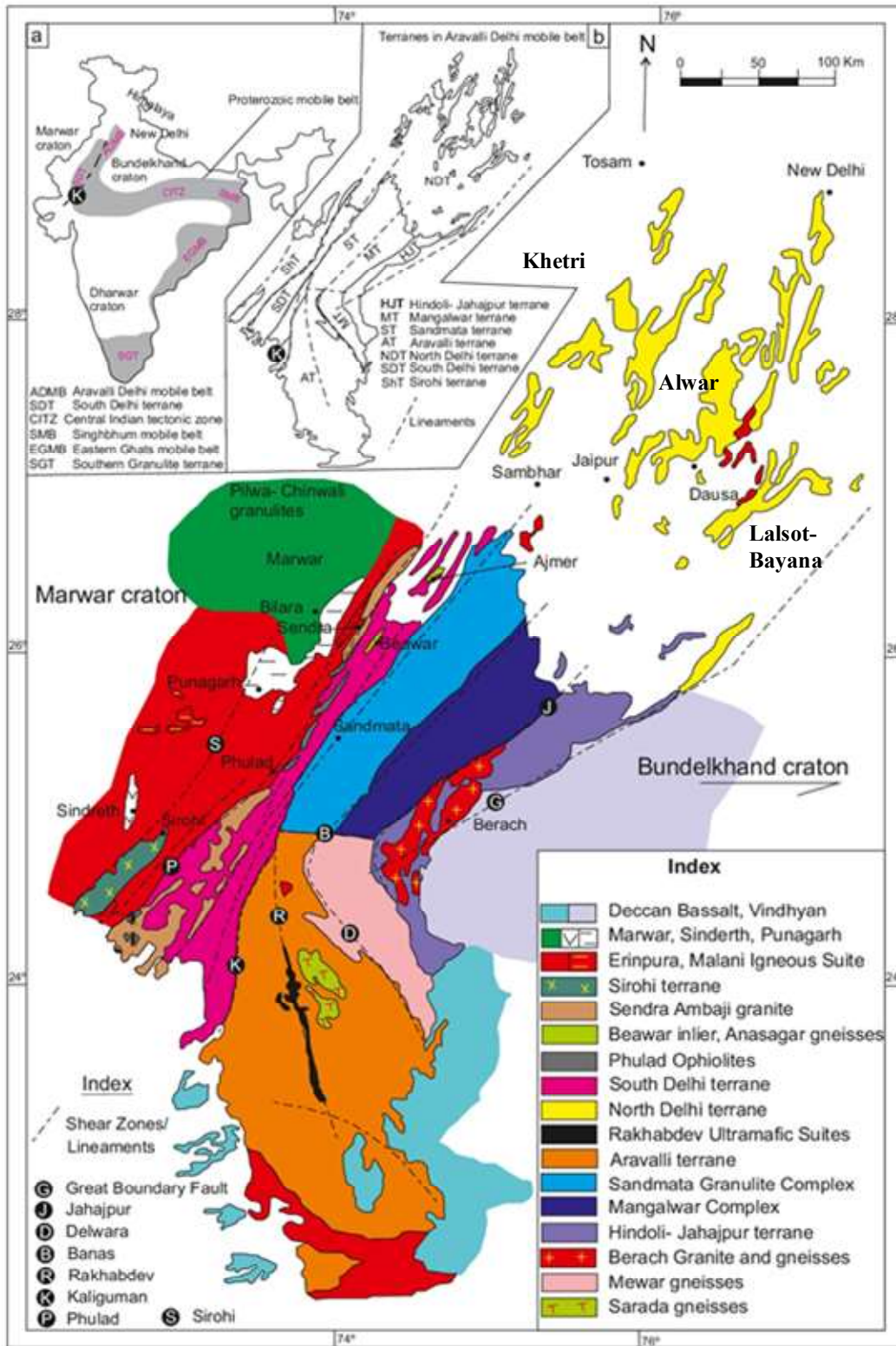


Figure 2.1 Geological map of the Aravalli Mobile Belt (after Singh et al., 2010).

The Aravalli terrane is characterized by low to medium-grade rocks showing multiple phases of folding and granitic intrusions (Gupta, 1934; Heron, 1953; Bose and Sharma, 1992; Roy and Jakhar, 2002). Synsedimentary felsic volcanic rocks are of Proterozoic age (1.8 Ga), of the terrane (Deb et al., 2001). There are two facies domains (i) shallow water stromatolites-bearing facies in the east, and, (ii) deep water carbonate-pelite facies in the west. These facies are separated by the ophiolite-bearing Rakhabdev shear zone.

The Hindoli-Jahajpur terrane is separated by Great Boundary Fault from the Vindhyan basin in the east. Earlier studies considered them as a part of the Aravalli Terrane on the basis of lithological association, structure and the Proterozoic age of the synsedimentary felsic volcanic rocks (Gupta, 1934; Heron, 1953). However, few researchers have considered it to be Archaean and part of Bhilwara Supergroup, along with the Sandmata-Mangalwar terrane (Gupta et al., 1980; Sinha-Roy et al., 2013). Still some regard it as an independent sequence of Palaeo-proterozoic age (Porwal et al., 2006). The Banas Lineament or Jahazpur thrust separates Hindoli belt from Mangalwar complex in the north and Mewar Gneiss in the south.

The Sandmata- and Mangalwar terrane are dominated by migmatitic gneisses, with isolated enclaves of amphibolite and metapelite within it. The gneisses have been considered to be the product of migmatization of the Aravalli rocks. The Delwara Lineament marks a gradational metamorphic-migmatitic or sheared tectonic contact between Mangalwar and Sandmata Complexes.

The Sirohi Terrane occurs to the west of the South Delhi terrane and consists of low-grade metasedimentary rocks exhibiting multiple phases of deformation (Roy and Sharma, 1999). It is extensively intruded by the Erinpura granites, the Malani igneous suite and Sindreth volcanic.

The Delhi terrane is subdivided into the North and South Delhi terrane. The Kaliguman Lineament separates the Delhi terrane from Sandmata Complex in the North and Aravalli fold belt in the South, both are separated by Sambhar-Jaipur-Dausa strike slip fault (Sinha et al., 2013). The South Delhi Fold Belt (SDFB) occurs as a linear belt along the western edge of the Aravalli Mobile Belt and has been subdivided into a number of longitudinal tectonic zones. In general, the rocks of the SDFB show amphibolite facies of metamorphism and multiple stages of folding. It is dominated by arenaceous facies in the east and calcareous facies in the west with sporadic occurrence of granulite, tectonic slices of ophiolite, blue schist and basement gneiss (Biswal, 1988; Biswal et al., 1998a, b; Khan et al., 2005). The South Delhi Orogeny is constrained between ca. 1.7 and 0.8 Ga based on synkinematic Sendra-Ambaji granite and diorite (Choudhary et al., 1984). The North Delhi Fold Belt (NDFB) exhibits more extensive outcrops of quartzites and schist unconformably overlying the sialic basement rocks. The NDFB is marked by late-stage open folding, axial planar shearing and low-grade metamorphism, and has been constrained between 1.8 and 1.5 Ga (Kaur et al., 2009).

Aravalli mountain belt is classified into three lithostratigraphic units:

- (i) Bhilwara Supergroup
- (ii) Aravalli Supergroup
- (iii) Delhi Supergroup

The Bhilwara Supergroup forms the basement of the Aravalli mountain belt and consists of Banded Gneissic Complex (BGC). It has been classified as Sandmata Complex, Mangalwar Complex and Hindoli group; Rajpura Dariba, Pur-Banera, Jahazpur, Sawar and Ranthambor groups (table 2.1). The Aravalli Supergroup overlies the Banded Gneissic Complex and comprises thick pile of predominantly argillaceous sediments which show

prograde metamorphosed character towards the core of Aravalli range. The Delhi Supergroup is confined to the Delhi Fold Belt (NDFB and SDFB) and unconformably overlies pre-Delhi schist and gneisses. Here, the study area is confined to Delhi Supergroup.

Table 2.1 Lithostratigraphic classification of Rajasthan and Northern Gujarat (Gupta et al., 1980).

Deccan Trap			
PROTEROZOIC	Marwar Supergroup		Malani plutonic Suite (~740-771 Ma) Erinpura Granite (~750 Ma) Godhra Granite (~995 Ma)
	Vindhyan Supergroup		Upper Vindhyan (~1000-650Ma) Lower Vindhyan (~1750-1500Ma)
	Delhi Supergroup (2000-800Ma)	Punagarh Group Sindreth Group Sirohi Group Kumbhalgarh Group Ajabgarh Group Gogunda Group Alwar Group	Sendra-Ambaji Granite (800-1550Ma) Kishangarh Syenites (1475-1910 Ma) Granulite (Phulad Ophiolite Suit)
	Aravalli Supergroup (2500-1600 Ma)	Champaner Group Lunavada Group Jharol Group Dovda Group Nathdwara Group Bari Lake Group Kankorli Group Udaipur Group Debari Group	Udaipur Granites (~2275 Ma) Serpentinites, Talc Schist (Rakhabdev Ultramafic Suit)
ARCHEAN	Bhilwara Supergroup (>2500 Ma)	Ranthambor Group Rajpura-Dariba Group Pur-Banera Group Jahazpur Group Sawar Group Hindoli Group Mangalwar Complex Sandmata Comlex	Berach Granite/Jahazpur Granite (2585 Ma) Dolerite Sill and Dykes Untala, Gingla Granite (~2960 Ma) Mafic and Ultramafic body Acidic bodies

The North Delhi Fold Belt (NDFB) is further divided into three main sedimentary sub-basins (Singh, 1984). From east to west, these are the Bayana-Lalsot, the Alwar and the Khetri sub-basins. The Bayana-Lalsot and the Alwar sub-basins taper in the south, whereas the southern continuation of the Khetri sub-basin is uncertain due to scarcity of continuous outcrops.

2.1 Geology of Alwar sub-basin

The Alwar sub-basin extends from Jaipur in the south to beyond Rajasthan-Haryana border in the north, and is located between the Lalsot-Bayana sub-basin in the east and the Khetri sub-basin in the west separated by prominent faults or lineaments. The Alwar sub-basin tapers southward near Lalgah.

Heron (1917) classified Delhi System into Raialo series, Alwar series, Kushalgarh limestone, Hornstone breccia and Ajabgarh series in younging order. All the basic rocks and granites occurring within the Delhi System were given the status as post Delhi intrusive by him. The stratigraphic succession suggested by Heron (1917) is given in table 2.2.

Table 2.2 Stratigraphy of Delhi System (after Heron, 1917).

Post-Tertiary	Recent and sub-recent
Delhi SystemUnconformity.....
	Ajabgarh series
	Hornstone breccia
	Kushalgarh limestone
	Alwar series
Unconformity.....
	Raialo series
Unconformity.....
Pre Delhis	Mica schist, limestone, quartzite and conglomerate

After his work in central Rajasthan, Heron (1953), placed the Raialo Series between the Aravalli and the Delhi Systems, separated by strong unconformities representing Eparchean interval. This seminal framework of Heron (1917, 1953) has remained the basis for all subsequent stratigraphic revisions. The systematic geological study in Alwar, Jaipur and Bharatpur districts in the north-eastern part of Rajasthan and adjoining areas by many researchers have led to the refinement of geology of Alwar sub-basin. A brief geological classification of the area is provided in table 2.3.

The Mangalwar Complex (Archaean) of the Bhilwara Supergroup forms the basement of the Alwar sub-basin. The Raialo, the Alwar and the Ajabgarh Groups of the Delhi Supergroup (Palaeo to Mesoproterozoic) occur as cover rocks. Unconsolidated to semi-consolidated alluvium of sub-recent to recent age occupy vast plains in the north. The survey area falls in the south-eastern part of Alwar sub-basin (fig. 2.2). The basement Mangalwar Complex (Archean) of the Bhilwara Supergroup comprising gneisses, amphibolites, quartzite, phyllite, mica schist, marble, banded-magnetite-hematite-jasper quartzite, tuff conglomerate and granite occurs as isolated exposures towards south, around Tholai, Sainthal, Kundal, Golana and Thatra. The rocks of the Delhi Supergroup occupy major part of the area. The Raialo Group unconformably overlies the Mangalwar Complex and has been divided into the Dogeta, Serrate and Tehla Formations in the younging order. The lower unit of the Dogeta Formation comprises pebbly and gritty quartzite and schist while the upper unit is thick dolomitic marble, tremolite-bearing at places, with minor intercalatory quartzite. The basal part of the Raialo Group is restricted around Raialo, south of Dogeta, Baldeogarh and Palpur. This unit is overlain by fine grained, white, mature quartzite (Serrate Quartzite; Heron, 1917) of the Serrate Formation. The overlying Tehla Formation begins with metabasic volcanics and is interlayered with gritty biotite- feldspar-quartz schist and quartzite, minor phyllite and carbonate. It is exposed in the area around Talab, Tehla, Kanikhor, Kaled and South of Surer.

The thick quartzite horizon interlayered and capped by metabasic rocks south of Pandupol valley and at Kankwarhi, constitutes upper part of the Tehla Formation and rests over the lower part of this formation with angular relationship.

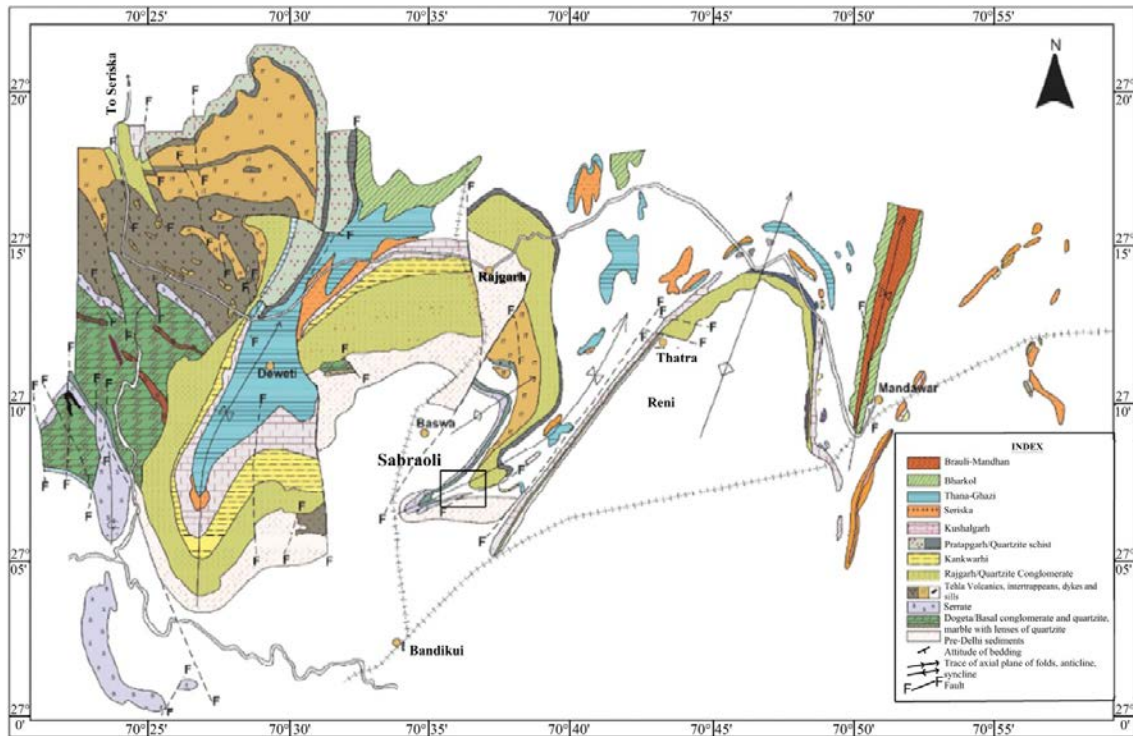


Figure 2.2 Generalized geological map of part of Alwar sub-basin, northeastern Rajasthan showing location of study area (after Khanam et al. 2020).

The rocks of the Alwar Group, overlying the Raijalo with an erosional and/or angular unconformity are widespread and have been classified into the Rajgarh, Kankwarhi and Pratapgarh Formations. The Rajgarh Formation comprises basal conglomerate, overlain by gritty, coarse and arkosic quartzite. The upper beds of the Rajgarh Formation grade into an assemblage of quartz-sericite schist and minor ferruginous marble with interbedded quartzite of the Kankwarhi Formation. Massive, thin bedded feldspathic and sericite quartzite and gritty, quartz schist constitute the youngest unit of the Alwar Group called the Pratapgarh Formation, preserving cross bedding, truncated tops of which serve as younging indicators.

Table 2.3 Stratigraphic sequence of the Delhi Super Group of northeastern Rajasthan (after Banerjee, 1980; Singh, 1988a, 1988b).

Group	Formation	Lithology
Ajabgarh	Acid intrusives	Granite, pegmatite & quartz veins
	Basic intrusives	Amphibolite and meta-dolerite
	Arauli-Mandhan Formation	Quartzite, staurolite-garnet schist, carbon phyllite, slate
	Bharkol Formation	Quartzite with interbedded phyllite and carbon phyllite
	Thana-Ghazi Formation	Carbon phyllite, tuffaceous phyllite, sericite schist, quartzite, and marble
	Seriska/Weir Formation	Brecciated and ferruginous quartzite, chert, breccia, carbon phyllite and marble
	Kushalgarh Formation	Impure marble with lenses of phosphorite, basic flows, agglomerate tuff.
.....Unconformity.....		
Alwar	Pratapgarh Formation (=Bayana and Damdama Formations)	Quartzite and quartz-sericite schist (conglomerate)
	Kankwarhi Formation (= Badalgarh Formation)	Quartz-sericite schist, quartzite schist, quartzite with thin lenses of marble and conglomerate.
	Rajgarh Formation (= Jogipura Formation)	Quartzite, marble, gritty quartzite, conglomerate
.....Unconformity.....		
Raialo (Rayanhalla)	Tehla Formation (-Jahaj-Govindpura Volcanics)	Lava flow, pillow lava, agglomerate, spatter, pyroclastic breccia, tuff, epiclastic breccia, and associated conglomerate, quartzite, schist, phyllite, marble
	Serrate Quartzite (-Nithar Formation)	Quartzite with wedge and lenses of oligomictic conglomerate
	Dogeta Formation	Banded siliceous marble, quartzite phyllite, dolomitic marble with bands of conglomerate, quartzite phyllite and schist.
.....Unconformity.....		
Pre-Delhi		Granite and gneisses, amphibolites, quartzite, phyllite, schist, marble, banded magnetite-hematite-jasper quartzite, tuff, granitised meta-sediments.

The rocks of the overlying Ajabgarh Group are dominantly tuffaceous and calcareous and occupy low lying areas and valleys between the high ridges of the Alwar Group. The basal part (black banded marble, calc schist and minor quartzite) constitutes the Kushalgarh Formation. Argillaceous content increases in the area south of Nangal Durgu with occurrence of staurolite-bearing phyllite and schist along with tremolite-bearing calc schist. At Baraud, the Kushalgarh Formation is rich in stromatolites. Species include *Baicalia baicalica*, *Collenia columnaris*, *Kusiella kusiensis* & *Jacutophyton* indicating age from 1700 m.y. to 1300 m.y. for the rocks of the Ajabgarh Group (Barman, 1980). The overlying Seriska Formation ("Hornstone breccia", Heron, 1917) includes brecciated, ferruginous quartzite with angular clasts of vein quartz, quartzite and intercalations of meta-tuff and phyllite. This formation occurs as a bedded horizon and has been folded along with the associated overlying and underlying lithologies. The Seriska Formation is overlain by grey dolomitic marble, phyllite, tuffaceous grey and black variegated beds and felsic rocks of the Thanaghazi Formation. It also contains minor ferruginous quartzite and hydroclastic breccia. In the Ajabgarh valley, this Formation is profusely traversed by quartz veins. The Bharkol Formation overlies the Thanagazi Formation and consists of intercalated and thinly bedded assemblage of phyllite, quartzite, grey and red tuffaceous beds and calcareous felsic rocks. Patches of hydroclastic breccia also occur at few places in this Formation. The Arauli Formation comprising slate, phyllite, and staurolite - garnet bearing phyllite and schist forms the youngest Formation in this sequence and is restricted in a few patches to the north and near Mandawar to the southeast.

The Delhi sequence is affected by three distinct types of intrusives. Few, small unmappable basic dykes intrude the basal part of the Raialo Group, probably represent feeder channels to the basic bodies occurring in the Tehla Formation. The Raialo Group is intruded by granite bodies, such as the Jhiri Granite and apophyses arising from the Bairath Granite.

Pegmatite and quartz veins constitute the latest intrusive bodies affecting mostly the Ajabgarh rocks. Large bodies of pegmatite and pegmatitic granite occur near Torara Kalan, east of Buchara.

The granite and granite gneiss bodies at Dadikar, Bairath, Barodia and smaller bodies around Harsora and Khairthal regarded as post- Delhi intrusive by Heron (1917), have been adjudged as basically basement granites, which have been remobilized during the Raialo deformation. Even the granite body at Jhiri may have basement component in it. Likewise the metabasic bodies in the Tehla Formation of the Raialo Group, recognised as post-Delhi intrusives by Heron (1917), have been established as metavolcanics of Tehla Formation (Banerjee and Singh, 1977).

The Alwar sub-basin has undergone at least three phases of deformation. The earliest deformation produced tight folds with ENE - WSW axial traces in the Raialo rocks. The first deformation of the Alwar - Ajabgarh sequence (II deformation of the Delhi's) produced isoclines with NNE- SSW striking axial planes and resulted in the development of slaty cleavage and axial planar schistosity. Superposed on these folds are a set of folds, which are isoclinal, tight to open on steep to vertical NNW-SSE to NNE-SSW striking axial planes. This superposition has produced type -3 interference pattern of Ramsay. The 2nd generation folds of the Alwar- Ajabgarh sequence have developed on all the scales and control the map pattern (Das, 1988). Subsequently, these folds were superposed by broad and open cross folds on ENE-WSW to ESE - WNW trending axial surfaces, producing culminations and depressions. A structural hiatus exists between the Raialo Group and the overlying Alwar - Ajabgarh Groups.

The average metamorphic grade in the area is low, but staurolite - biotite association with garnet has been recorded at some places, indicating that this region was metamorphosed up to the garnet-staurolite zone and middle grade (Gangopadhyay and Sen, 1972). The

absence of kyanite in this belt suggests a lower grade of metamorphism than that in the Khetri Copper Belt (Sharma, 1988).

The Raialo and the Alwar rocks were deposited in shallow environment as compared to the Ajabgarh Group. The repetitive sequence of argillite, meta-tuffs and carbonate - quartzite points towards a fluctuating environment during the deposition of the Ajabgarh metasediments. The talus or scree on the pediment slopes of the hillocks, and the alternating layers of sand, silt and loam on the plains and riverbeds, constitute the Quaternary deposits of recent to sub-recent age.

2.2 The Raialo Controversy

The stratigraphic position of Raialo and its contact with overlying Alwar Group have remained a subject of controversy ever since the times of Hacket and Heron. A chronological order of the status of Raialo Group is provided below.

- (i) Hacket (1877) included Raialo limestone and quartzite in 'Alwar Group' and later revised his own classification (1881) to include the Raialo limestone in 'Aravalli Series', thus, separating it from the 'Delhi Series'.
- (ii) Heron (1917), from his studies of the north-eastern Rajasthan, could not establish conclusively the unconformity between the rock units and preferred to put them together under 'Delhi System'.
- (iii) Subsequently, after the mapping of Central Rajasthan (1953), Heron modified the stratigraphic sequence assigning an independent status to the Raialo Series, based on 'pronounced unconformity below and above it'.
- (iv) Sant and Sharma (1973) assigned the status of a Group to the 'Raialo Series, within the Delhi Supergroup and shifted the contact between Raialo and Alwar Groups to 5 km, north across Tehla on the basis of angular unconformity between Serrate

Quartzite and the rocks of Alwar Group. They included the Serrate Quartzite (put within the Alwar series by Heron) and overlying conglomerate-quartzite schist assemblage into the Raialo Group. This group was divided into two Formations, namely, the Dogeta Formation and the Tehla Formation. In the former were included the basal conglomerate, feldspathic quartzite and dolomitic marble while the Serrate quartzite and overlying conglomerate-quartzite schist assemblage found their place in upper Formation. The basic rocks associated with the Tehla Formation were considered to be the post-Delhi intrusives.

- (v) On the basis of study of Banerjee and Singh (1977) about the volcanic origin of basic rocks of Tehla area and the nature of unconformity between the Raialo and Alwar Groups, Singh et al. (1978) gave a separate status of formation to Tehla volcanic and equated it with the Jahaj-Govindpura volcanics of Bayana area. They also shifted the contact between Raialo and Alwar Groups to a higher stratigraphic level at the base of Pandupole conglomerate.
- (vi) On the basis of descriptions by previous researchers and self observations from the field areas of Alwar sub-basin, it is inferred that the Raialo Group should be given an independent status of Delhi Supergroup having unconformable contacts with the underlying basement rocks and overlying Alwar Group of rocks. Although, the Raialo Group has an angular contact with Alwar Group around Tehla area, the contact seems to be disconformable around Surer and further southward up to Sabraoli.

2.3 Evolution of Alwar sub-basin

Evolutionary model of Alwar sub-basin has been suggested by S. P. Singh (1982a) on the basis of deposition of various stratigraphic units and their sedimentological framework. During initial stage, a down sag Dogeta graben was formed due to brittle deformation of the

crust which received carbonate sediment under stable shelf condition and no terrigenous sediment due to lack of drainage system and then up warping of the basement and its erosion followed by weak tectonic movement resulting in the Alwar basin and Baswa block (Singh, 1982a). Basement lithology of the Baswa block is demarcated by a fault on both side and being protected from erosion for a longer period before the onset of Delhi sedimentation. It indicates that both Surer and Riwas-Rajpura faults were active before Delhi sedimentation (fig. 2.3A). During the stage II, Dogeta Graben experienced down warping and reactivated block faulting in the eastern part gave rise to the Baswa horst and Surer Graben (fig. 2.3B). During stage III, basin development indicates reactivation of Surer fault and subsidence of the individual depositories and outpouring of basic volcanics along these ruptures (fig. 2.3C). The stage IV, marks the initiation of Alwar sedimentation with the tilting of the basin towards north and subsidence of Baswa horst and eastern part of Surer graben. Transverse Thatra fault and longitudinal Ancheri fault developed. At this stage the southern source area suffered rapid upliftment increasing the relief many folds. Coarse clastic of Alwar deposited in fluvial to marginal marine environment (fig. 2.3D). The facies associations include river-dominated estuary, tidal flat/ intertidal and wave dominated shore face to foreshore (Khanam et al. 2020). The eastern tectonic units could not keep pace with the rapidly subsiding main basin and hence, they were exposed during last phase of Alwar sedimentation. Subsidence of the wider areas submerged entire Alwar sub-basin and also submerged the eastern barrier between this and the Bayana sub-basin (fig. 2.3E). Psammopelitic sequence of Ajabgarh Group was deposited in a coastal complex environment including lagoonal basins with circulation and tidal bars and flats.

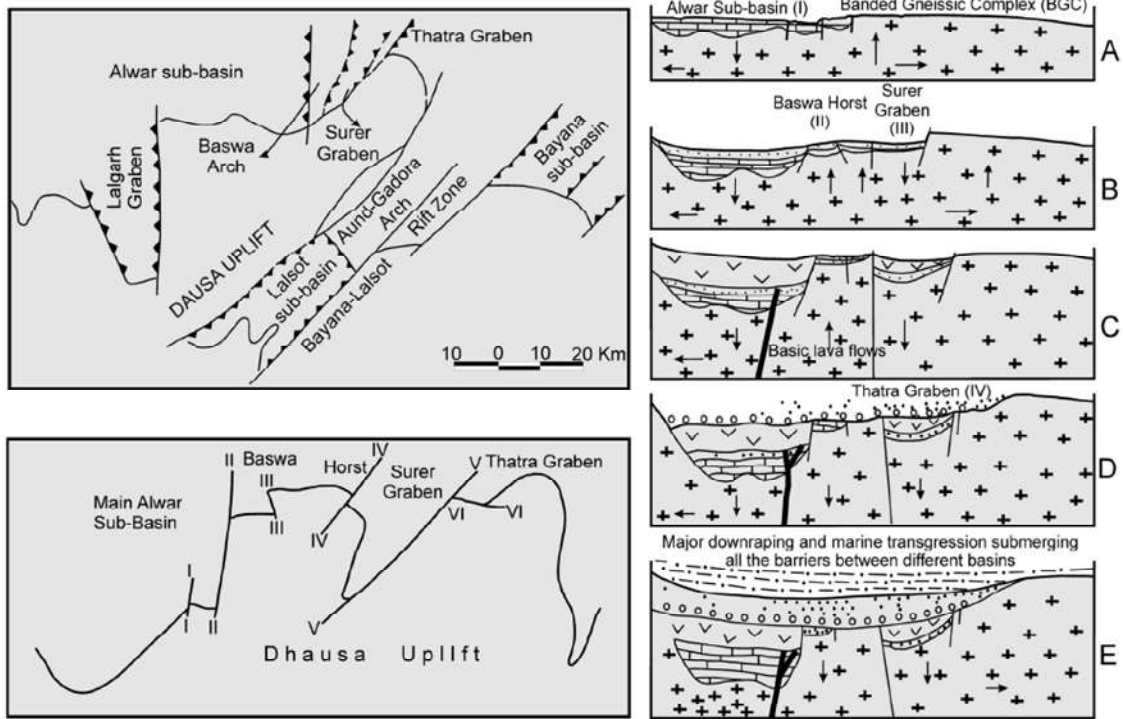


Figure 2.3 Map showing location, syn-sedimentary dislocation and various tectonic blocks of the eastern part of the Alwar sub-basin. Evolutionary trend of Alwar sub-basin (mainly eastern part): A. Development of main Alwar sub-basin (I); B. Down warping and reactivated block faulting, birth of Baswa horst (II) and Surer graben (III); C. Eruption of basic flows; D. Wider down warping and origin of Thatra graben (IV); E. Major down warping and marine transgression submerging all the barriers between different basins (after Khanam et al. 2020 & Singh, 1982a).

CHAPTER 3

LOCAL GEOLOGY

3.1 Detailed Geological Mapping around Sabraoli

Sabraoli area lies at the south-eastern part of the Alwar sub-basin. The area is characterized by a folded map pattern. It lies along the Gullana-Sabraoli-Jamrauli-Buchpuri-Babeli synclinal axis. The major litho units exposed in the area are granite-gneiss, quartz sericite schist, quartzite, quartz-hornblende schist, quartz-biotite-sericite schist of Raialo and quartzite of Alwar Group. The detailed geological map around Sabraoli-Uprera area is presented in fig. 3.1.

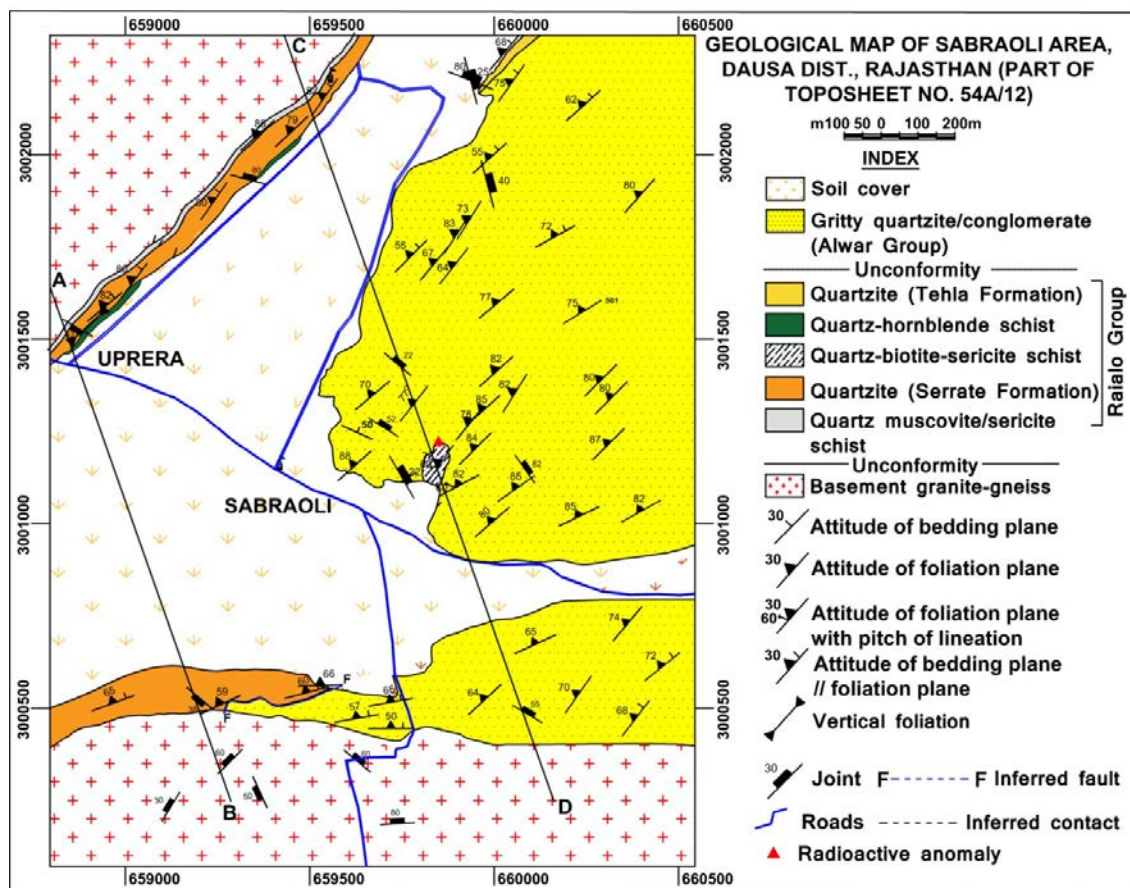


Figure 3.1 Geological map around Sabraoli-Uprera area.

Towards southern part of the mapped area, basement granite-gneiss is unconformably overlain by ferruginized gritty quartzite (Alwar Group) on the east (fig.3.2a). However, the granite is directly overlain by serrate quartzite (Raialo Group) on the west (fig.3.2.b), juxtaposed with the gritty quartzite of Alwar Group (fig.3.2.c,d). Geological disposition of the litho units and field evidences suggest a faulted contact between the two quartzites. The granite is massive, leucocratic, grey to dark grey in colour with patches of pink granite at places, medium to coarse grained having porphyritic texture and is composed of phenocryst of feldspars with groundmass composed of quartz, feldspar, biotite, muscovite (fig.3.2e). The granite has been foliated. Along with this granite, some lensoidal patches of very fine grained, cryptocrystalline, dark colored xenoliths are also observed (fig.3.2f). The granite is not exposed on surface towards NW side of the mapped area, but study of well dump material indicates its presence below the soil cover.

The north-western part of the study area around Uprera is characterised by small hillocks. Here, the soil covered area inferred to be granite gneiss of Mangalwar Complex is followed by 5-10m thick quartz sericite schist. It is highly sheared with well developed foliation. The quartz-sericite schist has a sharp contact with massive Serrate quartzite (fig. 3.3a) on the SE flank, which is successively in contact with the meta-basic rock (quartz-hornblende schist) of Tehla Formation. The Serrate quartzite is primarily composed of serrated orthoquartzite (fig.3.3b) with sporadic, thin oligomictic conglomerate at the basal part. The Serrate quartzite has a strike of $N40^{\circ}E-S40^{\circ}W$ with sub-vertical dip towards NW. It is affected by number of joint sets with ferruginization along the joint planes. Chunks of magnetite were observed within the quartzite at places. Outcrops of co-folded quartz-sericite schist and serrate quartzite are prominent. The quartz-sericite schist shows higher radioactive counts as compared to the serrate quartzite. From the geological setting and disposition of

rock units, the hillocks are inferred to be the extension of the NE-SW trending hill near Sera ka Bas-Golana.

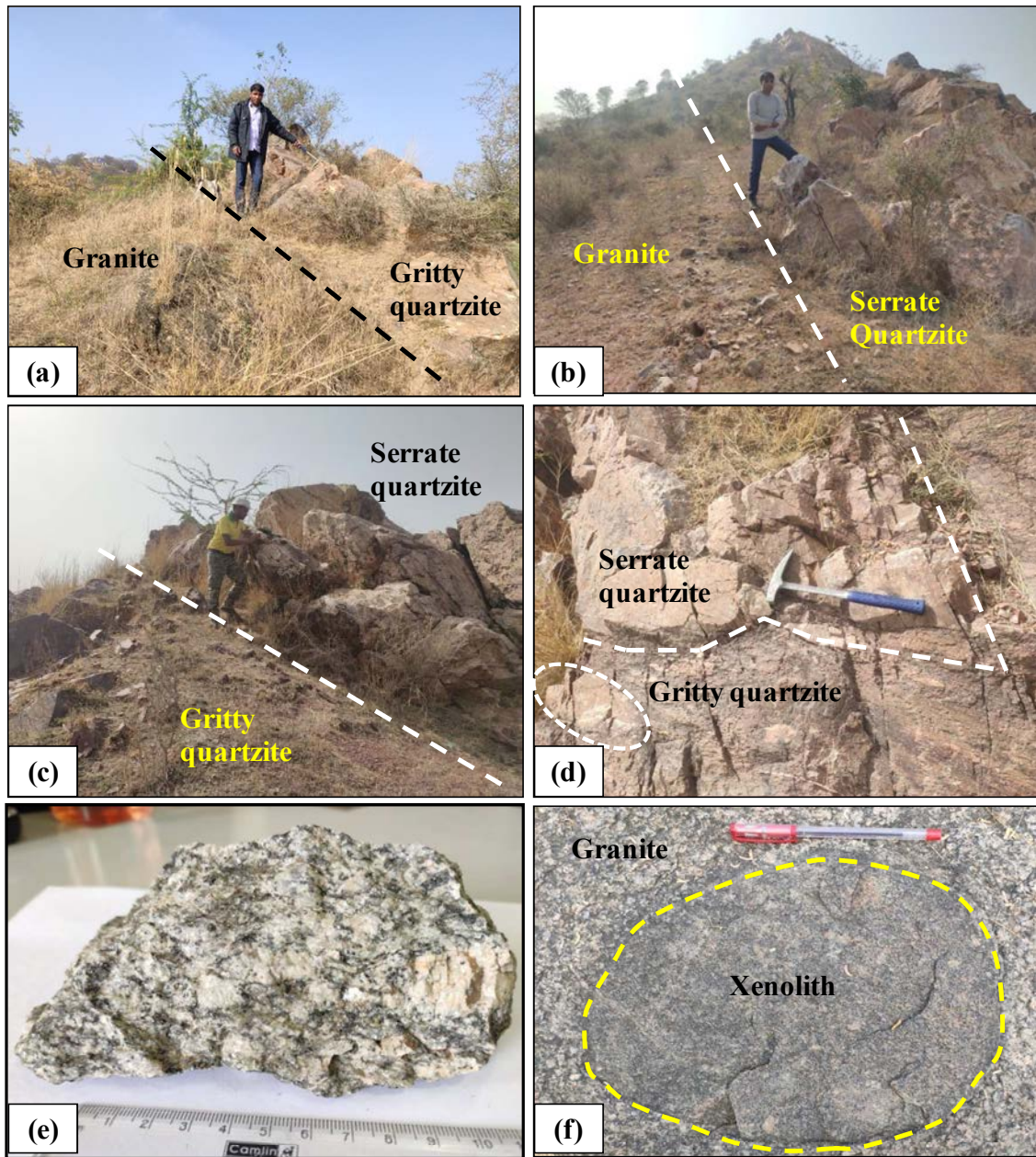


Figure 3.2 (a) Contact of basement granite with gritty quartzite of Rajgarh Formation, (b) Contact of basement granite with serrate quartzite, (c), (d) Juxtaposition of quartzite of Rajgarh Formation and Serrate Formation, (e) Megascopic view of granite gneiss showing phenocryst of feldspar, (f) Lensoidal xenolith within basement granite-gneiss.

The Tehla Formation conformably overlies the Serrate Formation and comprises meta-basic, quartzite and quartz-biotite-sericite schist units. The meta-basic rock is dark green coloured rock, very fine grained, cryptocrystalline in nature and is composed of quartz and hornblende (fig.3.3c). Although the overall grain size is fine, but at some places medium grained, euhedral, recrystallized grains of amphiboles (primarily hornblende) are observed. It is mainly altered in the surficial conditions. The quartzite of Tehla Formation is compact, massive, and fine to medium grained in nature. Thin, lenticular patches of intra-formational oligomictic conglomerates are observed in few places (fig.3.3d). It is interlayered or interbanded with metavolcanics in and around Surer (North of Sabraoli). Quartz-biotite-sericite schist is another component of Tehla Formation. It is exposed near to the Sabraoli uranium mineralization. The soil covered area in between the Serrate quartzite and gritty quartzite of Alwar Group is inferred (from the bore well dumps) to be quartz-biotite-sericite schist. It is very fine grained, foliated and is dominantly composed of quartz, biotite, sericite and disseminated magnetite (fig.3.3e). It has a very a high specific gravity and magnetic susceptibility due to higher content of disseminated magnetite. Numerous quartzo-feldspathic veins (varying from 2cm to 10cm) are observed within the litho-unit (fig.3.3.f).

The Raialo Group of rocks are unconformably overlain by gritty quartzite/conglomerate of Rajgarh Formation (Alwar Group). Moderately thick, polymictic, at some places oligomictic (fig.3.4a), boulder conglomeratic horizon has been observed at the basal part of the Rajgarh Formation at Kalesan around 10 km NE of Sabraoli, which denotes the unconformable contact with the underlying Raialo Group. The gritty quartzite exposed near Sabraoli is coarse to very coarse grained with intra-formational pebble layers, poorly sorted, angular- to sub-rounded having low to medium sphericity (fig.3.4b) in nature with 2-5m thick conglomerate horizon at the basal part. It is composed of clasts of quartz, feldspar (mostly microcline), tourmaline, muscovite and sericite. It is characterized as sub-feldspathic

arenite to feldspathic arenite. The litho-unit has been metamorphosed with well developed foliation. Highly stretched and elongated clasts parallel to the foliation direction are observed near to Sabraoli uranium mineralization (fig.3.4c, d). Some of the quartzo-feldspathic veins observed within the underlying quartz-biotite-sericite schist are persistent within the gritty feldspathic quartzite of Rajgarh Formation. The gritty quartzite is ferruginized near the contact with granite-gneiss in the southern part of the study area. The contact between quartzite of Rajgarh Formation with the quartz-biotite-sericite schist of Raialo Group is well exposed at Sabraoli.

Uranium mineralization (659846E, 3001178N) has been located within gritty quartzite/meta-conglomerate at the basal part of Rajgarh Formation overlying quartz-biotite-sericite schist of Raialo Group (fig.3.4e). The meta-conglomerate is composed of pebbles/cobbles of quartz, feldspar embedded in a matrix of quartz, feldspar, tourmaline, biotite, sericite, and magnetite (fig.3.4f). Higher content of biotite, sericite, magnetite in matrix part of basal Rajgarh Formation have been derived from the underlying quartz-biotite-sericite schist. Though radioactivity is mainly confined within basal gritty quartzite/meta-conglomerate of Rajgarh Formation, some part of the quartz-biotite-sericite schist is radioactive. Besides, few quartzo-feldspathic veins show radioactivity. Malachite stains are also observed within the quartz-biotite-sericite schist.

3.2 Lithostratigraphy of study area

The rocks exposed in the study area belong to the meta-sediments of the Delhi Supergroup resting unconformably over gneissic basement of the Mangalwar Complex. Raialo and Alwar Group of rocks are encountered in the mapped area although rocks of Ajabgarh Group of are present away from the area along Jamrauli-Buchpuri-Babeli tract. The following litho-units are mapped: (a) Granite gneiss with xenoliths of Mangalwar Complex

(b) Quartz-sericite schist, quartzite, quartz-biotite-sericite schist and metabasic rocks of the Raialo Group (c) Quartzite of the Rajgarh Formation.

The established stratigraphic succession within the mapped area based on the present work is as follows:

Delhi Supergroup	Alwar Group	Rajgarh Formation	Gritty feldspathic quartzite
	----- Unconformity -----		
	Raialo Group	Tehla Formation	Quartzite, Schist, Metabasic
Serrate Formation		Quartzite	
	----- Unconformity -----		
Mangalwar Complex (BGC)		Granite gneiss	

3.3 Structure

The litho-units are strongly foliated which corresponds to axial planar cleavage of the regional fold. Foliation planes within massive serrate quartzite of Raialo Group has an average strike of N46°E with dip of 83° towards N44°W (fig. 3.5), whereas that of gritty quartzite of Rajgarh Formation (Alwar Group) has an average strike of N46°E with dip of 77° towards N44°W (fig. 3.6). Sabraoli uranium mineralization has been located around the hinge zone regional syncline having a northeasterly trending fold axis. Bedding plane data is scarce in the area due to development of intense foliation. Cross laminations are identified at certain outcrops. On the north-western flank, bedding is parallel to the foliation suggesting a disconformable contact between Raialo and Alwar Group of rocks. Numerous joint planes and fractures have been observed in the area. Stereonet plot of joint planes in the area suggest an average strike of NW-SE with moderate to high dip either towards NE or SW (fig. 3.7). Kink folds have been developed at certain places representing later phase of deformation (fig. 3.8).

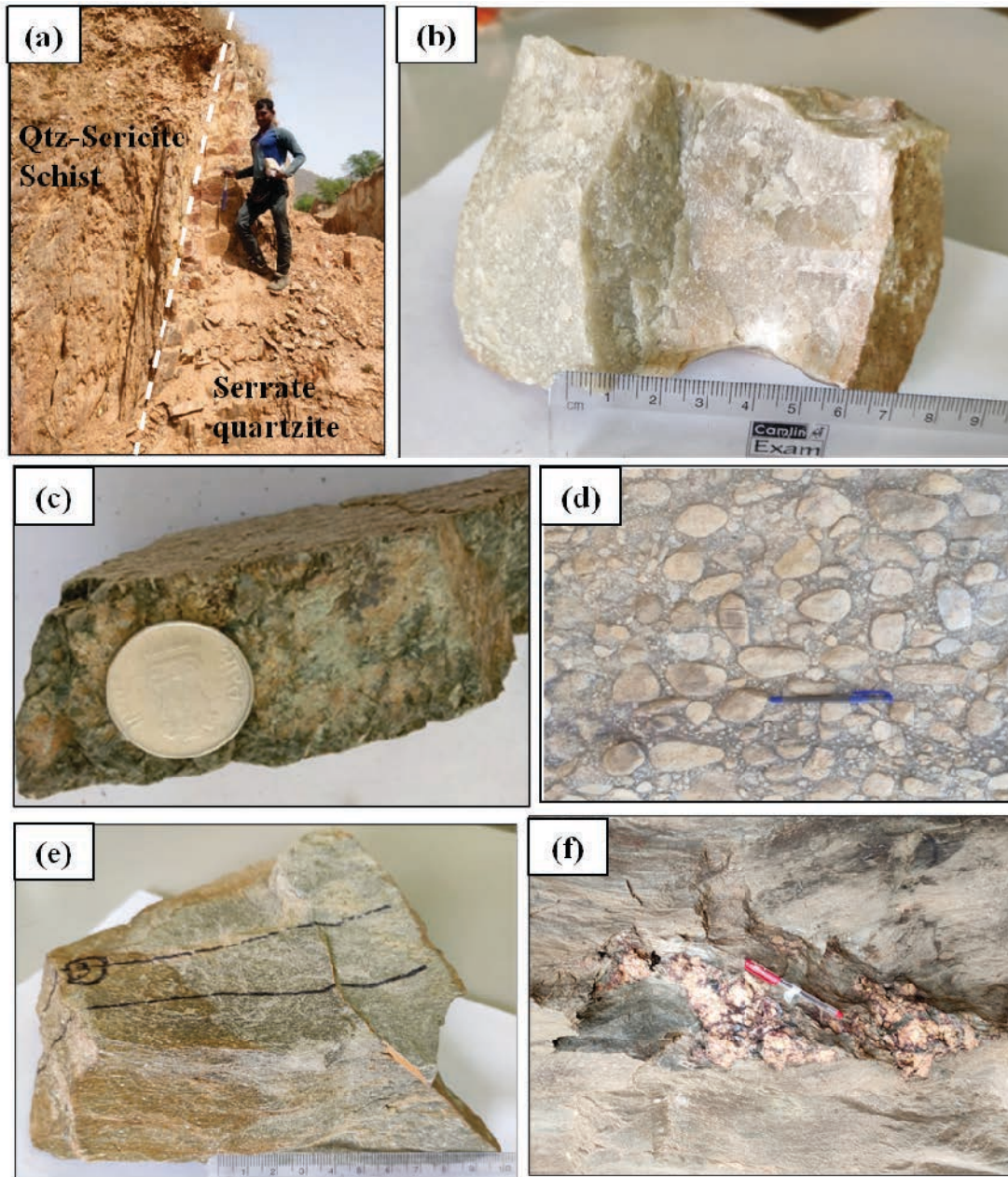


Figure 3.3 (a) Sharp contact of quartz-sericite schist with serrate quartzite, (b) Serrate quartzite, (c) Quartz-hornblende schist, (d) Oligomictic conglomerate within quartzite of Tehla Formation, (e) Quartz-biotite-sericite schist (QBSS), (f) Quartzo-feldspathic vein within quartz-biotite-sericite schist.

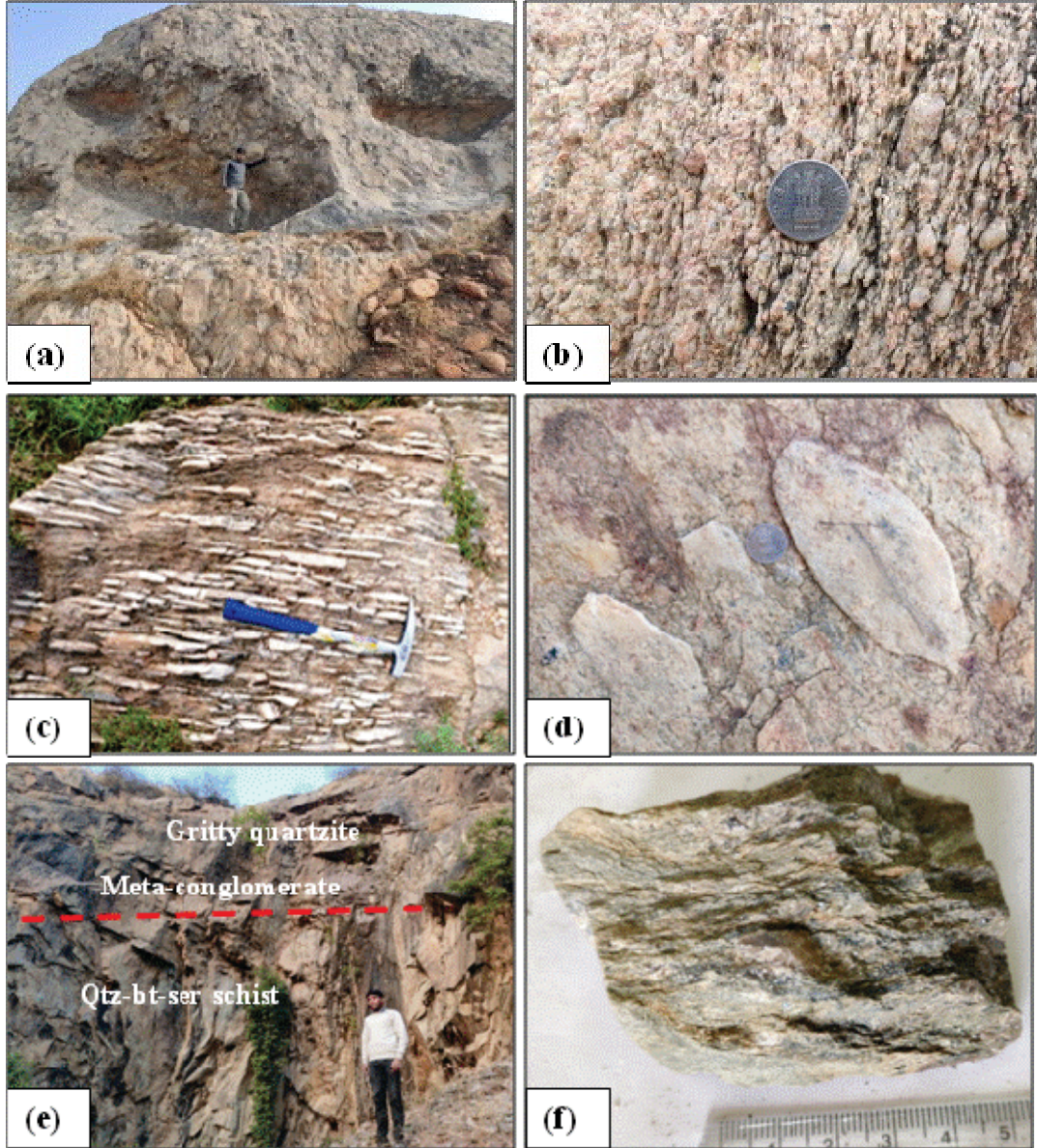


Figure 3.4 (a) Polymictic boulder conglomerate at Kalesan, representing basal part of the Rajgarh Formation, (b) Gritty quartzite of Rajgarh Formation, (c) Highly stretched, elongated quartz pebbles/cobbles of Rajgarh Formation, (d) Flattened cobble along foliation plane, (e) Cliff face exposing meta-conglomerate, basal part of Rajgarh quartzite, (f) Meta-conglomerate.

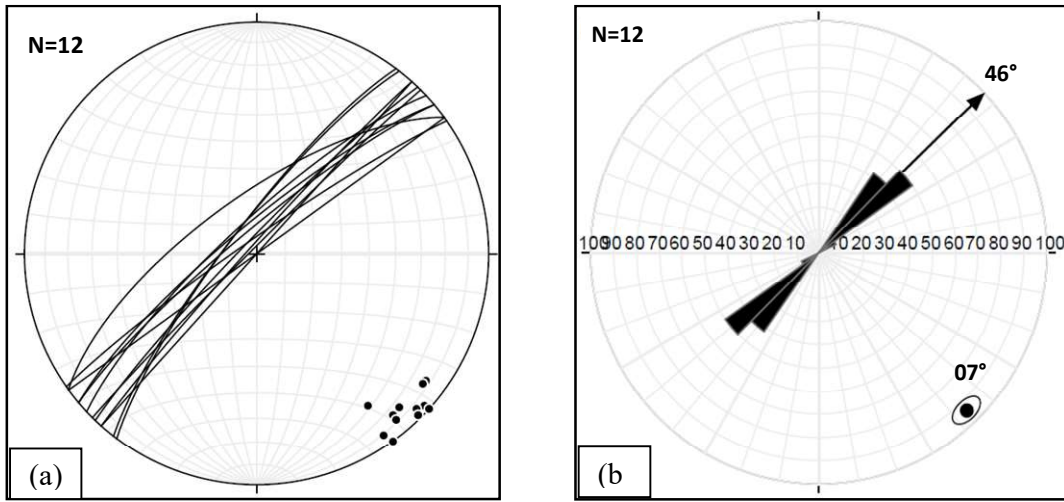


Figure 3.5 (a) Stereonet plot of foliation data and poles to the foliation (n=12) for Serrate quartzite (Raialo Group). (b) Rose diagram of the foliation planes (arrow points in the average direction and bulls eye represents pole to the average foliation plane) Average strike of the foliation plane is N46°E with dip 83° towards N44°W.

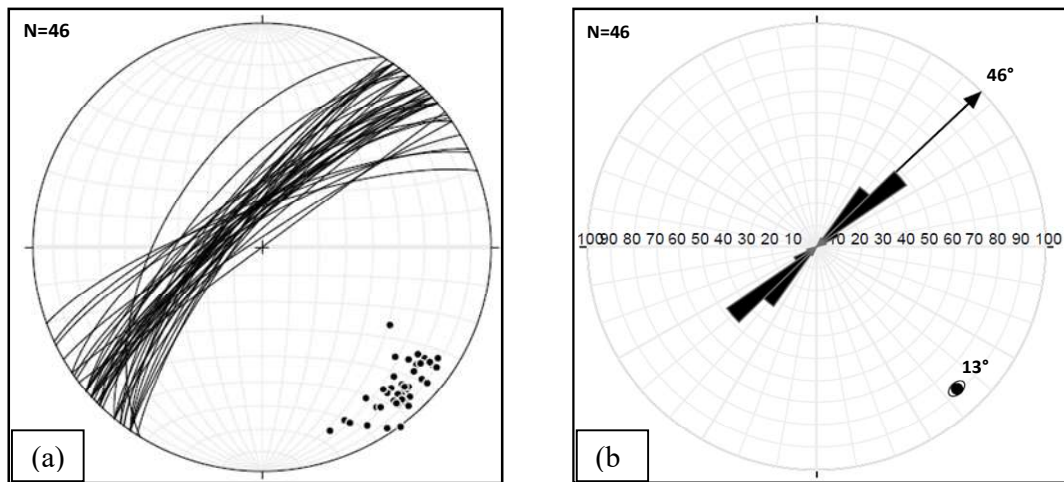


Figure 3.6 (a) Stereonet plot of foliation data and poles to the foliation (n=46) for gritty feldspathic quartzite of Rajgarh Formation (Alwar Group). (b) Rose diagram of the foliation planes (arrow points in the average direction and bulls eye represents pole to the average foliation plane). Average strike of the foliation plane is N46°E with dip 77° towards N44°W.

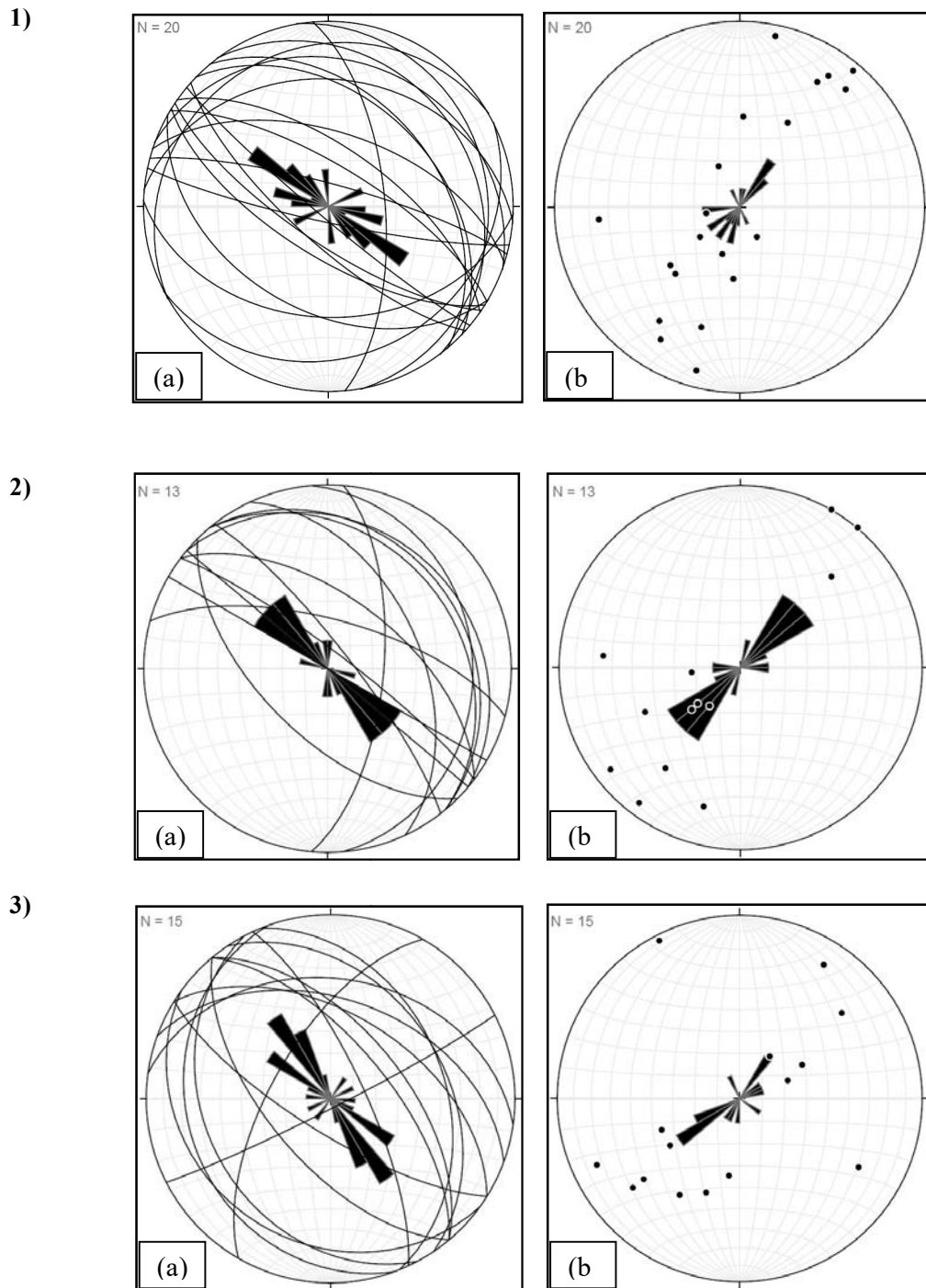


Figure 3.7 Rose diagrams for 1(a), 2(a), 3(a) strike of joint planes, 1(b), 2(b), 3(b) poles to joint planes. The plots show joint planes around Sabraoli-Uprera area have average strike of NW-SE with moderate to high dip either towards NE or SW.

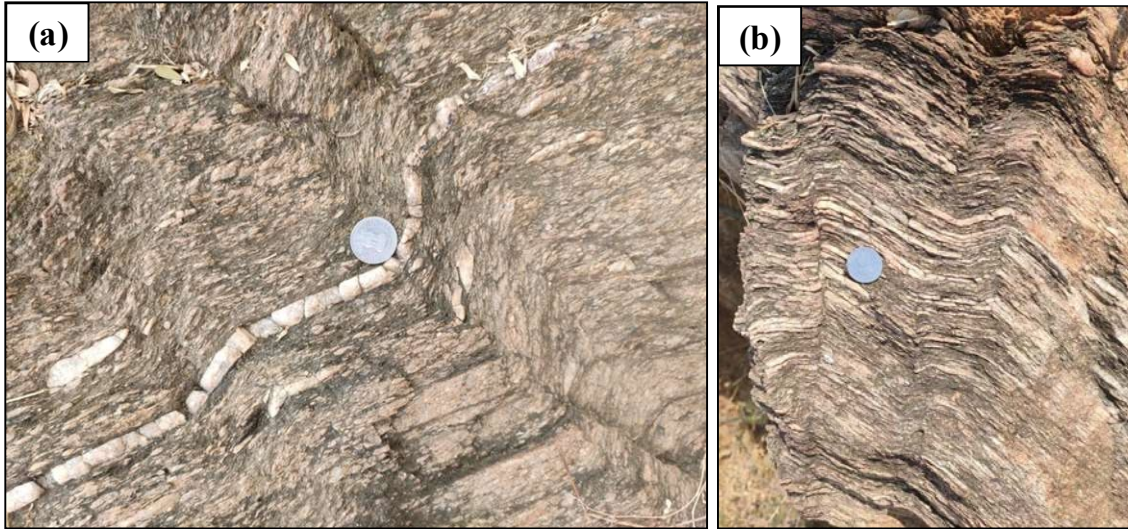


Figure 3.8 (a), (b) Kink folds developed within quartzite of Rajgarh Formation around Sabraoli.

3.4 Geological sections across Sabraoli occurrence

The Raialo Group of rocks consisting of quartz-muscovite/sericite schist, serrate quartzite, quartz-hornblende schist and quartz-biotite-sericite schist deposited over the basement granite-gneiss. The Raialo Group of rocks was followed by gritty feldspathic quartzite / conglomerate of Alwar Group. Rock units of both the Groups have undergone later deformations. The cross sections across the litho-units depict co-folding of both Raialo and Alwar Group of rocks in the area (fig. 3.9 & 3.10).

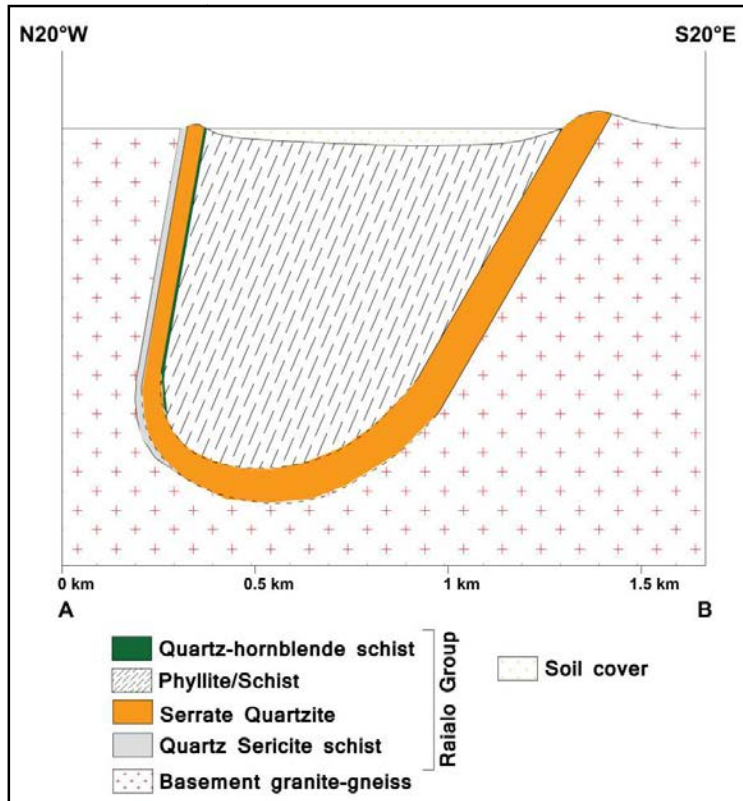


Figure 3.9 Hypothetical geologic cross section along AB line.

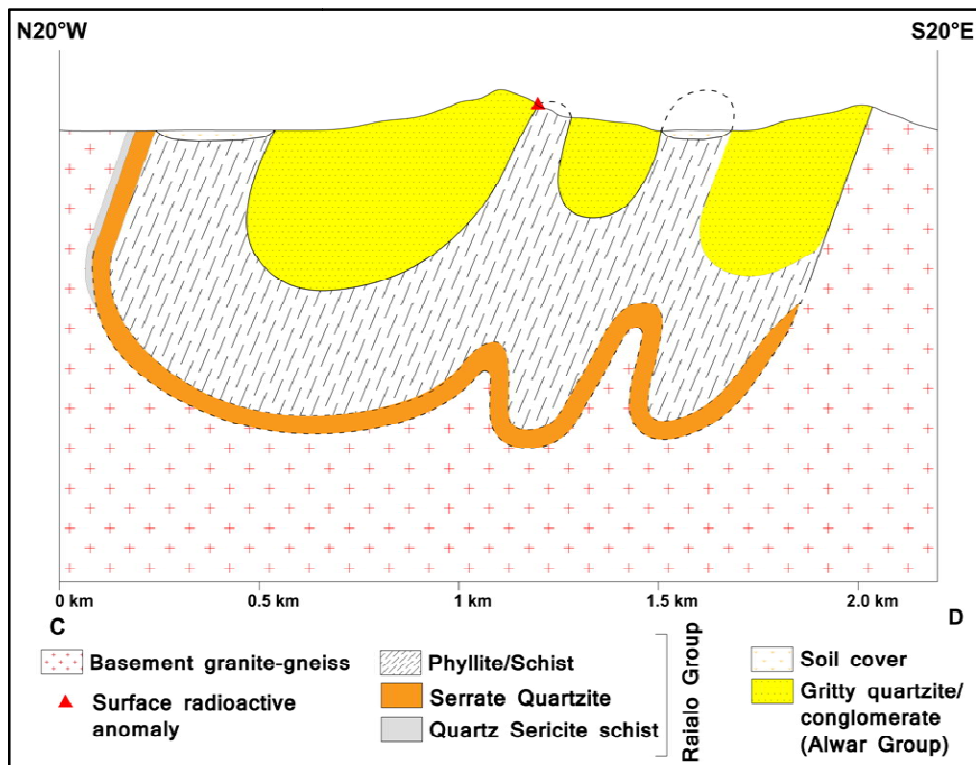


Figure 3.10 Hypothetical geologic cross section along CD line.

3.5 Subsurface investigation from core samples

From the detailed study of borehole cores from SBR-2 (50° inclination towards S55°E), it has been observed that the gritty feldspathic quartzite with intra-formational pebble layers of Alwar Group is encountered up to depth of 277.00m (fig. 3.11a). The gritty feldspathic quartzite is underlain by meta-conglomerate (fig. 3.11b), which is the basal part of the Rajgarh Formation (Alwar Group). The meta-conglomerate has a thickness of around 5m. It is successively underlain by quartz-biotite-sericite schist (QBSS, fig. 3.11c) with intermittent layers of quartz-biotite-amphibole schist (Raialo Group). Injection of thin veins of amphibole within quartz-biotite-sericite schist is also observed with depth. Biotite content of the QBSS unit increases at places. The quartzite of Rajgarh Formation has low magnetic susceptibility whereas the QBSS shows very high magnetic susceptibility due to presence of disseminated magnetite. Numerous quartzo-feldspathic veins are observed within the litho-units (fig. 3.11d). Epidote bands associated with increased biotite content are common within QBSS. Dip of the foliation varies from 70° to 80°. The litho-units are having similar compositions to that of surface outcrops.

Uraniferous radioactivity has also been recorded in basal gritty quartzite/conglomerate of Rajgarh Formation within borehole SBR-2 at Sabraoli area (fig. 3.12). The matrix of the radioactive unit is having higher content of magnetite, biotite, and sericite and has been derived from the underlying quartz-biotite-sericite schist as evidenced from the geological set up of the litho-units observed both in outcrop and core samples.



Figure 3.11 (a) Gritty feldspathic quartzite of Rajgarh Formation, (b) Meta-conglomerate composed of pebbles/cobbles of quartz embedded in matrix of quartz, feldspar, tourmaline, magnetite, sericite/muscovite (c) Contact between met-conglomerate and quartz-biotite-sericite schist, (d) Lensoidal quartzo-feldspathic material within quartz-biotite-sericite schist.

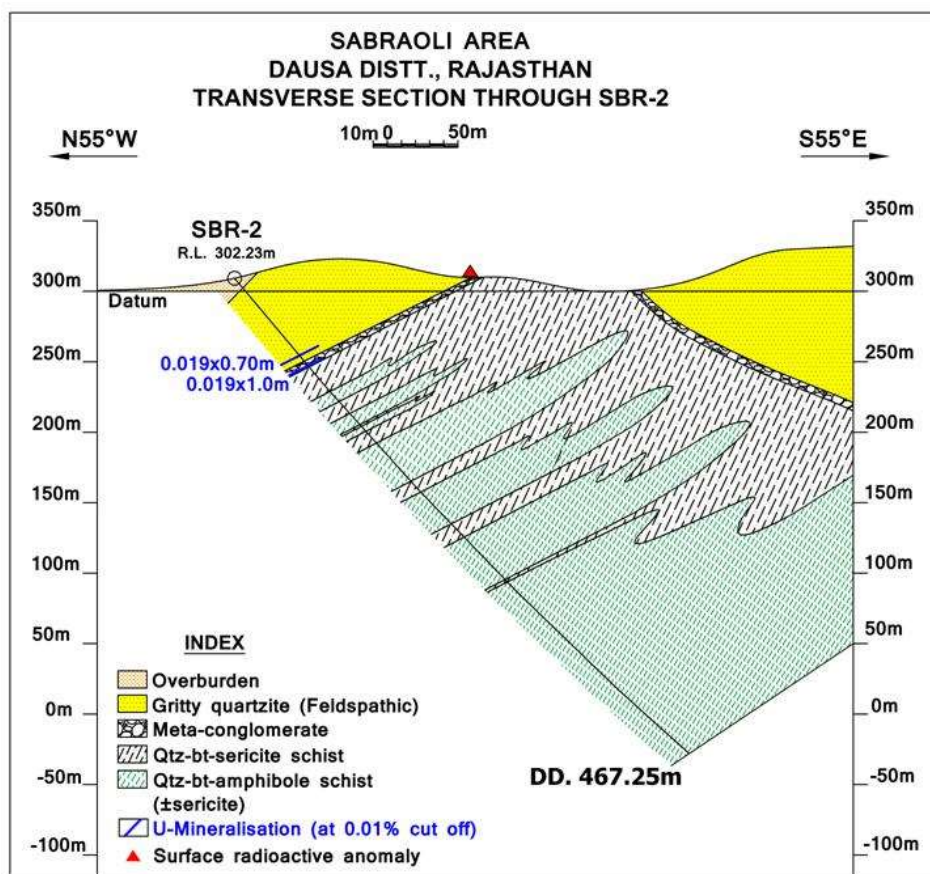


Figure 3.12 Transverse section through borehole SBR-2, Sabraoli area, Dausa district, Rajasthan.

3.6 Delineation of lineaments and other structural features over satellite imagery

Satellite imagery shows tightly folded lines (developed over quartzite of Rajgarh Formation) defining M/W pattern indicative of hinge of the regional syncline around Sabraoli (fig.3.13). Another hinge of similar pattern is demarcated near Golana (defined by Serrate quartzite). The regional fold axes have an average trend of NE-SW. Two NE-SW faults pass through east of Sabraoli U-mineralization anomaly whereas, another similar trending fault is evident near Golana. Besides, WNW-ESE, ENE-WSW trending faults are discernable around Sabraoli and Jhajhi Rampura-Jamrauli tract respectively. A NNE-SSW trending fault separating basement and Raialo Group of rocks passes through east of Kaled.

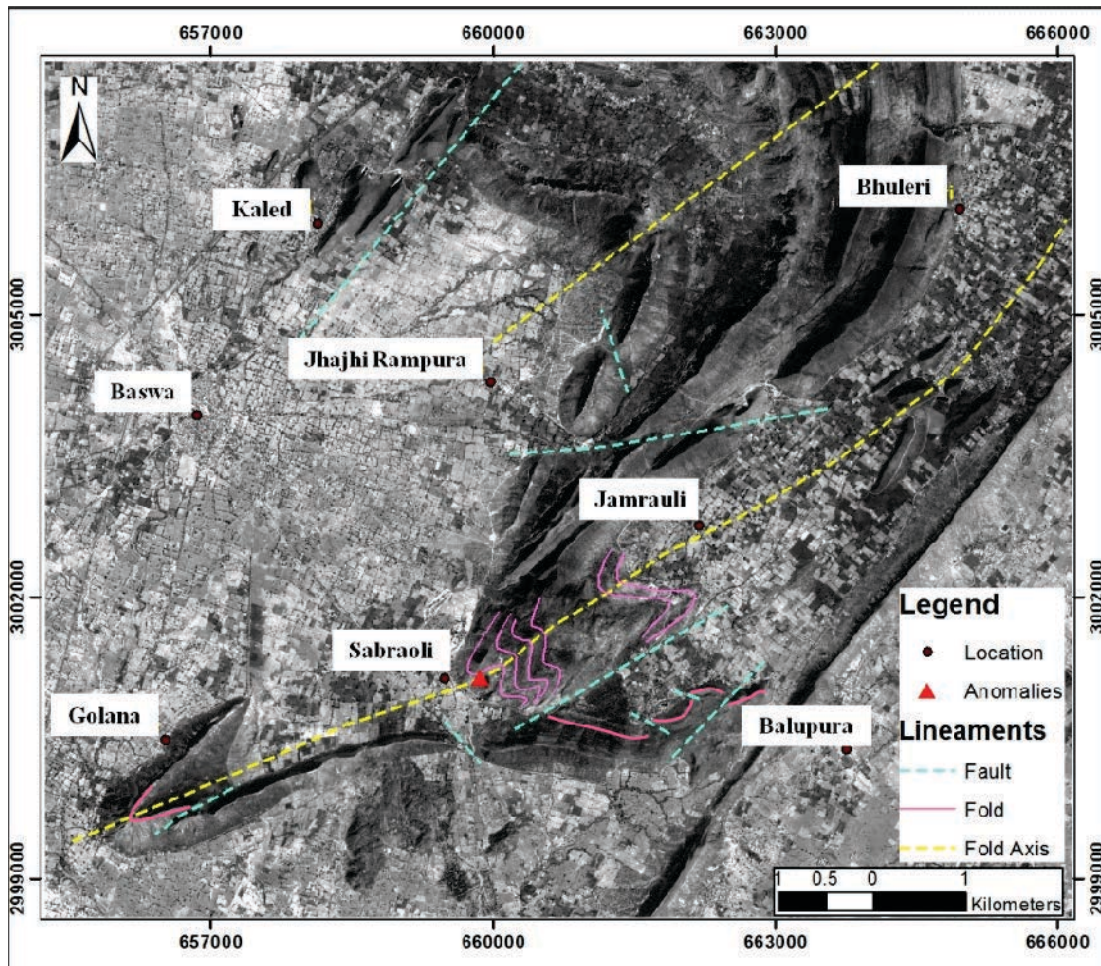


Figure 3.13 Cartosat satellite image with interpreted structural elements around Sabraoli area, Dausa district, Rajasthan.

CHAPTER 4

METHODOLOGY

Surface grab rock samples from various litho-units were collected from different locations from the mapped area. During sampling, proper care was taken to collect representative and oriented samples. The petrographic studies were carried out by self in petrology laboratory, AMD/WR. Radiometric assay has been carried out in Physics laboratory and geo-chemical analysis has been undertaken in XRF and Chemical laboratories, AMD/WR. The brief description of techniques used for analysis and studies are mentioned in following paragraphs.

4.1 Petrology Laboratory

Oriented parts of the grab samples were cut into thin-section size or cut to appropriate size slab for mounting on a slide with a diamond-blade circular saw. Friable samples were impregnated in Canada balsam and diluted with xylene before slicing. The slab was labeled on one side. Hand grinding of the other side is carried out by making a paste of 400 mesh size silicon carbide powder with water over a glass plate. The procedure is repeated with 600 and 800 size silicon carbide powder afterwards. The fine grinded face of the specimen is glued with cleaned, thin glass slide using epoxy (cold mounting). The thickness of the rock specimen on thin slide is reduced to 0.03mm by hand grinding using silicon carbide (Carborundum powder) of different sizes. The prepared section is washed in water and placed in a holder and polished on a polishing machine using nylon cloth and diamond paste. Hifin fluid has been used to avoid the sticking of the paste to the polishing cloth. Polished thin section was cleaned and ready to use for microscopic observations.

The prepared thin sections were studied under polarizing light microscope in both plane polarized and crossed polarized light.

4.2 Wavelength Dispersive X-Rays Fluorescence (WDXRF) Laboratory

Wavelength dispersive spectrometers are one of the most used methods for elemental composition of a sample, for both qualitative and quantitative determination. XRF brings advantages such as minor requirements for sample preparation, non-destructive analysis platform, relatively short analysis runtime, wide elemental analysis range from Be to U and linearity from ppm to 100%. XRF analysis instruments can be largely categorized into wavelength-dispersive X-ray spectroscopy (WDX) and energy-dispersive X-ray spectroscopy (EDX). In WDXRF, the fluorescent X-rays are physically separated before detection using diffraction crystals. It offers excellent signal-to-noise ratio and peak separation leading to very low background noise and high resolution.

4.2.1 Sample preparation

The samples were first ground to –200 mesh (75 µm) and thoroughly homogenized. Thereafter, the homogenized sample powder (1 g) were spread uniformly over a base of boric acid powder (20 g) in a cylindrical sample die of 40 mm diameter, and pelletized by applying a pressure of 20,000 kg/cm² in a semiautomatic pelletizer. Boric acid is an organic material which is highly stable under X-rays and is used to prevent X-rays from reaching the aluminum cup. A solid cylindrical pellet of 40 mm in diameter was obtained. Pellets of both the samples and reference standards, used for calibration, were prepared using this procedure. A suite of well-characterized natural rocks and Certified Reference Materials were used as calibration standards.

4.3 Chemical Laboratory

Grab rock samples from different litho-units were analyzed for trace elements and REE by wet chemical methods at Chemistry Laboratory, AMD, Western Region, Jaipur.

Representative samples were powdered to -200 mesh and the same analyzed by wet chemical methods for trace and REE elements. About 0.5gm of each fine powdered sample was taken for analysis. The samples were digested in acid media (1:1HF-HNO₃) to remove the silicate phases. The treated filtrate was then fused with Na₂CO₃ followed by pre-concentration and separation using HNO₃. The separated solution was analyzed in Inductive Couple Plasma Optical Emission Spectrometer (ICP-OES) for the analysis of REE and other trace elements.

CHAPTER 5

RESULTS

5.1 Petrography

Petro-mineralogical studies of prepared thin sections of different lithologies were carried under optical microscope. The detailed microscopic description of these litho-units is given below.

5.1.1 Basement granite-gneiss

The basement granite is primarily composed of quartz, microcline, plagioclase, biotite, muscovite, sericite (fig. 5.1a). Microcline is the dominated over plagioclase feldspars. Magnetite, apatite are the accessory minerals. Phenocrysts of feldspars with occasionally larger quartz grains show overall porphyritic texture (fig. 5.1b). Quartz grains show undulose extinction. Cross hatched twinning in microcline and lamellar twinning in plagioclase are common. The alignment of micaceous minerals has developed gneissosity within the granite. Numerous cracks have been observed within quartz grains. These features show strong deformation of the basement granite. Alteration of feldspar to sericite is very common. Hematitization of magnetite grains are also observed (fig. 5.1c).

5.1.2 Xenoliths

The major minerals present are quartz, biotite, muscovite, plagioclase, sericite (fig. 5.1d). Apatite, zircon and magnetite occur as accessory minerals. Lamellar twinning in plagioclase feldspars is common. The rock has approximately equigranular texture with occasionally larger laths of biotite (fig. 5.1e). Foliation is defined by the alignment of biotite and muscovite. Apatite, zircon, magnetite occur as accessory mineral. Serrated boundary of quartz with undulose extinction is observed. Alteration of feldspar to sericite is very common (fig. 5.1f).

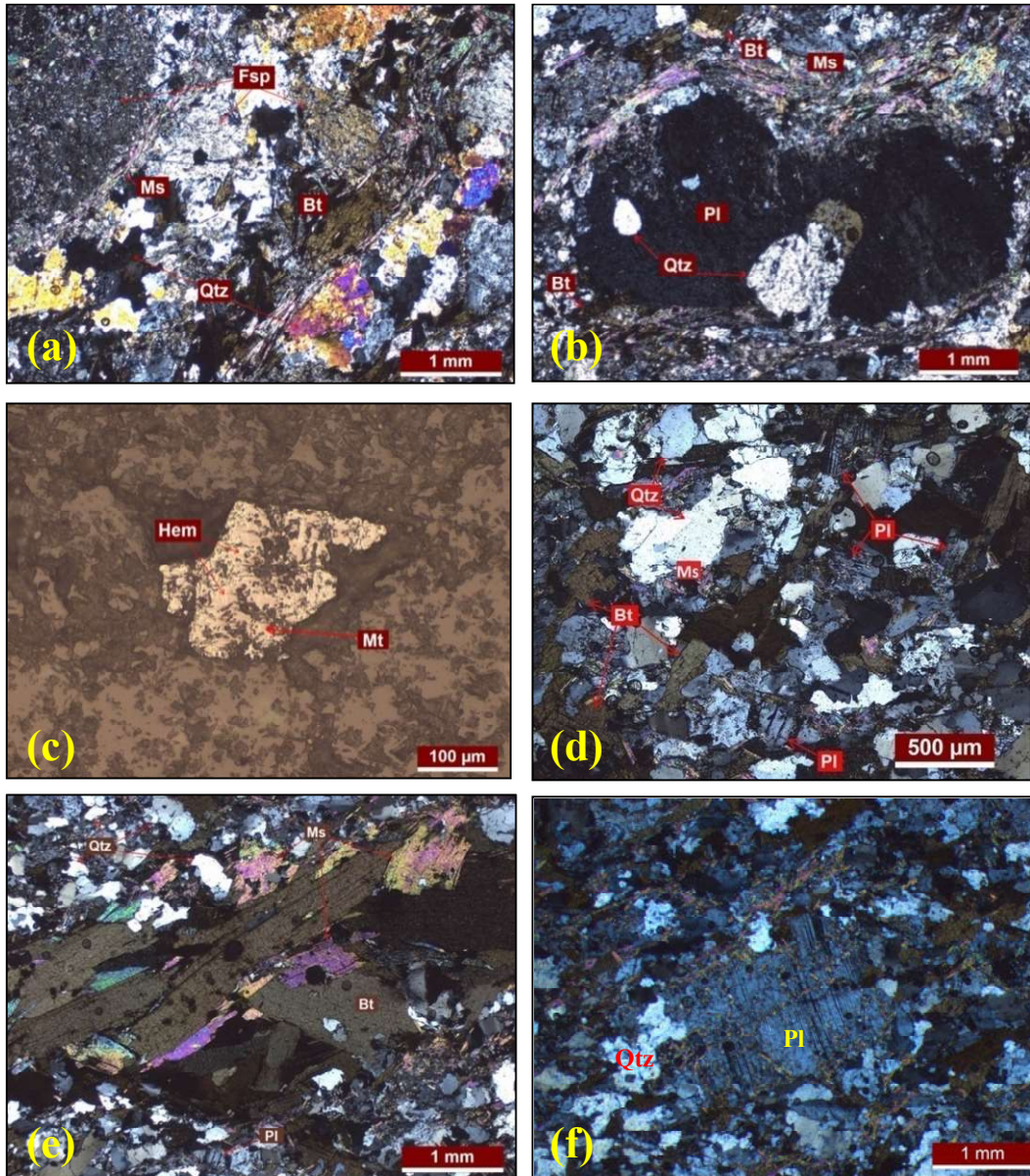


Figure 5.1 (a) Textural view of basement granite-gneiss showing gneissosity defined by alignment of flaky minerals (TL, 2N, MA-216), (b) Warping of muscovite/sericite around phenocryst of plagioclase enclosing quartz grain (TL, 2N, MA-216), (c) Hematitization of magnetite within granite samples (RL, 1N, MA-259), (d) Textural view of xenolith within basement granite (TL, 1N, MA-219), (e) Occasionally larger laths of biotite occur with groundmass of quartz, feldspar, biotite, muscovite/sericite (TL, 2N, MA-219) (f) Sericitization of plagioclase feldspar within xenoliths of basement granite (TL, 2N, MA-218). Bt = biotite, Fsp = feldspar, Hem = hematite, Ms = muscovite, Mt = magnetite, Pl = plagioclase, Qtz = quartz.

5.1.3 Quartz muscovite/sericite schist

The rock is mainly composed of quartz, muscovite/sericite with few opaque minerals. Magnetite grains having brownish gray colour and isotropic nature are observed in some thin sections under reflected light. It is highly foliated defined by highly stretched quartz and alignment of muscovite/sericite. Polycrystalline quartz clasts are common. Shearing is prominent as indicated by presence of S-C fabric. Warping of muscovite/sericite around shear lenses of polycrystalline quartz is dominant (fig. 5.2).

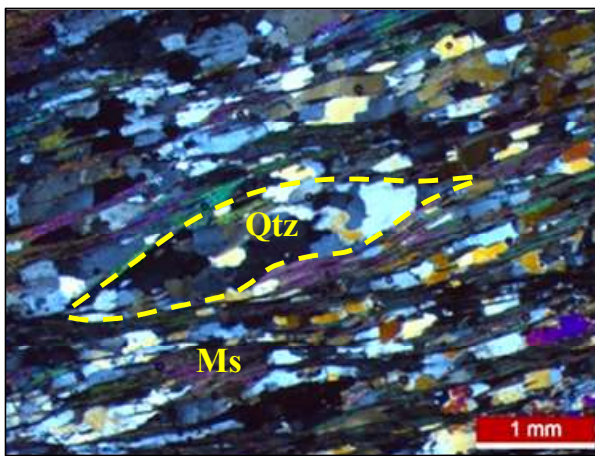


Figure 5.2 Shear lenses of polycrystalline quartz (Qtz) with muscovite (Ms)/sericite warping and few opaque mineral grains (TL, 2N, MA-264).

5.1.4 Quartzite (Serrate Formation)

This is composed of highly stretched quartz with minor flakes of muscovite along the bedding parallel schistosity (fig. 5.3a). Tourmaline and minor zircon grains occur as accessory minerals (fig. 5.3b). Serrated boundaries of quartz with undulose extinction are also observed. These features show high strain conditions and shearing is prominent as evidenced from highly stretched quartz along foliation plane.

5.1.5 Meta-basic rock (Quartz-hornblende schist)

Hornblende and quartz are major minerals within the rock (fig. 5.4a). Quartz is fine grained and present in between larger grains of hornblende which is mostly prismatic in

shape, deep greenish coloured showing preferred orientation. The rock is crudely foliated. Very minor feldspar (<1%) are also observed (fig. 5.4b).

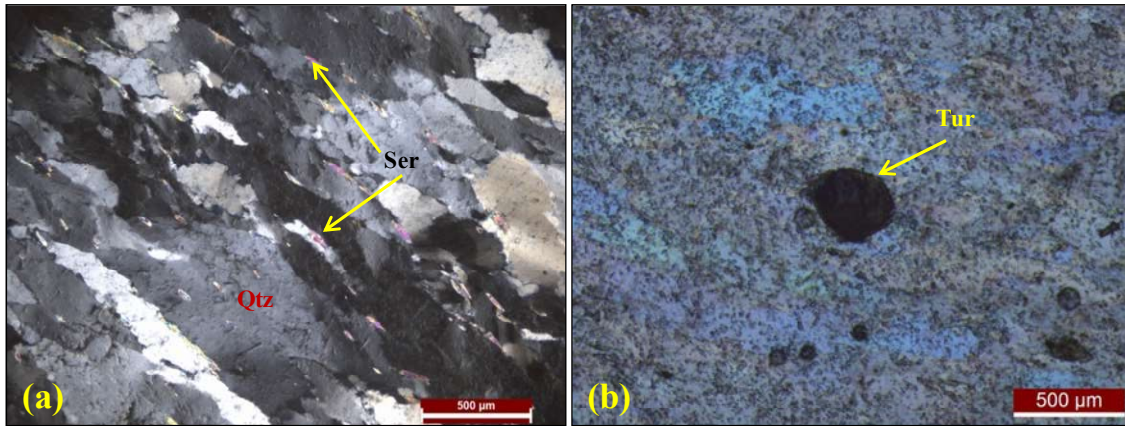


Figure 5.3 (a) Highly stretched quartz (Qtz) clasts with minor flakes of sericite (Ser) aligned parallel to the foliation (TL, 2N, MA-221), (b) Tourmaline (Tur) clast within Serrate quartzite (TL, 2N, MA-221).

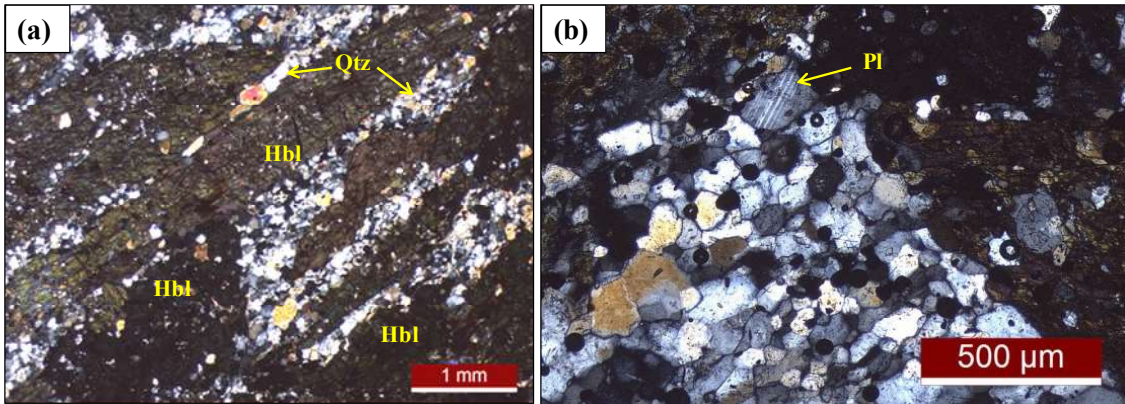


Figure 5.4 (a) Alignment of prismatic hornblende (Hbl) with quartz (Qtz) grains filling the interstices, (b) Very minor plagioclase (Pl) within qtz-hornblende schist.

5.1.6 Quartzite (Tehla Formation)

Quartzite of Tehla Formation shows grain supported, clastic, granulose texture which consist mostly quartz with very minor sericite. Polygonization of quartz clasts are common (fig. 5.5a). Tourmaline (fig. 5.5b) occur as heavy mineral fraction, which has high relief and is greenish coloured, strongly pleochroic in nature. Grain boundary migration (bulging) is also observed within some clasts. Undulose extinction of quartz is prominent. Crude foliation

has been developed. Numerous micro-fractures are observed within quartz. Limonitic material is encountered at locales.

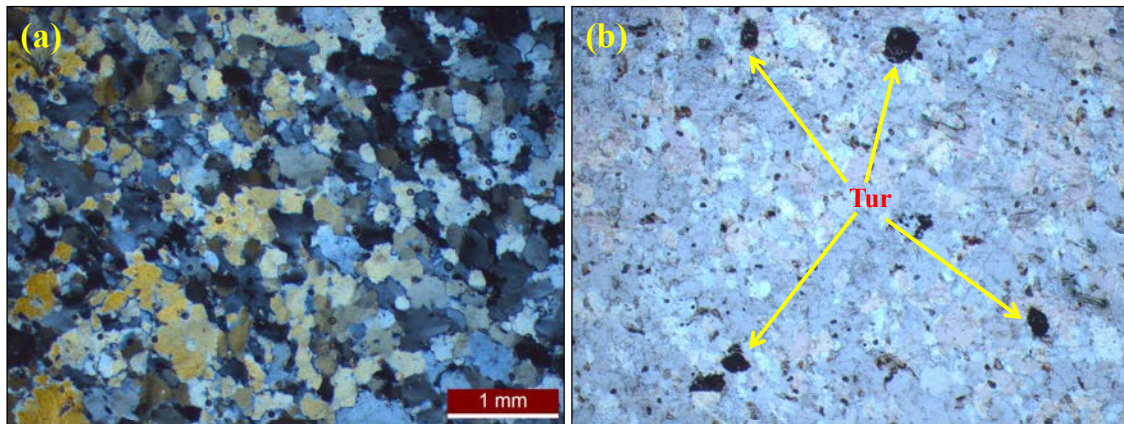


Figure 5.5 (a) Polygonal mosaic of quartz clasts (TL, 2N, MA-269), (b) Tourmaline (Tur) clasts within quartzite of Tehla Formation (TL, 2N, MA-269).

5.1.7 Quartz-biotite-sericite schist

It is primarily composed of quartz, biotite sericite, and magnetite (fig. 5.6a). The rock is very fine grained, well foliated, and the foliation plane is defined by the alignment of flaky minerals. Quartz clasts are highly stretched (elongated) along the foliation plane. Quartz rich layers with polygonal mosaic are also present intermittently (fig. 5.6b). The litho-unit is rich in magnetite. Magnetite occurs as disseminated, medium sized, idiomorphic grains. Highly elongated opaque minerals (ilmenite) are observed. Biotite is present both as aligned along foliation plane as well as in random orientation. Development of shear lenses towards south of Sabraoli are prominent under microscope (fig. 5.6c). Warping of flaky minerals around larger clasts of quartz is also observed (fig. 5.6d).

5.1.8 Gritty Feldspathic Quartzite (Rajgarh Formation)

Under the microscope, quartzite of Rajgarh Formation is coarse grained and shows overall a clast supported texture consisting dominantly of quartz, feldspars (fig. 5.7a). Microcline is the dominant feldspar over plagioclase. Tourmaline occurs as heavy mineral

fraction within the rock. Minor magnetite grains occur as opaque. The rock is sub-arkose type as the feldspar content varies from 5% to 15% within the rock. It is texturally and mineralogically sub-mature, poorly sorted and individual clasts are angular to sub-rounded. Both mono- and polycrystalline quartz are observed. Sericitization of feldspars are common.

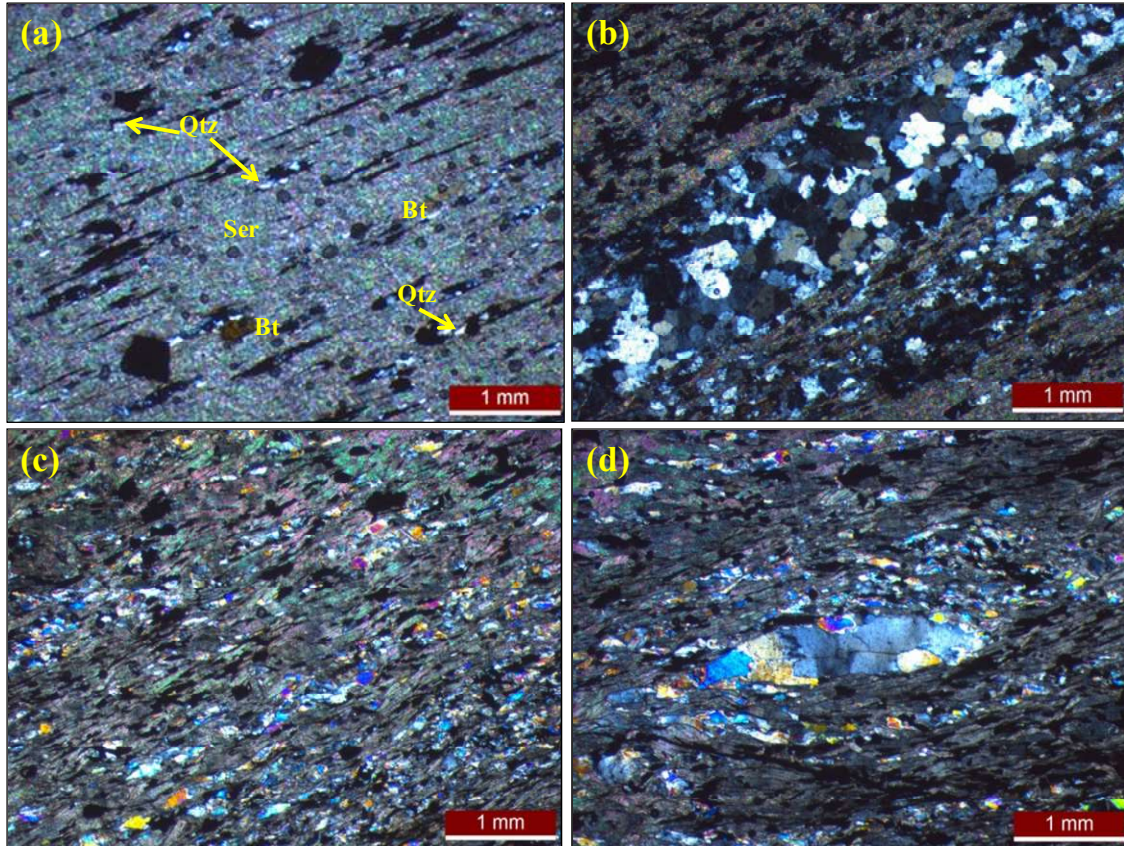


Figure 5.6 (a) Fine grained quartz (Qtz)-biotite (Bt)-sericite (Ser) schist with highly elongated quartz clasts and opaque minerals (TL, 2N, MA-254), (b) Polycrystalline quartz lens with polygonal mosaic of sub-grains (TL, 2N, MA-254), (c) Kinks within qtz-bt-sericite schist with development of shear lenses (TL, 2N, MA-280), (d) Polycrystalline quartz shear lens (TL, 2N, MA-280).

The rock is foliated with stretched quartz aligned along the schistosity plane (fig. 5.7b). Layers of sericite aligned parallel to the foliation plane are also observed. Even some elongated feldspar clasts are observed. Occasionally flakes of muscovite are seen. Serrated boundaries with grain boundary bulging and highly elongated clasts are observed within

samples from central part of the study area near to Sabraoli uranium mineralisation. S-C fabric has been developed with warping of flaky minerals around quartz and feldspar porphyroclasts. These features represent high strain conditions in the area. Quartz clasts show undulose extinction. Sample from southern part of the study area shows higher content of ferruginized material.

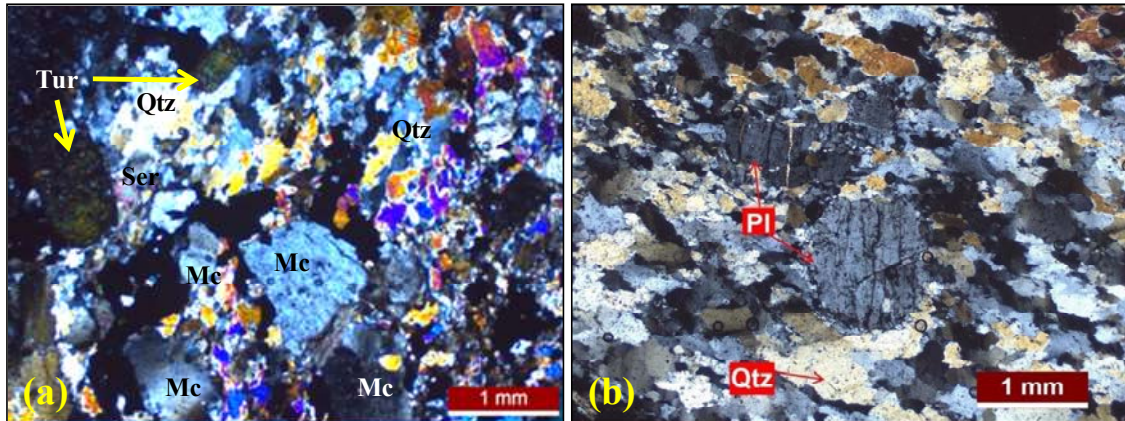


Figure 5.7 (a) Prismatic tourmaline (Tur) clast showing high order interference colour (TL, 2N, MA-273); Mc = microcline, Qtz = quartz, Ser = sericite. Note higher content of feldspars (mostly microcline), (b) Plagioclase (Pl) with stretched quartz (Qtz) clast aligned along the schistosity plane (TL, 2N, MA-223).

5.1.9 Radioactive samples (basal part of Rajgarh Formation)

Radioactivity is primarily confined to the basal part of the gritty quartzite/conglomerate of Rajgarh Formation. However, part of the quartz-biotite-sericite schist underlying the Rajgarh Formation is active at places.

The radioactive gritty quartzite/conglomerate is comprised of quartz, muscovite/sericite, apatite, magnetite, biotite and tourmaline. Under microscope shear fabric (S-C) is prominent which is also observable in megascopic samples. Quartz is the most dominant mineral. Polycrystalline quartz fish/sigmoid/lozenges wrap-around by muscovite is observed (fig. 5.8a). Quartz grains are stretched, elongated and sutured within polycrystalline quartz-fish. Porphyroclasts of quartz, feldspar, and magnetite are observed (fig. 5.8b). Apatite

is important constituent present as granular aggregate in groundmass (fig. 5.8b, c). Grain boundary migration (GBM) and grain boundary bulging (GBL) is prominent within quartz clasts (fig. 5.8d). It indicates dynamic recrystallization of the clasts under metamorphism. Narrow muscovite flakes are preferably oriented along schistosity (S-fabric) and also wrap around quartz-augen (C-plane). Magnetite occurs as disseminated, medium sized, ididioblastic grains. Tourmaline (schorl) is occasionally present as large pre-kinematic fabric.

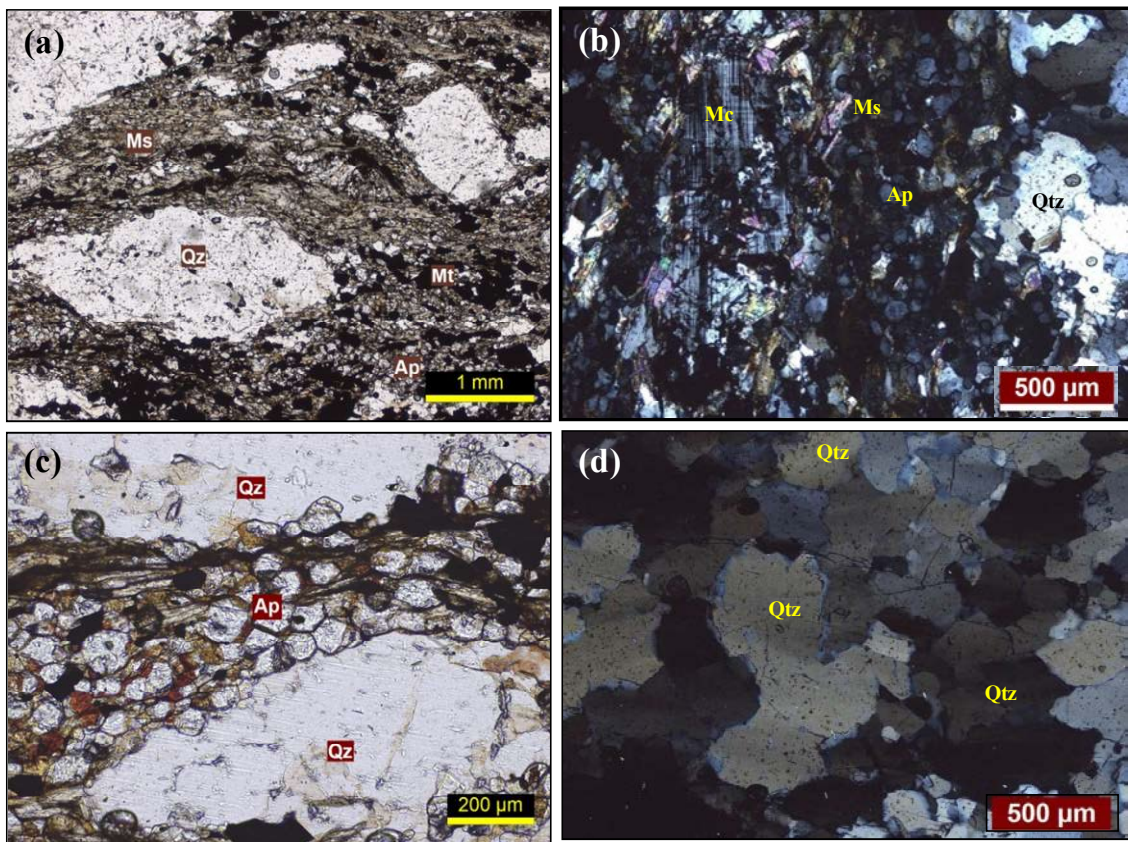


Figure 5.8 (a) Quartz (Qtz) augen wrapped by muscovite (Ms), TL, 1N, (b) Microcline (Mc) clast in the groundmass of quartz (Qtz), apatite (Ap), muscovite (Ms), (c) Granular apatite (Ap) aggregate in groundmass, (d) Grain boundary bulging (GBL)/migration of quartz (Qtz) clasts.

Martitization is very common in magnetite (fig. 5.9a). Hematitization of magnetite are prominent. Hydrated iron oxide/goethite masks intergranular spaces and micro-fractures. A few discrete medium density & occasional high density alpha tracks are recorded on CN-film

which corresponds to hydrated iron oxide/goethitized grains (fig. 5.9b). High density alpha tracks signify presence of some primary radioactive phase but due to iron-masking and fine size, identification is difficult. However, few suspected grains of uranothorite are observed occurring as inclusion within quartz clast and surrounded by chloritic rims indicating marginal alteration (fig. 5.9c). Alignment of medium density alpha tracks corresponding to fine grained mineral phase with iron masking have been observed, which indicate later mobilization due to shearing (fig. 5.9d).

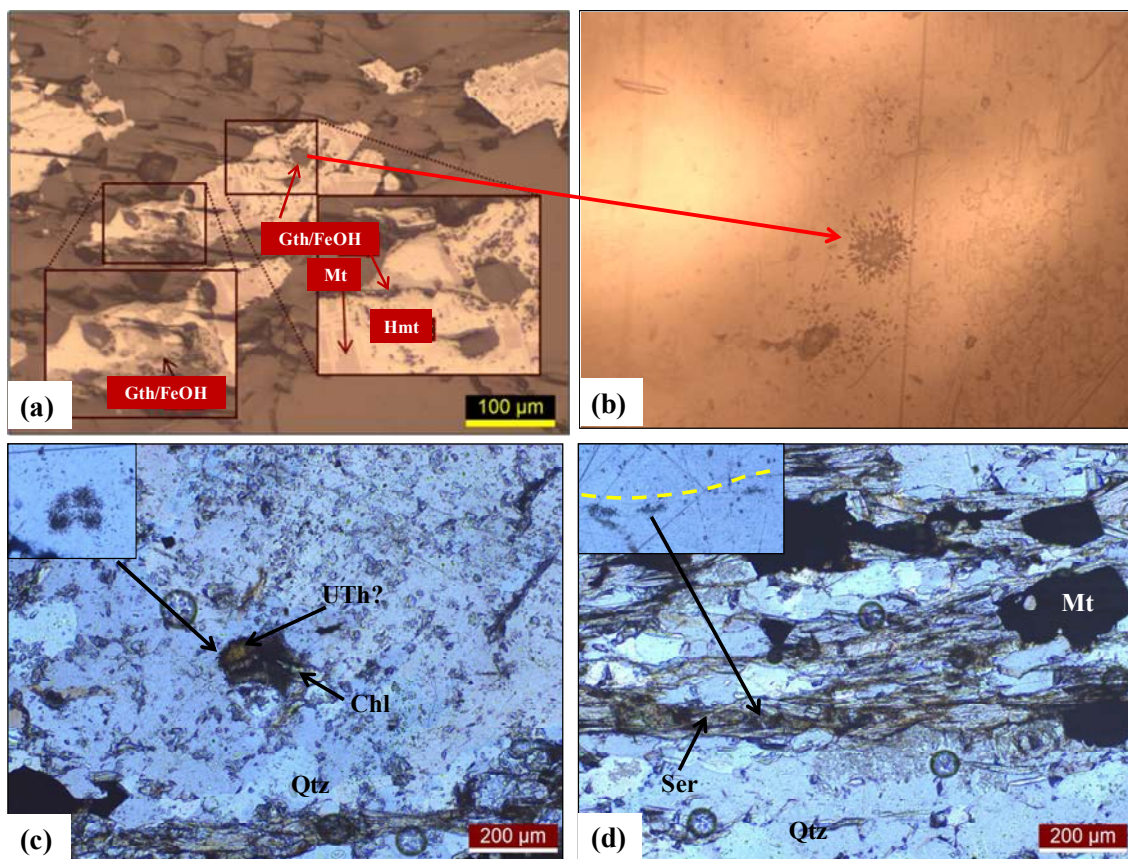


Figure 5.9 (a) Martitised magnetite with hydrated iron oxides/goethite, E-665, (b) High density alpha tracks corresponding to hydrated iron oxide/goethitised patch in fig. 5.8a, (c) Suspected inclusion of uranothorite grain within quartz surrounded by chloritic rims, corresponding alpha track shown inset, (d) Fine grained radioactive phase with iron masking and corresponding alpha track showing alignment. Chl = chlorite, FeOH = hydrated iron oxide, Gth = goethite, Hmt = hematite, Mt = magnetite, Qtz = quartz, Ser = sericite, UTh = uranothorite.

Radioactive quartz-biotite-muscovite/sericite schist is medium grained and has foliated texture (fig. 5.10a). Foliation is pervasive and continuous type. Quartz, biotite, muscovite/sericite are the major constituents. Apatite, epidote and allanite are minor minerals and zircon is in trace quantities. Quartz grains are irregular shaped having serrated grain margins and are surrounded by mica flakes (fig. 5.10b). Polycrystallinity and marginal subgrains on quartz is noted at places. Biotite flakes are medium sized, dark brown (sometimes opaque due to deep colors), and have preferred orientation. Muscovite occurs as oriented bundles of fine flakes around quartz grains. Apatite form medium sized elongated grains, roughly oriented along foliation.

Allanite (REE-epidote) is main radioactive mineral present as fine sized irregularly dispersed grains. Allanite is often mantled by colourless epidote (fig.5.10c). Zircon is also present in trace quantities. Zircon grains are prismatic with sharp terminations and very high length to width ratio (fig.5.10d). Rare presence of uranothorite (?) is observed. The suspected uranothorite is ~0.01mm, cubic form, transparent with brown mask (fig.5.10e), metamict and gives low-medium density alpha tracks on CN-film. Uranothorite is occasionally enclosed within biotite (fig.5.10f).

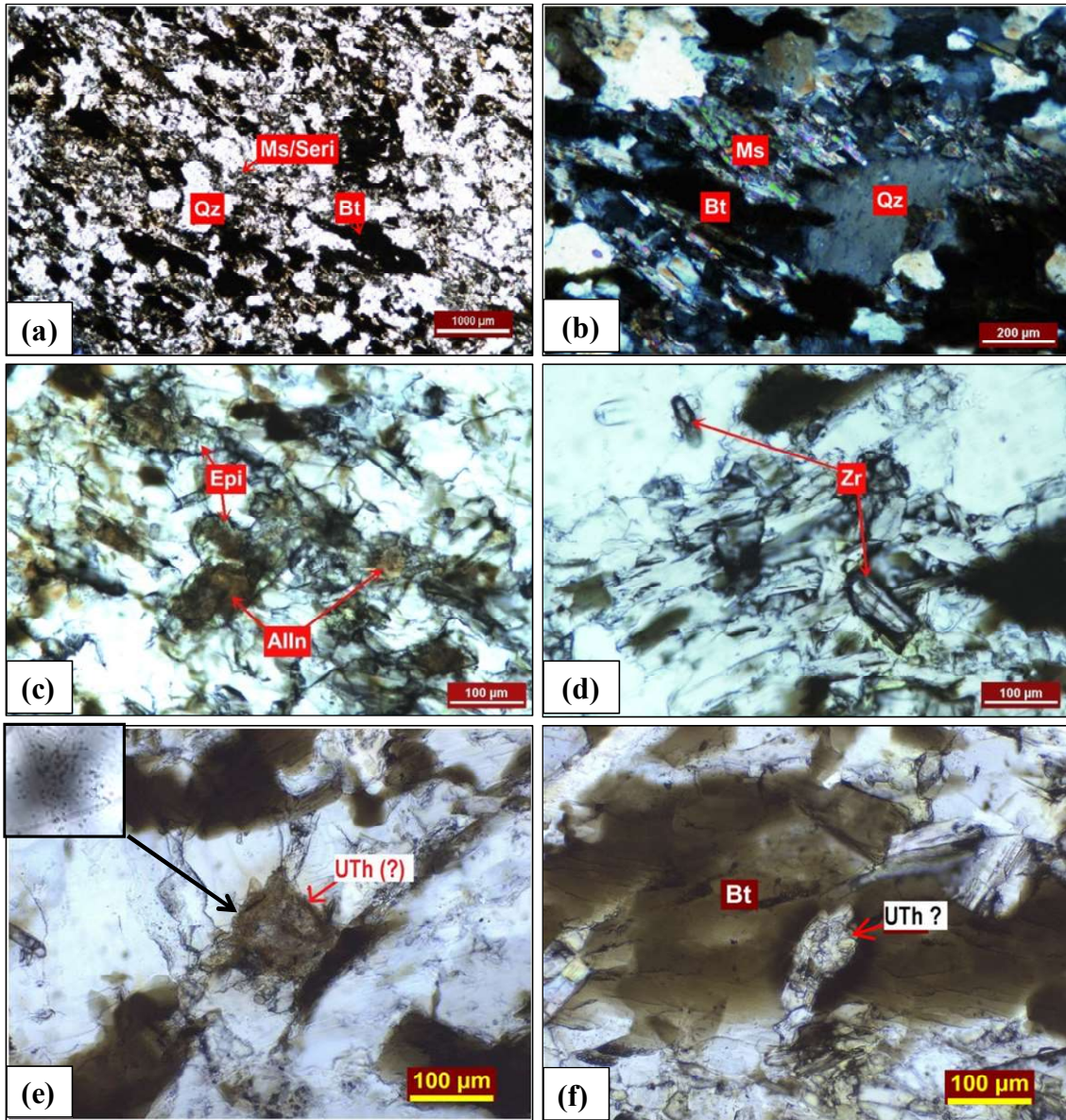


Figure 5.10 (a) General texture of quartz (Qz)-biotite (Bt)-muscovite (Ms)/sericite (Seri) schist (QBMS), (b) Quartz with mica beard in QBMS, (c) Allanite (Alln) grains (brown core) having epidote (Epi) overgrowth (clear rim). (d) Longitudinal zircons (Zr) in QBMS, (e) Suspected cubic grain of uranothorite (Uth) and corresponding alpha tracks shown in inset, QBMS, TL,1N,E-914, (f) Uraniothorite (UTh?) is making strong pleochroic haloes in host biotite, QBMS, TL,1N,E-914.

5.2 XRD Laboratory

During X-Ray Diffraction studies, Metanatroautunite $((\text{NaUO}_2\text{PO}_4)_3\text{H}_2\text{O})$ has been identified as radioactive phase in quartz-biotite-sericite schist (table 5.1). Rutile has been identified within meta-conglomerate of basal Rajgarh Formation.

Besides, hematite and magnetite have been identified as other ore minerals within meta-conglomerate whereas hematite is present within quartz-biotite-sericite schist. Biotite, flourapatite, muscovite and quartz have been identified as rock forming minerals in both quartz-biotite-sericite schist and meta-conglomerate. Presence of magnetite, hematite and other rock forming minerals are also observed under petro-mineralogical studies. Geochemical analysis data also support the presence of these minerals.

Table 5.1 X-ray diffraction analysis of radioactive samples from Sabraoli area, Dausa district, Rajasthan.

Rock type	Sample No.	Atomic Minerals Identified	Ore Minerals Identified	Other Rock Forming Minerals Identified
Quartz-biotite-sericite schist	AA03638	Metanatroautunite (traces) $(\text{NaUO}_2\text{PO}_4)_3\text{H}_2\text{O}$	Hematite	Biotite, Flourapatite, Muscovite and Quartz
Meta-conglomerate	AA03639	-	Hematite and magnetite	Biotite, Flourapatite, Muscovite and Quartz
Meta-conglomerate	AA03640	Rutile	Hematite and magnetite	Biotite, Flourapatite, Muscovite and Quartz

5.3 Radiometric assay of representative rock samples

Physical assay of gritty quartzite/meta-conglomerate occurring at the basal part of the Rajgarh Formation indicates 0.014-0.096 % eU₃O₈, 0.012-0.11% U₃O₈, <0.010% ThO₂, 0.013-0.095% Ra (eU₃O₈) (n=10). One sample of quartz-biotite-sericite schist assayed 0.053 % eU₃O₈, 0.047% U₃O₈, <0.010% ThO₂, 0.051% Ra (eU₃O₈). Besides, one quartzo-feldspathic vein analyzed 0.015% eU₃O₈, 0.015% U₃O₈, <0.010% ThO₂, 0.014% Ra (eU₃O₈) (table 5.2).

Table 5.2 Physical assay results of radioactive samples, Sabraoli area, Dausa district, Rajasthan.

Rock type	Sample No.	eU ₃ O ₈ (%)	U ₃ O ₈ (%)	ThO ₂ (%)	Ra (eU ₃ O ₈) (%)
Gritty quartzite/ Conglomerate	20P/145	0.017	0.012	< 0.010	0.016
	20P/146	0.027	0.027	< 0.010	0.026
	20P/147	0.014	0.015	< 0.010	0.013
	20P/148	0.034	0.034	< 0.010	0.032
	20P/149	0.063	0.066	< 0.010	0.062
	20P/150	0.096	0.11	< 0.010	0.095
	20P/152	0.020	0.021	< 0.010	0.019
	20P/153	0.019	0.015	< 0.010	0.018
	20P/154	0.027	0.021	< 0.010	0.026
	20P/155	0.057	0.064	< 0.010	0.056
Quartz-biotite-sericite schist	20P/151	0.053	0.047	< 0.010	0.051
Quartzo-feldspathic Vein	20P/181	0.015	0.029	<0.010	0.014

Samples of basement granite-gneiss are thoriferous in nature with 28-30 ppm of eU₃O₈, 33-38 ppm of ThO₂, <5 ppm of Ra (eU₃O₈) and 3.8-5 % K (n=5). Two xenolith samples from basement granite-gneiss recorded 22-38 ppm of eU₃O₈, 19-40 ppm of ThO₂, 3-9 ppm of Ra (eU₃O₈) and 4.4-4.7 % K. Quartz sericite schist samples (n=3) from north-western part of Sabraoli area analysed 15-20 ppm of eU₃O₈, <10-17 ppm of ThO₂, <5 ppm of Ra (eU₃O₈) and 3.3-4.4% K. Samples (n=3) of Quartz-amphibole (hornblende) schist (Tehla

Formation) assayed <2-4 ppm of eU₃O₈, <10 ppm of ThO₂, <5 ppm of Ra (eU₃O₈) and <0.5-0.6 % K. Quartzite of Tehla Formation analysed 4-8 ppm of eU₃O₈, 3 to <10 ppm of ThO₂, 4 to <5 ppm of Ra (eU₃O₈) and 0.4-1.3 % K (n=4). The quartz-biotite-sericite schist samples recorded 22-73 ppm of eU₃O₈, 3 to <10 ppm of ThO₂, 10-55 ppm of Ra (eU₃O₈) and 3-7.2 % K. Physical assay of samples from gritty quartzite of Rajgarh Formation indicates 10-23 ppm of eU₃O₈, 6-15 ppm of ThO₂, 3-10 ppm of Ra (eU₃O₈) and 2.5-4.0 % K. One quartzofeldspathic vein analysed 77 ppm of eU₃O₈, <10 ppm of ThO₂, 60 ppm of Ra (eU₃O₈) and 4.7% K (table 5.3).

Table 5.3 Physical assay results of non-radioactive samples, Sabraoli area, Dausa district, Rajasthan.

Rock type	Sample No.	eU ₃ O ₈ (ppm)	ThO ₂ (ppm)	Ra (eU ₃ O ₈) (ppm)	K (%)
Granite	20P/99	30	34	<5	4.8
	20P/100	28	33	<5	4.4
	20P/101	30	35	<5	4.5
	20P/119	30	38	<5	4.4
	20P/120	30	34	<5	5
Xenolith	20P/103	24	25	<5	3.8
	20P/104	24	28	<5	3.1
	20P/117	28	32	<5	4
	20P/179	22	19	3	4.4
	20P/180	38	40	9	4.7
Qtz-sericite schist	20P/105	22	23	<5	2.9
	20P/160	15	<10	<5	4.4
	20P/161	20	17	<5	3.3
	20P/162	20	17	<5	3.4
Serrate quartzite	20P/110	<5	---	---	---
	20P/111	<5	---	---	---
	20P/184	3	<10	<5	<0.5
	20P/185	4	<10	<5	<0.5
Qtz-amphibole schist	20P/112	<5	---	---	---
	20P/163	4	<10	<5	0.6
	20P/164	<2	<10	<5	<0.5
	20P/165	<2	<10	<5	<0.5
Quartzite (Tehla)	20P/175	8	3	4	1.3
	20P/176	5	<10	<5	0.6
	20P/177	5	1	4	0.4
	20P/178	4	<10	<5	<0.5

Qtz-biotite-sericite schist	20P/113	43	<10	25	6.6
	20P/114	43	<10	24	6.6
	20P/115	36	<10	17	6.7
	20P/116	47	<10	29	6.2
	20P/166	38	<10	19	7.2
	20P/167	30	<10	11	7.1
	20P/168	73	<10	55	6.5
	20P/169	39	3	23	6.5
	20P/170	22	<10	10	3
Gritty quartzite (Rajgarh)	20P/102	25	12	9	2.5
	20P/106	16	11	<5	3.6
	20P/107	16	<10	<5	3.5
	20P/108	13	10	<5	2.5
	20P/109	10	<10	<5	1.5
	20P/171	10	<10	<5	2.6
	20P/172	20	6	10	3.1
	20P/173	14	9	3	3
	20P/174	23	15	6	4.0
	20P/183	14	<10	5	2.5
Quartzo-feldspathic vein	20P/182	77	<10	60	4.7

5.4 Geochemistry

5.4.1 Major oxides of basement granite

Geochemical analysis (table 5.4) of basement granite gneiss (n=10) from the southern part of the study area shows SiO₂ from 69.32% to 71.87% (av. 70.35%), TiO₂ from 0.33% to 0.52% (av. 0.42%), Al₂O₃ from 14.67% to 15.34% (av. 15.02%), Fe₂O₃ from 3.12% to 4.04% (av. 3.57%), MgO from 0.81% to 1.56% (av. 1.14%), MnO from 0.04% to 0.06% (av. 0.04%), CaO from 1.16% to 1.78% (1.51%), Na₂O from 1.48% to 3.08% (av. 2.36%), K₂O from 4.58% to 5.81% (av. 5.13%), P₂O₅ from 0.19% to 0.47% (av. 0.27%).

In the normative QAP classification diagram (fig.5.11a), all samples plot in the monzogranite field. On the other hand, on the total alkali silica (TAS diagram), all the samples plot in the granite field (fig.5.11b). The samples define a typical calc-alkaline trend on the AFM diagram (fig.5.11c). The granite gneisses have alumina saturation index from

1.61 to 1.75 (n=10) with an average of 1.67, indicating that they are essentially peraluminous type (fig.5.11d). According to the classification of Frost et al. (2001), all samples belong to the magnesian granite except sample XA-8384 which plot in the ferroan granite on Fe^* $[FeO^t / (FeO^t + MgO)]$ vs. SiO_2 diagram (fig.5.11e), whereas on the MALI-index diagram, the samples plot near to the boundary between alkali-calcic to cal-alkalic fields.

The relationship of major elements with SiO_2 is shown in Harker diagram (fig. 5.12). The overall pattern of decreasing Fe_2O_3 (t), MgO , CaO with increasing SiO_2 is characteristic of fractionating granitic systems. The distribution of Al_2O_3 shows a slightly negative trend. The variation of MnO , K_2O remains almost constant with respect to SiO_2 . The TiO_2 content first shows slightly decreasing trend and then slightly increasing trend with increasing amount of SiO_2 . The variation of Na_2O however, is independent of the SiO_2 .

5.4.2 Trace elements and rare earth elements of basement granite

The basement granite gneiss contain higher Rb content ranging from 218ppm to 313ppm (avg. 252ppm), Sr from 88ppm to 145ppm (avg. 116ppm), highly variable Ba from 365ppm to 1540ppm (avg. 767ppm), Zr from 124ppm to 190ppm (avg. 156ppm), low V from 24ppm to 43 ppm (avg. 33ppm), Co from 8ppm to 15ppm (avg. 11ppm), Ni from 10ppm to 21ppm (avg. 15ppm), Cu from 11ppm to 28ppm (avg. 20ppm), Zn from 13ppm to 33ppm (avg. 23ppm), Ga from 18ppm to 22ppm (avg. 20ppm), Y from 17ppm to 71ppm (avg. 41ppm), Nb from 11ppm to 44ppm (avg. 19ppm), Pb from 11ppm to 49 ppm (avg. 33ppm).

The variations of trace elements with reference to SiO_2 are shown in fig. 5.13 with Rb, Sr, Ba, and Zn show little positive correlation with SiO_2 . V, Ni, Cu, Zr, Y generally decrease with increasing SiO_2 . Pb shows little or no correlation with increasing silica.

REE plots (fig.5.14) show a depleted HREE compared to LREE because LREEs are more incompatible so left behind in the liquid phase. The negative Eu anomaly indicates that

that the liquid was at one time in equilibrium with now-absent plagioclase. The Eu^{2+} replaced some of the Ca^{2+} in the plagioclase structure and got separated from the liquid. The remaining liquid is thus depleted in Eu. This means that significant quantity of plagioclase feldspars have been removed from the system. The removal of plagioclase is also indicated by decreasing Al_2O_3 with increasing SiO_2 .

5.4.3 Major oxides of xenoliths within basement granite

Xenoliths within the basement granite (table 5.5) are characterized by bimodal distribution of geochemical data. One set of samples (n=3) contains moderate SiO_2 from 59.47% to 61.25% (av. 60.39%), low TiO_2 from 0.80% to 1.16% (av. 1.03%), high Al_2O_3 from 14.84% to 15.80% (av. 15.26%), high Fe_2O_3 from 7.69% to 10.64% (av. 9.45%), MgO from 2.88% to 3.68% (av. 3.20%), MnO from 0.08% to 0.14% (av. 0.11%), CaO from 0.85% to 2.32% (1.69%), Na_2O from 1.01% to 2.97% (av. 2.25%), K_2O from 4.96% to 6.70% (av. 5.62%), P_2O_5 from 0.21% to 0.34% (av. 0.29%).

Another set of samples (n=4) contain high SiO_2 from 91.55% to 95.25% (av. 93.63%), low TiO_2 of 0.03%, moderate Al_2O_3 from 2.34% to 4.79% (av.3.55%), low Fe_2O_3 from 0.31% to 0.50% (av. 0.37%), MgO from 0.08% to 0.12% (av. 0.10%), low MnO , CaO from 0.04% to 0.19% (avg. 0.12%), Na_2O from 0.49% to 2.07% (av. 1.08%), K_2O from 0.01% to 1.18% (av. 1.12%), P_2O_5 from 0.01% to 0.04%.

Table 5.4 Major oxides (wt %) and trace elements (ppm) of basement granite-gneiss from southern part of the study area.

Sample No.	XA-5384	XA-5385	XA-5386	XA-5387	XA-5388	XA-5389	XA-5390	XA-5391	XA-5392	XA-5393	Min	Max	Avg.	Std.
SiO₂	70.66	70.77	70.01	70.25	70.11	71.87	69.75	70.87	69.84	69.32	69.32	71.87	70.34	0.72
TiO₂	0.4	0.46	0.36	0.52	0.33	0.44	0.46	0.42	0.45	0.38	0.33	0.52	0.42	0.06
Al₂O₃	14.9	15.17	14.67	15.34	15.02	14.75	15.14	14.7	15.27	15.21	14.67	15.34	15.02	0.25
Fe₂O₃	3.75	3.17	4.04	3.26	3.67	3.12	3.79	3.4	3.67	3.86	3.12	4.04	3.57	0.32
MgO	0.81	1.07	1.14	1.28	1.1	0.97	1.21	1.01	1.27	1.56	0.81	1.56	1.14	0.21
MnO	0.04	0.06	0.05	0.04	0.05	0.04	0.04	0.04	0.04	0.04	0.04	0.06	0.04	0.01
CaO	1.2	1.36	1.65	1.54	1.77	1.16	1.55	1.6	1.48	1.78	1.16	1.78	1.51	0.21
Na₂O	3.08	2.3	2.71	2	2.44	1.48	2.05	2.61	2.46	2.45	1.48	3.08	2.36	0.44
K₂O	4.58	5.21	4.74	5.32	5.06	5.81	5.55	4.91	5.12	5.01	4.58	5.81	5.13	0.37
P₂O₅	0.32	0.21	0.47	0.24	0.27	0.19	0.26	0.25	0.23	0.23	0.19	0.47	0.27	0.08
A/NK	1.95	2.02	1.97	2.1	2	2.02	1.99	1.95	2.01	2.04	1.95	2.04	2.01	0.04
A/CNK	1.68	1.71	1.61	1.73	1.62	1.75	1.65	1.61	1.69	1.65	1.61	1.75	1.67	0.05
V	35	38	27	33	40	24	30	25	34	43	24	43	32.9	6.40
Co	9	11	15	12	11	8	10	11	14	12	8	15	11.3	2.11
Ni	11	19	17	14	21	10	15	18	16	17	10	21	15.8	3.43
Cu	18	22	15	20	19	11	28	19	27	21	11	28	20	5.06
Zn	23	13	25	18	28	21	20	26	22	33	13	33	22.9	5.55
Ga	19	21	18	22	21	18	21	18	22	22	18	22	20.2	1.75
Rb	227	285	313	260	219	246	251	271	218	232	218	313	252.2	30.81
Sr	145	128	95	126	111	104	125	120	88	117	88	145	115.9	16.92
Y	48	35	50	64	47	28	17	21	71	29	17	71	41	18.01
Zr	125	177	148	185	165	124	146	190	140	164	124	190	156.4	23.54
Nb	11	19	44	21	15	17	13	23	16	19	11	44	19.8	9.24
Ba	1540	946	365	789	690	647	755	643	738	559	365	1540	767.2	311.20
Pb	43	25	11	49	32	44	47	41	13	30	11	49	33.5	13.71

Normative Minerals

	XA-5384	XA-5385	XA-5386	XA-5387	XA-5388	XA-5389	XA-5390	XA-5391	XA-5392	XA-5393	Min.	Max.	Avg.
Quartz	32.35	33.54	32.20	33.73	31.89	37.64	32.20	32.68	31.53	30.41	40.03	26.91	32.82
Corundum	3.46	3.78	3.21	4.07	2.96	4.37	3.56	2.78	3.54	3.07	5.62	1.87	3.48
Orthoclase	27.07	30.79	28.01	31.44	29.90	34.34	32.80	29.02	30.26	29.61	27.07	34.34	30.32
Albite	26.06	19.46	22.93	16.92	20.65	12.52	17.35	22.09	20.82	20.73	12.52	26.06	19.95
Anorthite	3.86	5.38	5.12	6.07	7.02	4.51	5.99	6.31	5.84	7.33	4.51	5.76	5.74
Hypersthene	2.02	2.67	2.84	3.19	2.74	2.42	3.01	2.52	3.16	3.89	2.02	3.89	2.84
Ilmenite	0.09	0.13	0.11	0.09	0.11	0.09	0.09	0.09	0.09	0.09	0.09	0.13	0.09
Hematite	3.75	3.17	4.04	3.26	3.67	3.12	3.79	3.40	3.67	3.86	3.12	4.04	3.57
Rutile	0.36	0.39	0.30	0.48	0.27	0.40	0.42	0.38	0.41	0.34	0.28	0.45	0.37
Apatite	0.76	0.50	1.11	0.57	0.64	0.45	0.62	0.59	0.55	0.55	0.45	1.11	0.63

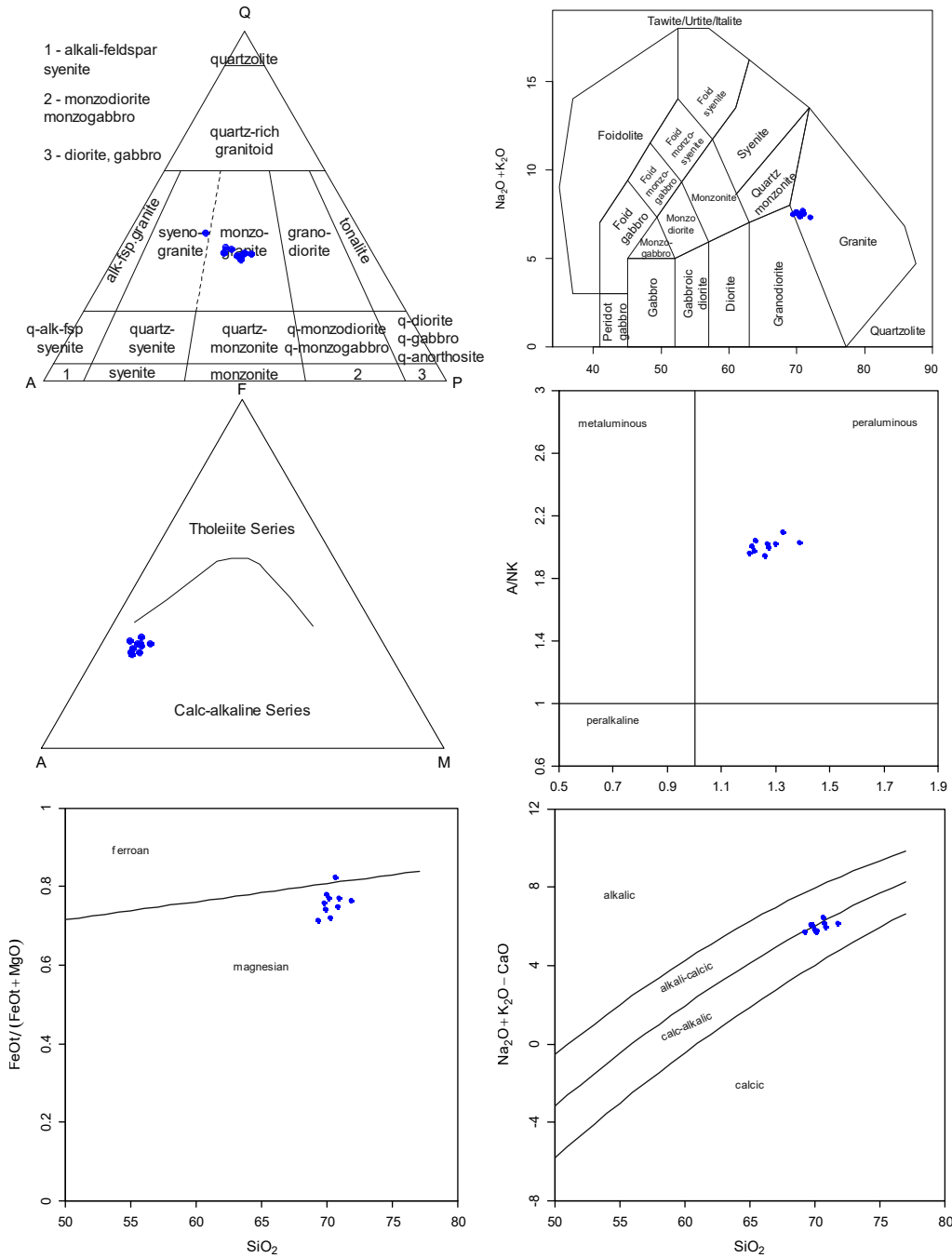


Figure 5.11 (a) Q-A-P normative plot after Le Maitre et al. (2002) and (b) TAS diagram (Middlemost, 1994) showing granitic composition for the samples, (c) AFM diagram showing calc-alkaline trend of the samples (d) A/CNK [Alumina Saturation Index, ASI, molar $\text{Al}_2\text{O}_3/(\text{CaO}+\text{Na}_2\text{O}+\text{K}_2\text{O})$] vs. A/NK [molar $\text{Al}_2\text{O}_3/(\text{Na}_2\text{O}+\text{K}_2\text{O})$] (e) Fe^* [$\text{FeO}^t/(\text{FeO}^t + \text{MgO})$] vs. SiO_2 , and (f) MALI-index ($\text{Na}_2\text{O}+\text{K}_2\text{O}-\text{CaO}$) vs. SiO_2 diagrams after Frost et al. (2001).

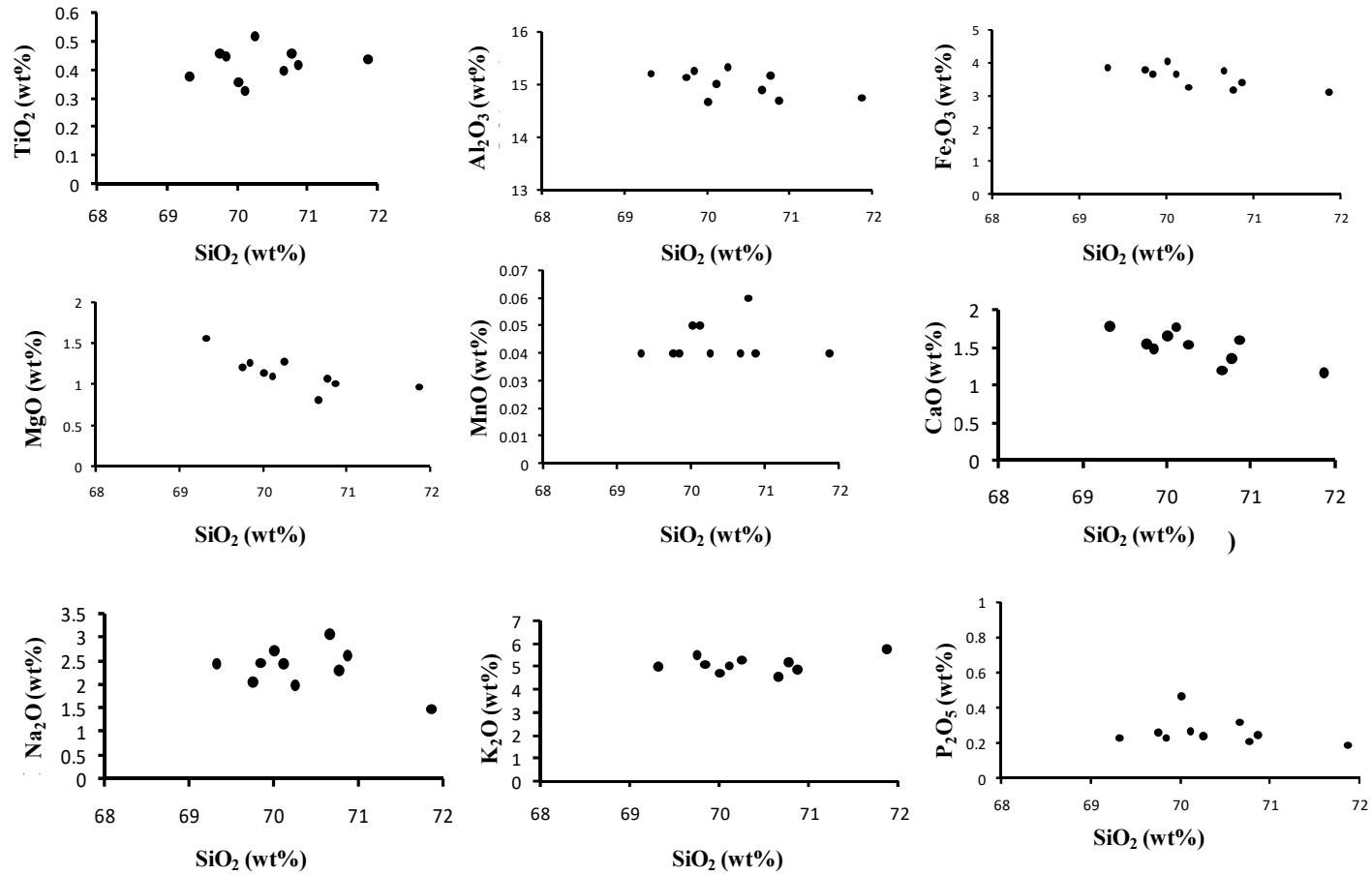


Figure 5.12 Harker's variation diagram (Harker, 1909) of SiO_2 vs. major oxides for the granite from southern part of study area.

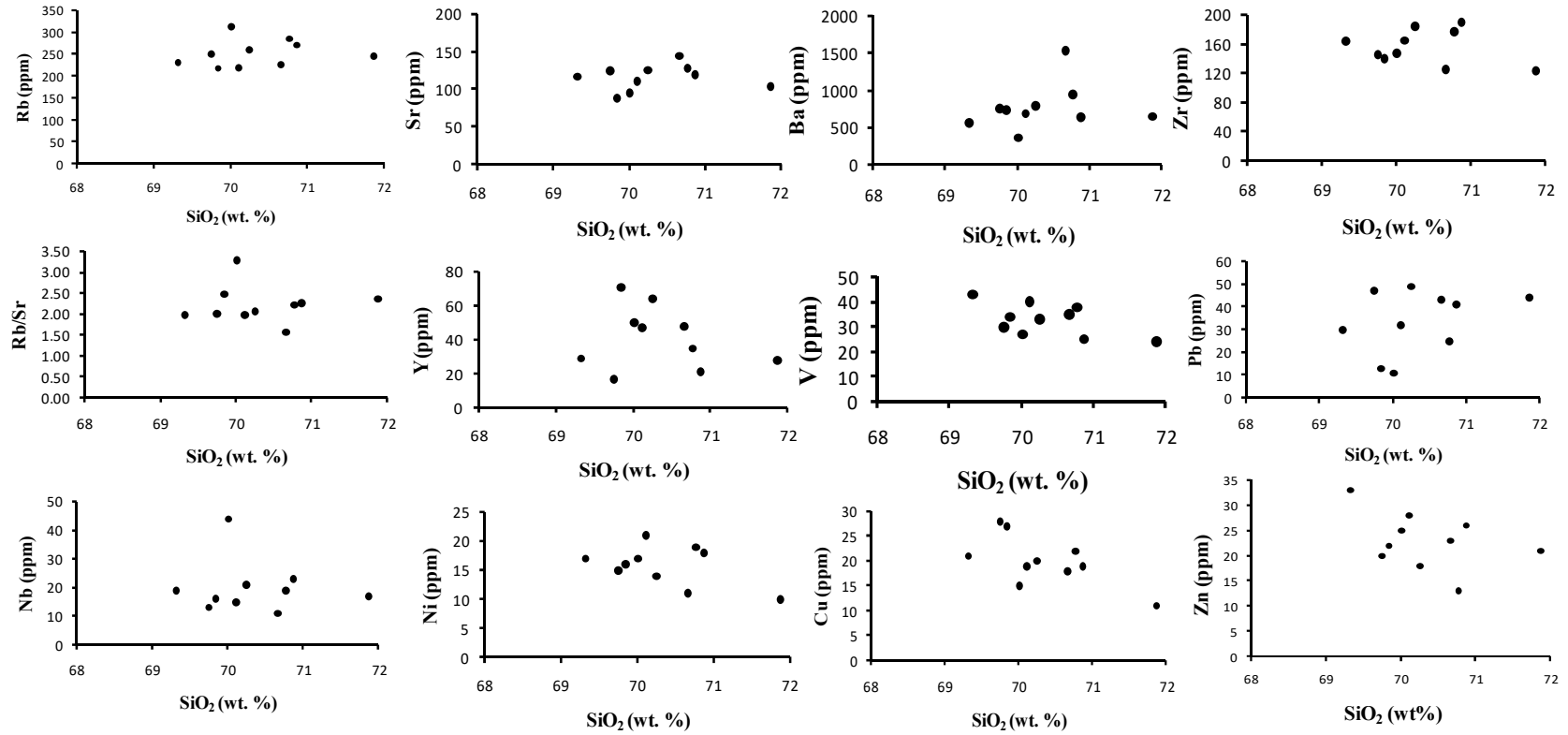


Figure 5.13 Harker's variation diagram (Harker, 1909) of SiO₂ vs. trace elements for the granite from southern part of study area.

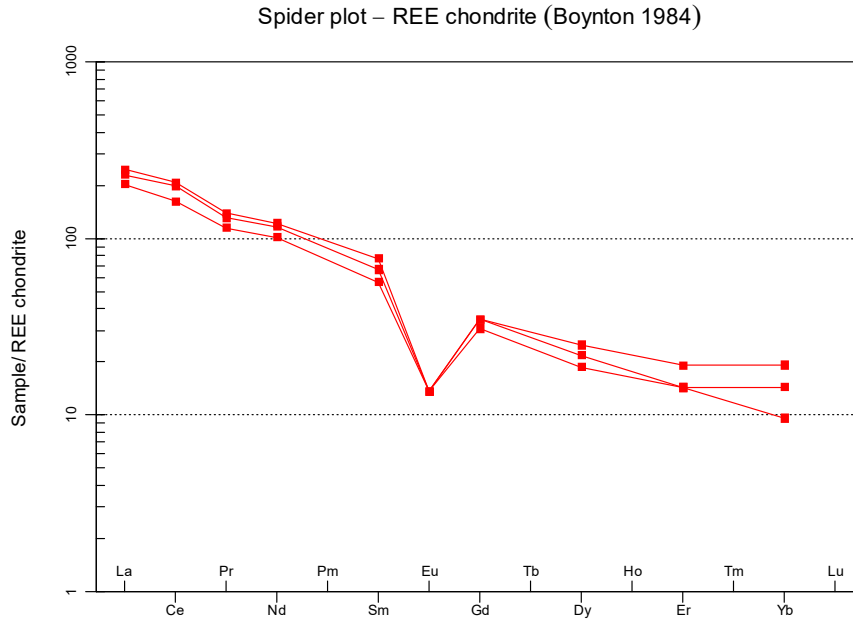


Figure 5.14 Chondrite-Normalized REE pattern (Boynton, 1984) of basement granite gneiss (n=3).

5.4.4 Trace elements and rare earth elements of xenoliths within basement granite

The first set of samples (n=3, table-5.5) contain higher content of Rb (241-315ppm, 275.67ppm), Ba (384-706ppm, avg. 507.67ppm), Cr from 83 to 102ppm (n=2), Zn (61-107ppm, avg. 89.33ppm), low Ni (<10-23ppm, avg. 21ppm), Cu from <10ppm to 114ppm (65ppm), V 125ppm (n=1), Ga (16-21ppm, avg. 19.33ppm), low to moderate Sr (<10-70ppm, avg. 58.50ppm), low Nb (<10 to 18ppm), low Pb (<10 to 16ppm), low Co (24ppm, n=1).

The second set of samples (n=4, table-5.5) contain low V (<5ppm), Co (<5), Moderate Cr (126-140ppm, avg. 133ppm, n=2), low Ni (8-20ppm, avg. 14.25ppm, n=4), Cu (5-22ppm, avg. 13.25), Zn (5-31ppm, 17.75ppm), Ga (7-28ppm, 17.25ppm), Rb (<10-42ppm), Sr (15-66ppm, avg. 35ppm), Y (<5-46ppm), Zr (12-109ppm, 53.75ppm), Nb (<5-63ppm), Ba (<25-27ppm), Pb (<5ppm) except for sample no. XA-5069 (110ppm) and XA-

5070 (146ppm). REE data (n=4) shows depleted HREE as compared to the LREE within the xenoliths (table 5.13).

Table 5.5 Major oxides (wt %) and trace elements (ppm) of xenoliths within basement granite.

Sample No.	XA5067	XA5068	XA5073	Avg.	XA5069	XA5070	XA5071	XA5072	Avg.
SiO ₂	60.44	59.47	61.25	60.39	92.62	91.55	95.25	95.11	93.63
TiO ₂	0.80	1.16	1.12	1.03	0.03	0.03	0.03	0.03	0.03
Al ₂ O ₃	15.80	14.84	15.13	15.26	4.57	4.79	2.48	2.34	3.55
Fe ₂ O ₃	7.69	10.01	10.64	9.45	0.36	0.32	0.31	0.5	0.37
MgO	3.68	2.88	3.04	3.20	0.08	0.08	0.11	0.12	0.10
MnO	0.14	0.08	0.1	0.11	<0.01	<0.01	<0.01	0.01	0.01
CaO	0.85	2.32	1.9	1.69	0.04	0.05	0.19	0.18	0.12
Na ₂ O	2.78	2.97	1.01	2.25	1.21	2.07	0.55	0.49	1.08
K ₂ O	6.70	4.96	5.19	5.62	<0.01	<0.01	1.06	1.18	1.12
P ₂ O ₅	0.31	0.34	0.21	0.29	0.03	0.04	<0.01	<0.01	0.035
V	-	-	125	125.00	-	-	<5	5	5.00
Co	-	-	24	24.00	-	-	<5	<5	-
Cr	102	83	-	92.50	140	126	-	-	133.00
Ni	23	<10	19	21.00	20	20	8	9	14.25
Cu	16	<10	114	65.00	21	22	5	5	13.25
Zn	61	100	107	89.33	29	31	5	6	17.75
Ga	21	21	16	19.33	27	28	7	7	17.25
Rb	315	241	271	275.67	<10	23	39	42	34.67
Sr	<10	70	47	58.50	41	66	15	18	35.00
Y	<10	<10	32	32.00	<10	46	<5	<5	46.00
Zr	91	97	142	110.00	79	109	15	12	53.75
Nb	<10	<10	18	18.00	37	63	<5	<5	50.00
Ba	706	433	384	507.67	27	27	<25	<25	27.00
Pb	<10	<10	16	16.00	110	146	<5	<5	128.00

5.4.5 Major oxides of quartz-muscovite/sericite schist

Geochemical analysis (table 5.6) of quartz-muscovite/sericite schist shows moderate SiO₂ from 64.42% to 68.61% (avg. 67.29%), low TiO₂ from 0.08% to 0.78% (avg. 0.30%), high Al₂O₃ from 16.61% to 21.93% (avg. 19.99%), moderate to high Fe₂O₃ from 2.09% to 7.85% (avg. 4.09%), low MgO from 0.30% to 2.28% (avg. 0.97%), low MnO from 0.01% to 0.08% (avg. 0.03%), low CaO from 0.09% to 0.96% (avg. 0.33%), moderate Na₂O from

1.36% to 2.6% (2.07%), high K₂O from 4.03% to 5.84% (avg. 4.71%), low P₂O₅ from 0.02% to 0.15% (avg. 0.06%).

5.4.6. Trace elements and rare earth elements of quartz-muscovite/sericite schist

The quartz-muscovite/sericite schist exhibit low V (9-82ppm), Co (<5-21 ppm), moderate Cr (145ppm), low Ni (6-34ppm), low Cu (8-42ppm), low Zn (9-77ppm), low Ga (18-28ppm), variable content of Rb (149-233ppm), low Sr (<10-75ppm), low Y (16-30ppm), highly variable Zr (28-174ppm), low Nb (9-17ppm), variable content of Ba (190-416ppm), low Pb (<5-18ppm).

5.4.7 Major oxides of quartzite (Serrate Formation)

The quartzites of Serrate Formation (n=8) are characterized by high and narrow range of SiO₂ (86.84-95.57%), dominantly low TiO₂ (0.01-0.07%), Al₂O₃ (2.47-8.06%), Fe₂O₃ (t), MgO (0.08-0.45%), MnO (0.01%), CaO (0.03-0.21%), Na₂O (0.20-1.77%), K₂O (0.10-1.34%), P₂O₅ (<0.01-0.14%). The samples are characterized by high SiO₂/Al₂O₃ (10.77-38.55), variable Na₂O/K₂O (0.26-17.70) (table 5.7).

In the geochemical classification diagram proposed by Pettijohn et al. (1987), quartzite samples of Serrate Formation plotted in the fields of sub-litharenite and litharenite (fig.5.15).

5.4.8 Trace elements and rare earth elements of quartzite (Serrate Formation)

The quartzites of Serrate Formation area deficient in most of the trace elements (n=8). They contain V from 5 to 8ppm, Co from <5 to 6ppm, moderate Cr from 147 to 174ppm, Ni from 5 to 21ppm, Cu from 7 to 23ppm, Zn from 5 to 29ppm, Ga from 6 to 29ppm, low Rb from 22 to 95ppm, Sr from 6 to 85ppm, Y from <5 to 85 ppm, Zr from 5 to 115ppm, Nb from <5 to 83ppm, highly variable Ba from <25 to 218ppm, Pb from <5 to 164ppm (table 5.7).

They are also depleted in most of the REE elements (n=2) except for low abundance of La (12-66ppm), Ce (24-114) (table 5.13).

Table 5.6 Major oxides (wt%) and trace elements (ppm) of quartz-muscovite/sericite schist.

Sample No.	XA5102	XA5264	XA5491	XA5492	XA5493	Min.	Max.	Avg.
SiO₂	67.45	64.42	67.7	68.61	68.28	64.42	68.61	67.29
TiO₂	0.36	0.78	0.08	0.16	0.1	0.08	0.78	0.30
Al₂O₃	19.01	16.61	21.67	20.71	21.93	16.61	21.93	19.99
Fe₂O₃	4.19	7.85	3.29	3.05	2.09	2.09	7.85	4.09
MgO	1.47	2.28	0.3	0.5	0.32	0.30	2.28	0.97
MnO	0.01	0.08	<0.01	0.01	<0.01	0.01	0.08	0.03
CaO	0.09	0.96	0.19	0.19	0.24	0.09	0.96	0.33
Na₂O	1.36	1.44	2.56	2.61	2.37	1.36	2.61	2.07
K₂O	5.84	5.03	4.1	4.03	4.56	4.03	5.84	4.71
P₂O₅	0.07	0.15	0.03	0.02	0.02	0.02	0.15	0.06
V		82	9	30	22	9.00	82.00	35.75
Co		21	<5	<5	<5	<5	21.00	-
Cr	145					145.00	145.00	145.00
Ni	13	34	6	8	10	6.00	34.00	14.20
Cu	42	27	8	9	13	8.00	42.00	19.80
Zn	37	77	12	9	10	9.00	77.00	29.00
Ga	28	18	27	25	28	18.00	28.00	25.20
Rb	197	233	149	172	165	149.00	233.00	183.20
Sr	<10	36	75	21	38	21.00	75.00	42.50
Y	25	28	16	30	17	16.00	30.00	23.20
Zr	115	174	28	109	39	28.00	174.00	93.00
Nb	16	17	9	11	12	9.00	17.00	13.00
Ba	366	416	190	258	214	190.00	416.00	288.80
Pb	18	12	<5	<5	<5	<5	18.00	-

Table 5.7 Major oxides (wt %) and trace elements (ppm) of quartzite (Serrate Formation).

Sample No.	XA5075	XA5079	XA5080	XA5081	XA5082	XA5084	XA5085	XA5494	Min	Max	Avg.
SiO ₂	86.84	95.46	95.57	95.21	95.09	89.15	90.64	92.8	86.84	95.57	92.60
TiO ₂	0.07	0.02	0.02	0.03	0.01	0.04	0.03	0.05	0.01	0.07	0.03
Al ₂ O ₃	8.06	2.75	2.58	2.47	2.8	5.54	5.53	3.83	2.47	8.06	4.20
Fe ₂ O ₃	1.33	1.03	0.89	0.95	0.85	0.45	0.50	1.61	0.45	1.61	0.95
MgO	0.45	0.08	0.13	0.12	0.15	0.36	0.24	0.25	0.08	0.45	0.22
MnO	<0.01	<0.01	<0.01	<0.01	<0.01	<0.01	<0.01	0.01	<0.01	0.01	-
CaO	0.18	0.13	0.13	0.14	0.18	0.03	0.05	0.21	0.03	0.21	0.13
Na ₂ O	1.52	0.2	0.28	0.48	0.32	1.77	1.56	0.23	0.20	1.77	0.80
K ₂ O	1.34	0.3	0.37	0.57	0.57	0.10	0.14	0.9	0.10	1.34	0.54
P ₂ O ₅	0.14	<0.01	<0.01	<0.01	<0.01	0.02	0.04	0.05	<0.01	0.14	-
SiO ₂ / Al ₂ O ₃	10.77	34.71	37.04	38.55	33.96	16.09	16.39	24.23	10.77	38.55	26.47
Na ₂ O/ K ₂ O	1.13	0.67	0.76	0.84	0.56	17.70	11.14	0.26	0.26	17.70	4.13
V		<5	6	7	5			8	<5.00	8	-
Co		6	5	5	5			<5	<5	6	-
Cr	152					147	174		147.00	174	157.67
Ni	18	7	6	8	5	20	21	7	5.00	21	11.50
Cu	21	9	10	8	7	23	23	16	7.00	23	14.63
Zn	29	5	8	8	7	28	29	6	5.00	29	15.00
Ga	27	8	8	8	8	28	29	6	6.00	29	15.25
Rb	95	32	31	36	35	22	46	76	22.00	95	46.63
Sr	38	8	6	9	10	53	85	28	6.00	85	29.63
Y	41	<5	<5	<5	<5	33	85	11	<5	85	-
Zr	99	5	7	6	9	86	115	52	5.00	115	47.38
Nb	29	<5	<5	<5	<5	54	83	5	<5	83	42.75
Ba	218	<25	<25	<25	<25	35	45	186	<25	218	-
Pb	82	<5	<5	<5	<5	122	164	<5	<5	164	-

5.4.9 Major oxides of quartz-hornblende schist

Geochemical analysis (table 5.8, n=4) of quartz-amphibole schist shows SiO₂ from 54.24% to 58.71% (av. 56.75%), TiO₂ from 0.64% to 2.01% (av. 1.26%), Al₂O₃ from 10.85% to 12.67% (av. 11.56%), Fe₂O₃ from 8.45% to 10.40% (av. 9.85%), MgO from 5.89% to 7.66% (av. 6.78%), MnO from 0.09% to 0.25% (av. 0.19%), CaO from 4.15% to 8.72% (7.06%), Na₂O from 1.75% to 3.99% (av. 2.88%), K₂O from 0.25% to 2.64% (av. 0.90%), P₂O₅ from 0.09% to 0.45% (av. 0.26%).

5.4.10 Trace elements and rare earth elements of quartz-hornblende schist

The quartz-amphibole schist contain Rb content ranging from 22ppm to 156ppm (avg. 64.50ppm), Sr from 77ppm to 187ppm (avg. 150.75ppm), Ba from 175ppm to 280ppm (avg. 222.50ppm), Zr from 37ppm to 187ppm (avg. 93.75ppm), V from 126ppm to 225 ppm (avg. 185.25ppm), Co from 24ppm to 31ppm (avg. 27.75ppm), Ni from 16ppm to 56ppm (avg. 42.75ppm), Cu from 30ppm to 262ppm (avg. 104ppm), Zn from 34ppm to 85ppm (avg. 61.25ppm), Ga from 14ppm to 16ppm (avg. 14.50ppm), Y from 14ppm to 26ppm (avg. 18.50ppm), Nb from 6ppm to 19ppm (avg. 11.67ppm), Pb from 7ppm to 8 ppm (avg. 7.33ppm) (table 5.8).

Table 5.8 Major oxides (wt %) and trace elements (ppm) of quartz-amphibole schist.

Sample No.	XA5265	XA5488	XA5489	XA5490	Min.	Max.	Avg.
SiO ₂	54.24	58.71	58.55	55.48	54.24	58.71	56.75
TiO ₂	0.64	1.03	1.35	2.01	0.64	2.01	1.26
Al ₂ O ₃	12.67	11.6	10.85	11.12	10.85	12.67	11.56
Fe ₂ O ₃	8.45	10.34	10.19	10.4	8.45	10.4	9.85
MgO	7.66	7.07	5.89	6.48	5.89	7.66	6.78
MnO	0.09	0.18	0.22	0.25	0.09	0.25	0.19
CaO	4.15	7.14	8.22	8.72	4.15	8.72	7.06
Na ₂ O	1.75	2.55	3.21	3.99	1.75	3.99	2.88
K ₂ O	2.64	0.4	0.29	0.25	0.25	2.64	0.90
P ₂ O ₅	0.09	0.21	0.3	0.45	0.09	0.45	0.26
V	126	185	205	225	126	225	185.25
Co	28	28	31	24	24	31	27.75
Ni	49	56	50	16	16	56	42.75
Cu	30	67	262	57	30	262	104.00
Zn	47	79	85	34	34	85	61.25
Ga	16	14	14	14	14	16	14.50
Rb	156	22	43	37	22	156	64.50
Sr	77	187	160	179	77	187	150.75
Y	14	14	20	26	14	26	18.50
Zr	97	37	54	187	37	187	93.75
Nb	6	<5	10	19	6	19	11.67
Ba	280	227	175	208	175	280	222.50
Pb	<5	7	8	7	7	8	7.33
Th*	<5	<5	<5	14	14	14	14.00
U*	<5	<5	<5	<5	0	0	-

The quartz-amphibole schist (n=1) is depleted in REE elements except lower abundance of La (13ppm), Ce (29ppm), Y (21ppm), Sc (2ppm).

5.4.11 Major oxides of quartzite (Tehla Formation)

Quartzites of Tehla Formation (n=3) are characterized by high SiO₂ (90.93-92.34%, avg. 91.67%) and contain lower abundance of other major oxides. They contain TiO₂ from 0.03% to 0.04% (avg. 0.04%), Al₂O₃ from 2.85% to 3.51% (avg. 3.17%), Fe₂O₃ from 1.85% to 2.01% (avg. 1.93%), MgO from 0.34% to 0.72% (avg. 0.57%), MnO from <0.01% to 0.01% (avg. 0.01%), CaO from 0.71% to 0.84% (avg. 0.78%), Na₂O from 0.21% to 1.52% (avg. 1.02%), K₂O from 0.57% to 0.86% (avg. 0.71%), P₂O₅ from 0.05% to 0.07% (avg. 0.06%). They are also characterized by low Na₂O/K₂O (0.30 to 2.67, avg. 1.51) and high SiO₂/Al₂O₃ (25.91 to 32.19, avg. 29.17) (table 5.9).

In the geochemical classification diagram proposed by Pettijohn et al. (1987), quartzite samples of Tehla Formation plotted in the field of sub-litharenite (fig.5.15).

5.4.12 Trace elements and rare earth elements of quartzite (Tehla Formation)

Quartzite of Tehla Formation (n=3) contain lower abundance of trace elements. They contain V from 6ppm to 10 ppm (avg. 8.33ppm), Co from <5ppm to 6ppm, Ni from 8ppm to 9ppm (avg. 8.33ppm), Cu from 7ppm to 9ppm (7.67ppm), Zn from 11ppm to 24ppm (avg. 17.67ppm), Ga from <5ppm to 5ppm, Rb from 41ppm to 52ppm (avg. 46.33ppm), Sr from 12ppm to 26ppm (avg. 20ppm), Y from <5ppm to 5ppm, Zr from 32ppm to 52ppm (avg. 43ppm), Nb <5ppm, Ba from <25ppm to 45ppm, Pb <5ppm (table 5.9).

The quartzite of Tehla Formation is also depleted in REE elements except for lower abundance of La (14-16ppm), Ce (27-32ppm), Y (3ppm).

Table 5.9 Major oxides (wt %) and trace elements (ppm) of quartzite (Tehla Formation).

Sample No.	XA5485	XA5486	XA5487	Min	Max	Avg.
SiO ₂	92.34	90.93	91.75	90.93	92.34	91.67
TiO ₂	0.04	0.04	0.03	0.03	0.04	0.04
Al ₂ O ₃	3.14	3.51	2.85	2.85	3.51	3.17
Fe ₂ O ₃	1.93	1.85	2.01	1.85	2.01	1.93
MgO	0.72	0.64	0.34	0.34	0.72	0.57
MnO	0.01	0.01	<0.01	0.01	0.01	0.01
CaO	0.8	0.84	0.71	0.71	0.84	0.78
Na ₂ O	0.21	1.52	1.34	0.21	1.52	1.02
K ₂ O	0.7	0.57	0.86	0.57	0.86	0.71
P ₂ O ₅	0.06	0.05	0.07	0.05	0.07	0.06
Na ₂ O/K ₂ O	0.30	2.67	1.56	0.30	2.67	1.51
SiO ₂ /Al ₂ O ₃	29.41	25.91	32.19	25.91	32.19	29.17
V	9	10	6	6.00	10.00	8.33
Co	<5	<5	6	<5	6.00	-
Ni	9	8	8	8.00	9.00	8.33
Cu	9	7	7	7.00	9.00	7.67
Zn	24	11	18	11.00	24.00	17.67
Ga	5	5	<5	<5	5.00	-
Rb	52	46	41	41.00	52.00	46.33
Sr	12	22	26	12.00	26.00	20.00
Y	<5	5	<5	5.00	5.00	5.00
Zr	52	45	32	32.00	52.00	43.00
Nb	<5	<5	<5	-	-	-
Ba	39	45	<25	<25	45.00	-
Pb	<5	<5	<5	-	-	-
Th*	<5	<5	<5	-	-	-
U*	<5	<5	<5	-	-	-

5.4.13 Major oxides of quartz-biotite-sericite schist

The quartz-biotite-sericite schist of Raialo Group underlying the quartzite of Rajgarh Formation are characterized by variable content of SiO₂ (44.11-65.69%, avg. 53.11), higher content of TiO₂ (0.94-2.58%, avg. 1.94%), high Al₂O₃ (14.41-21.99%, avg. 19.32%) and Fe₂O₃ (7.74-14.02%, avg. 11.26%), high MgO (1.45-2.38%, avg. 1.98%), low MnO (0.02-0.17%, avg. 0.07%) and CaO (0.20-1.92%, avg. 0.85%), Na₂O ranging from 1.51% to 2.20% (avg. 1.80%), high K₂O (6.31-10.62%, avg. 8.65%), low P₂O₅ (0.16-1.61%, avg. 0.69%) (table 5.10).

5.4.14 Trace elements and rare earth elements of quartz-biotite-sericite schist

The quartz-biotite-sericite schist is depleted in Th, Mo, Ta, Pb. They are characterized by higher content of V (228-510ppm), Cr (101-360ppm), Zr (159-456ppm), Rb (299-348ppm), Sr (27-39ppm). They also contain Nb from 42 to 64ppm, Cu from <10 to 123ppm, Ni from <10 to 81ppm, Zn from 31 to 110ppm, Co from <10 to 52ppm, Sr from 27 to 58ppm, U(T) from 10 to 40ppm with U(L) <10 to 17ppm (table 5.11).

5.4.15 Major oxides of gritty quartzite (Rajgarh Formation)

The quartzites of Rajgarh Formation are characterized by high and wide range of SiO₂ (76.18-92.35%, avg. 85.30%), low TiO₂ (0.05-0.45%, avg. 0.21%), variable content of Al₂O₃ (3.96-12.48%, avg. 7.69%) and Fe₂O₃ (0.56-5.58%, avg. 1.79%), low MgO (0.06-0.83%, avg. 0.32%), MnO (<0.01-0.03%), CaO (0.09-0.27%, avg. 0.17%), Na₂O (0.18-2.37%, avg. 1.01%), high K₂O (2-5.47%) except sample no. XA-5089, which contains <0.01, low P₂O₅ (0.02-0.18%, avg. 0.09%). The samples show variable SiO₂/Al₂O₃ from 6.10 to 23.26 and low Na₂O/K₂O from 0.08 to 1.23 (table 5.12).

In the geochemical classification diagram proposed by Pettijohn et al. (1987), quartzite samples of Rajgarh Formation plotted in the fields of arkose to sub-arkose, sublitharenite to litharenite (Fig.5.15).

5.4.16 Trace elements and rare earth elements of gritty quartzite (Rajgarh Formation)

Quartzite samples of Rajgarh Formation exhibit lower abundance of V (9-19ppm), Co (<5-8ppm), Ni (8-15ppm), Cu (<5-16ppm except sample no. XA-5089 containing 330ppm), Zn (<5-21ppm), Ga (10-27ppm), Y (7-50ppm), Zr (30-73ppm), Nb (<5-36ppm), variable content of Cr (105-242ppm), Rb (<10-203ppm), Sr (22-116ppm), high and a relatively wider range of Ba (155-1997ppm), Pb (<5-83ppm). They are depleted in REE elements except lower abundance of La, Ce, Pr, Nd, Y, Sc (table 5.12).

5.4.17 Trace elements and rare earth elements of quartzo-feldspathic veins

The quartzo-feldspathic samples (n=2) analyzed U(T) from 30ppm to 60ppm with leachability from 8.48ppm to 16.96ppm. The samples are characterized by low Th (<10ppm), Mo (<10ppm), Nb (29ppm), Ta (<25ppm), variable Zr (80-189ppm). They also exhibit high V (208-294ppm), Cr (184-224ppm), Cu (57-398ppm), Ni (39-41ppm), Zn (86-105ppm), Co (36-46ppm), Pb (81-217ppm), Rb (111-276ppm), very high Ba (994-2104ppm), Sr (153-390ppm) (table 5.14). The samples are depleted in REE elements except low Ce (8-27ppm) (table 5.15).

5.4.18 Major oxides of radioactive samples (basal part of Rajgarh Formation)

Radioactive gritty quartzite/conglomerate (n=12, table 5.16) occurring at basal part of the Rajgarh Formation is characterized by variable SiO₂ (56.50-74.35%) depending upon the quartz content in the matrix part, high TiO₂ (0.17-0.93%), moderate Al₂O₃ (3.78-10.50%), moderate to high Fe₂O₃ (3.93-16.70%), low MgO (0.31-1.34%) and MnO (0.03-0.33%), high CaO (3.76-11.49%), variable Na₂O (<0.01-3.97%), moderate K₂O (1.47-2.83%), invariably high P₂O₅ (2.77-8.15%). FeO (data available for samples T-1303, T-1304) has a lower value as compared to Fe₂O₃ suggesting higher content of hematite compared to magnetite. Hematitization and geothitization of radioactive samples observed under the microscope support the above data.

One radioactive quartz-biotite-sericite schist sample analyzed 44.23% SiO₂, high TiO₂ (1.98%), very high Al₂O₃ (24.04%) and Fe₂O₃ (t) (10.47%), relatively high MgO (1.38%), low MnO (0.06%), high CaO (3.03%) and P₂O₅ (2.3%), low Na₂O (<0.01%), high K₂O (9.57%).

5.4.19 Trace elements and rare earth elements of radioactive samples (basal part of Rajgarh Formation)

The radioactive samples analyzed variable content of U(T) from 51ppm to 814ppm with leachability from 34ppm to 644ppm. The samples are characterized by low Th (<10-19ppm), Mo (<10ppm), Nb (<25-35ppm), Ta (<25ppm), low Zr (30-92ppm) for gritty quartzite/conglomerate whereas the quartz-biotite-sericite schist contain high Zr (151ppm), low Ni (<10-27ppm), Zn (<5-42ppm), Co (<10-18ppm), variable Pb (28-119), low Sr (24-82ppm). They also exhibit high V (42-228ppm), Cr (100-196ppm), Cu (71-443), Rb (52-128ppm, 285ppm for quartz-biotite-sericite schist), Ba (84-191ppm, 373ppm for quartz-biotite-sericite schist) (table 5.17). Relatively high Cu values (134 to 346 ppm) in six meta-conglomerate samples (FQ-6135, 6136, 6138, 6141, 6142 & 6143) indicate the presence of secondary Cu/sulphide phases. Presence of malachite stains support the above outcome.

The radioactive samples are depleted in REE elements with lower abundance of LREE, Y except sample no. AA02262 which shows enriched value of LREE (table 5.18).

Correlation matrix among the major oxides and trace elements of radioactive samples has been prepared (table 5.19). Very strong positive correlation has been observed for U(T) vs. Fe₂O₃, U(T) vs. U(L), U(T) vs. Pb. Strong positive correlation is observed for U(T) vs. V, U(T) vs. Cu, U(T) vs. Zn, Th vs. MnO, Th vs. Cr. Moderate positive correlation is observed for U(T) vs. Nb, U(T) vs. Co, U(T) vs. Sr, Th vs. MgO.

Strong negative correlation is observed for U(T) vs. MnO, Th vs. Fe₂O₃. Moderate negative correlation is observed for U(T) vs. MgO, U(T) vs. Th.

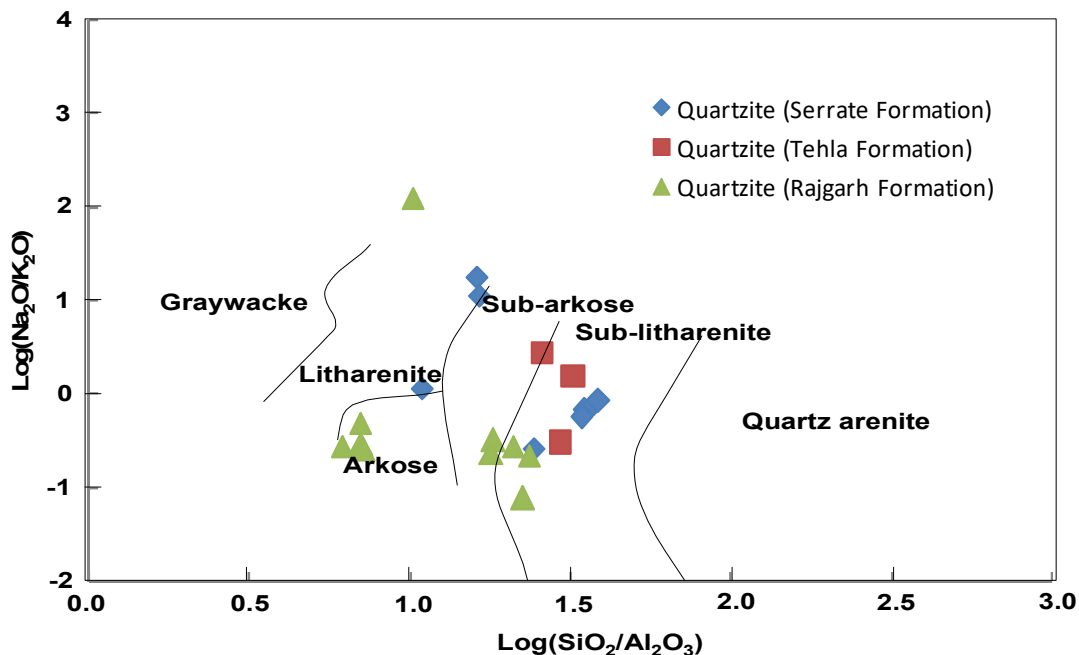


Figure 5.15 Sandstone classification diagram using $\log(\text{Na}_2\text{O}/\text{K}_2\text{O})$ vs. $\log(\text{SiO}_2/\text{Al}_2\text{O}_3)$ (after Pettijohn et al. 1987).

Table 5.10 Major oxides (wt %) of quartz-biotite-sericite schist.

Sample No.	XA5096	XA5097	XA5098	XA5266	XA5267	Min	Max	Avg.
SiO₂	65.69	47.84	56.56	47.77	44.11	44.11	65.69	53.11
TiO₂	0.94	2.10	2.12	2.32	2.58	0.94	2.58	1.94
Al₂O₃	15.41	20.17	18.28	21.99	21.97	15.41	21.99	19.32
Fe₂O₃	7.74	11.75	11.99	11.57	14.02	7.74	14.02	11.26
MgO	1.45	2.29	1.56	2.34	2.38	1.45	2.38	1.98
MnO	0.02	0.17	0.02	0.05	0.07	0.02	0.17	0.07
CaO	0.26	1.92	0.20	0.39	1.04	0.20	1.92	0.85
Na₂O	1.51	2.20	1.62	1.72	1.87	1.51	2.20	1.80
K₂O	6.31	9.25	7.29	10.62	10.18	6.31	10.62	8.65
P₂O₅	0.20	1.61	0.16	0.30	0.80	0.16	1.61	0.69

Table 5.11 Trace elements (ppm) of quartz-biotite-sericite schist.

Lab No.	Rock type	U(T)	U(L)	Th	Mo	V	Nb	Ta	Zr	Cr	Cu	Ni	Zn	Co	Pb	Rb	Ba	Sr
AA02803	Quartz-biotite-sericite schist	14	-	<10	<10	228	43	<25	159	101	93	<10	31	<10	<25	348	529	27
AA03179		20	<10	<10	<10	510	64	<25	456	244	60	53	76	32	<25	336	900	37
AA03180		10	<10	<10	<10	428	60	<25	418	274	<10	74	87	36	<25	312	892	36
AA03181		40	17	<10	<10	392	42	<25	368	172	24	76	110	52	<25	299	698	39
AA03182		30	<10	<10	<10	430	62	<25	384	360	123	81	97	36	<25	331	1134	58

Table 5.12 Major oxides (wt%) and trace elements (ppm) of gritty quartzite (Rajgarh Formation).

Sample No.	XA5076	XA5077	XA5078	XA5087	XA5088	XA5089	XA5092	XA5093	XA5094	XA5095	Min.	Max.	Avg.
SiO ₂	92.35	89.31	92.1	79.19	77.99	83.67	91.24	79.72	91.23	76.18	76.18	92.35	85.30
TiO ₂	0.05	0.2	0.09	0.45	0.30	0.13	0.06	0.25	0.13	0.45	0.05	0.45	0.21
Al ₂ O ₃	4.12	4.92	3.96	11.27	11.20	8.26	5.11	11.17	4.37	12.48	3.96	12.48	7.69
Fe ₂ O ₃	0.64	2.49	0.91	1.24	1.50	5.58	0.56	1.76	0.97	2.20	0.56	5.58	1.79
MgO	0.06	0.18	0.13	0.49	0.65	0.14	0.11	0.52	0.13	0.83	0.06	0.83	0.32
MnO	<0.01	0.01	0.03	<0.01	<0.01	<0.01	0.01	<0.01	0.01	<0.01	<0.01	0.03	-
CaO	0.14	0.17	0.16	0.14	0.17	0.23	0.18	0.09	0.27	0.18	0.09	0.27	0.17
Na ₂ O	0.18	0.63	0.46	1.44	2.37	1.23	0.49	1.22	0.58	1.51	0.18	2.37	1.01
K ₂ O	2.37	2	2.06	4.98	4.77	<0.01	2.15	4.87	2.08	5.47	<0.01	5.47	-
P ₂ O ₅	0.02	0.02	0.02	0.11	0.13	0.18	0.02	0.07	0.15	0.14	0.02	0.18	0.09
(SiO ₂ /Al ₂ O ₃)	22.42	18.15	23.26	7.03	6.96	10.13	17.86	7.14	20.88	6.10	6.10	23.26	13.99
(Na ₂ O/K ₂ O)	0.08	0.32	0.22	0.29	0.50	1.23	0.23	0.25	0.28	0.28	0.08	1.23	0.37
V	9	12	10	-	-	-	10	-	19	-	9.00	19.00	12.00
Co	<5	8	6	-	-	-	5	-	<5	-	<5	8.00	-

Cr				112	227	242		148		105	105	242	166.80
Ni	9	8	10	10	12	<10	15	10	9	<10	8	15	-
Cu	9	10	10	16	16	330	16	16	<5	14	<5	330	-
Zn	<5	<5	5	21	21	19	8	21	<5	21	<5	21	-
Ga	10	12	10	26	26	22	14	27	12	26	10	27	18.50
Rb	108	116	92	175	183	<10	102	203	92	202	<10	203	-
Sr	27	30	22	46	57	116	44	52	25	60	22	116	47.90
Y	8	15	10	<10	28	<10	14	50	7	39	7	50	-
Zr	32	35	40	59	61	30	49	65	37	73	30	73	48.10
Nb	<5	5	<5	14	22	14	<5	36	8	31	<5	36	-
Ba	203	236	247	695	498	1997	174	343	155	407	155	1997	495.50
Pb	18	12	<5	65	75	43	<5	83	<5	77	<5	83	-
Th*	<5	8	<5	39	43	30	<5	46	11	45	<5	46	-
U*	<5	<5	<5	<10	10	<10	<5	15	<5	27	<5	27	-

Table 5.13 Rare Earth Elements (REE) of different non-radioactive litho-units.

Lab No.	Rock type	La	Ce	Pr	Nd	Sm	Eu	Gd	Tb	Dy	Ho	Er	Tm	Yb	Lu	Y	Sc
AA03175	Granite	63	131	14	61	11	1	8	<2	6	<2	3	<2	2	<0.5	28	9
AA03176		71	160	16	70	13	1	9	<2	7	<2	3	<2	3	<0.5	34	16
AA03177		76	168	17	73	15	1	9	<2	8	<2	4	<2	4	<0.5	36	10
AA02805	Xenolith	36	78	8	34	6	<0.5	8	<2	3	<2	<2	<2	<2	<0.5	16	4
AA02266		52	109	13	45	11	<1	8	<2	2	<2	2	<2	<2	<1	22	<2
AA02267		31	69	6	22	5	<1	<5	<2	2	<2	<2	<2	<2	<1	15	<2
AA02268		44	99	10	40	9	<1	6	<2	3	<2	<2	<2	<2	1	24	<2
AA02802	Qtz-Sericite schist	51	104	14	48	9	<0.5	14	<2	5	<2	<2	<2	<2	<0.5	22	11
AA02269		48	107	8	43	10	<1	7	<2	2	<2	2	<2	<2	<1	10	<2
AA02270		48	92	10	43	9	<1	6	<2	2	<2	2	<2	<2	<1	12	<2
AA02804	Quartzite (Serrate)	12	24	<5	10	<5	<0.5	<5	<2	<2	<2	<2	<2	<2	<0.5	10	<2

AA03178		66	121	13	58	8	1	3	<2	5	<2	2	<2	<2	<0.5	11	16
AA02271	Quartz-amphibole schist	13	29	<5	10	<5	<1	<5	<2	<2	<2	<2	<2	<2	<1	21	2
AA03183	Quartzite (Tehla)	14	27	<5	11	<5	<0.5	<5	<2	<2	<2	<2	<2	<2	<0.5	3	<2
AA03184		16	32	<5	14	<5	<0.5	<5	<2	<2	<2	<2	<2	<2	<0.5	3	<2
AA02803	Phyllite	9	20	<5	8	<5	<0.5	<5	<2	<2	<2	<2	<2	<2	<0.5	8	<2
AA03179		41	80	9	38	6	<0.5	6	<2	3	<2	2	<2	3	<0.5	42	76
AA03180		27	56	6	26	<5	<0.5	<5	<2	<2	<2	<2	<2	3	<0.5	31	52
AA03181		26	55	6	24	<5	<0.5	<5	<2	<2	<2	<2	<2	3	<0.5	30	66
AA03182		30	70	8	28	5	<0.5	<5	<2	<2	<2	<2	<2	3	<0.5	33	71
AA02806	Gritty feldspathic quartzite (Rajgarh Formation)	13	27	<5	12	<5	<0.5	<5	<2	<2	<2	<2	<2	<2	<0.5	8	<2
AA03187		29	63	6	26	<5	<0.5	<5	<2	<2	<2	<2	<2	<2	<0.5	8	2
AA03188		30	65	7	27	5	<0.5	<5	<2	<2	<2	<2	<2	<2	<0.5	8	3
AA03189		22	45	6	20	<5	<0.5	<5	<2	<2	<2	<2	<2	<2	<0.5	16	4
AA03190		17	37	<5	12	<5	<0.5	<5	<2	<2	<2	<2	<2	<2	<0.5	7	<2

Table 5.14 Trace elements concentration of quartzo-feldspathic veins.

Lab No.	U(T)	U(L)	Th	Mo	V	Nb	Ta	Zr	Cr	Cu	Ni	Zn	Co	Pb	Rb	Ba	Sr
AA03185	30	8.48	<10	<10	294	29	<25	80	224	398	41	86	46	81	111	994	153
AA03186	60	16.96	<10	<10	208	29	<25	189	184	57	39	105	36	217	276	2104	390

Table 5.15 Rare Earth Elements (REE) concentration of quartzo-feldspathic veins.

Lab No.	La	Ce	Pr	Nd	Sm	Eu	Gd	Tb	Dy	Ho	Er	Tm	Yb	Lu	Y	Sc
AA03185	<5	8	<5	<5	<5	<0.5	<5	<2	<2	<2	<2	<2	<2	<0.5	<2	<2
AA03186	13	27	<5	8	<5	<0.5	<5	<2	<2	<2	<2	<2	<2	<0.5	6	8

Table 5.16 Major oxides (wt %) composition of radioactive samples, Sabraoli, Dausa district, Rajasthan.

Lab No.	Rock type	SiO ₂	TiO ₂	Al ₂ O ₃	Fe ₂ O ₃	FeO	MgO	MnO	CaO	Na ₂ O	K ₂ O	P ₂ O ₅
T-1303	Gritty quartzite/ Conglomerate	61.87	0.2	4.14	16.7	1.5	0.45	0.05	8.2	0.37	1.74	4.98
T-1304		67.39	0.46	4.55	9.90	0.68	0.31	0.04	8.38	0.78	1.57	4.99
FQ6133		64.83	0.93	7.33	3.93	-	0.48	0.29	10.6	2.21	2.65	7.3
FQ6134		62.36	0.8	6.63	5.41	-	1.34	0.33	10.41	<0.01	2.83	6.96
FQ6135		74.35	0.17	6.41	7.72	-	1.01	0.12	3.76	<0.01	2.42	2.77
FQ6136		64.83	0.93	7.33	3.93	-	0.48	0.29	10.6	2.21	2.65	7.3
FQ6137		67.3	0.47	4.7	10.41	-	0.44	0.05	7.74	<0.01	1.99	5.19
FQ6138		68.47	0.27	3.78	10.64	-	0.5	0.05	7.66	<0.01	1.47	5.08
FQ6140		59.5	0.67	10.5	6.36	-	1.21	0.23	10.22	0.6	2.28	6.53
FQ6141		60.82	0.68	5.99	10.86	-	0.65	0.14	9.83	<0.01	2.62	6.47
FQ6142		72.32	0.34	4.26	6.85	-	0.49	0.03	7.36	<0.01	1.56	4.87
FQ6143		56.5	0.68	5.66	9.74	-	0.77	0.06	11.49	3.97	2.49	8.15
Min.		56.50	0.17	3.78	3.93	-	0.31	0.03	3.76	<0.01	1.47	2.77
Max.		74.35	0.93	10.50	15.20	-	1.34	0.33	11.49	3.97	2.83	8.15
FQ6139	Qtz-bt-sericite schist	44.23	1.98	24.04	10.47	-	1.38	0.06	3.03	<0.01	9.57	2.3

Table 5.17 Trace elements concentration of radioactive samples from Sabraoli area, Dausa district, Rajasthan.

Lab No.	Rock type	U(T)	U(L)	Th	Mo	V	Nb	Ta	Zr	Cr	Cu	Ni	Zn	Co	Pb	Rb	Ba	Sr
T-1301	Gritty Quartzite/ Conglomerate	814	644	<10	<10	180	30	<25	48	117	443	<10	38	16	105	63	136	81
T-1302		360	339	<10	<10	117	35	<25	58	136	82	<10	23	14	56	58	96	72
AA02255		102	76	18	<10	60	<25	<25	53	173	123	<10	<5	<10	52	80	186	56
AA02256		85	76	17	<10	82	<25	<25	37	163	72	<10	10	<10	39	63	85	32
AA02257		51	34	16	<10	42	<25	<25	36	176	71	<10	12	<10	28	75	95	24
AA02258		551	543	16	<10	228	35	<25	92	196	357	27	41	12	68	128	191	82
AA02259		441	407	<10	<10	107	30	<25	44	125	119	<10	42	<10	71	52	84	40
AA02260		551	534	<10	<10	103	<25	<25	42	109	109	<10	26	18	119	63	133	73

AA02262		85	68	19	<10	65	<25	<25	47	126	121	<10	21	<10	31	104	138	45
AA02263		102	93	<10	<10	55	<25	<25	47	125	180	<10	20	12	48	86	108	73
AA02264		254	204	<10	<10	64	<25	<25	30	134	207	<10	27	14	66	52	86	39
AA02265		594	492	<10	<10	96	<25	<25	41	125	423	<10	32	<10	62	64	102	33
Min.		51	34	<10	<10	42	<25	<25	30	109	71	<10	<5	<10	28	52	84	24
Max.		814	644	19	<10	228	35	<25	92	196	443	27	42	18	119	128	191	82
AA02261	Qtz-bt-sericite schist	348	339	11	<10	191	34	<25	151	100	267	26	36	<10	44	285	373	35

Table 5.18 Rare Earth Elements (REE) concentration in radioactive samples from Sabraoli area, Dausa district, Rajasthan.

Lab No.	Rock type	La	Ce	Pr	Nd	Sm	Eu	Gd	Tb	Dy	Ho	Er	Tm	Yb	Lu	Y	Sc	
T-1301	Gritty quartzite/ Conglomerate	6	13	<5	<5	<5	<5	<5	<2	<2	<2	<2	<2	<2	<0.5	<2	<2	
T-1302		16	34	<5	<5	<5	<5	<5	<2	<2	<2	<2	<2	<2	<0.5	<2	<2	
AA02255		15	33	5	12	5	1	5	<2	<2	<2	<2	<2	<2	<2	<1	34	<2
AA02256		12	27	<5	9	<5	<1	<5	<2	<2	<2	<2	<2	<2	<2	<1	14	<2
AA02257		20	42	5	18	6	<1	5	<2	2	<2	<2	<2	<2	<2	1	15	<2
AA02258		30	63	7	22	6	2	6	<2	2	<2	<2	<2	<2	<2	<1	84	2
AA02259		7	17	<5	<5	<5	<1	<5	<2	<2	<2	<2	<2	<2	<2	<1	17	<2
AA02260		6	15	<5	<5	<5	<1	<5	<2	<2	<2	<2	<2	<2	<2	<1	23	<2
AA02262		222	398	50	211	41	7	19	3	6	<2	5	<2	2	1	25	2	
AA02263		25	46	6	23	5	2	<5	<2	<2	<2	<2	<2	<2	2	1	66	<2
AA02264		12	22	<5	<5	<5	<1	<5	<2	<2	<2	<2	<2	<2	<2	1	16	<2
AA02265		7	18	<5	<5	<5	<1	<5	<2	<2	<2	<2	<2	<2	<2	<1	18	<2
Min.			6	13	<5	<5	<5	<1	<5	<2	<2	<2	<2	<2	<2	<1	<2	<2
Max.			222	398	50	211	41	7	19	3	6	<2	5	<2	2	1	84	2
AA02261	Qtz-bt-sericite schist	22	48	6	17	<5	<1	<5	<2	<2	<2	<2	<2	<2	<1	39	3	

Table 5.19 Correlation matrix of major oxides and trace elements composition of radioactive samples, Sabraoli area, Dausa district, Rajasthan.

	SiO ₂	TiO ₂	Al ₂ O ₃	Fe ₂ O ₃	MgO	MnO	CaO	Na ₂ O	K ₂ O	P ₂ O ₅	U(T)	U(L)	Th	V	Nb	Zr	Cr	Cu	Ni	Zn	Co	Pb	Rb	Ba	Sr	
SiO ₂	1.00																									
TiO ₂	-0.84	1.00																								
Al ₂ O ₃	-0.78	0.91	1.00																							
Fe ₂ O ₃	-0.13	-0.17	-0.05	1.00																						
MgO	-0.57	0.58	0.68	-0.34	1.00																					
MnO	-0.12	0.22	0.08	-0.72	0.49	1.00																				
CaO	-0.10	-0.16	-0.43	-0.33	-0.10	0.49	1.00																			
Na ₂ O	-0.25	0.09	-0.10	-0.20	-0.09	0.11	0.56	1.00																		
K ₂ O	-0.78	0.92	0.97	0.04	0.62	0.00	-0.46	-0.09	1.00																	
P ₂ O ₅	-0.13	-0.09	-0.38	-0.38	-0.04	0.51	0.99	0.63	-0.40	1.00																
U(T)	-0.07	-0.21	-0.18	0.81	-0.47	-0.69	-0.12	0.16	-0.10	-0.14	1.00															
U(L)	-0.06	-0.17	-0.15	0.80	-0.48	-0.71	-0.19	0.10	-0.06	-0.21	0.99	1.00														
Th	0.12	0.09	0.13	-0.63	0.43	0.77	0.06	0.01	-0.02	0.09	-0.57	-0.57	1.00													
V	-0.27	0.25	0.32	0.68	-0.13	-0.48	-0.51	-0.17	0.37	-0.53	0.70	0.75	-0.20	1.00												
Nb	-0.15	0.26	0.32	0.50	-0.22	-0.50	-0.55	-0.24	0.35	-0.60	0.44	0.51	-0.23	0.83	1.00											
Zr	-0.61	0.79	0.85	0.27	0.30	-0.22	-0.60	-0.16	0.87	-0.58	0.15	0.23	-0.03	0.70	0.70	1.00										
Cr	0.58	-0.25	-0.28	-0.38	-0.10	0.36	-0.14	0.01	-0.29	-0.10	-0.33	-0.31	0.67	-0.04	0.01	-0.14	1.00									
Cu	-0.32	0.06	0.07	0.64	-0.17	-0.46	-0.07	0.36	0.14	-0.05	0.74	0.68	-0.33	0.63	0.28	0.28	-0.15	1.00								
Ni	-0.32	0.55	0.63	0.30	0.19	-0.28	-0.70	-0.23	0.66	-0.66	0.21	0.30	0.09	0.79	0.68	0.89	0.16	0.38	1.00							
Zn	-0.17	0.01	0.11	0.78	-0.28	-0.78	-0.37	-0.12	0.15	-0.39	0.79	0.81	-0.56	0.74	0.60	0.39	-0.38	0.64	0.48	1.00						
Co	0.31	-0.48	-0.42	0.50	-0.56	-0.49	-0.05	-0.27	-0.39	-0.14	0.55	0.55	-0.52	0.22	0.09	-0.19	-0.33	0.14	-0.16	0.24	1.00					
Pb	0.18	-0.39	-0.41	0.61	-0.62	-0.52	0.02	-0.05	-0.33	-0.03	0.81	0.81	-0.56	0.39	0.11	-0.13	-0.36	0.37	-0.07	0.49	0.84	1.00				
Rb	-0.70	0.85	0.96	0.14	0.53	-0.09	-0.57	-0.17	0.95	-0.53	-0.03	0.03	0.07	0.52	0.47	0.95	-0.21	0.21	0.81	0.26	-0.29	-0.27	1.00			
Ba	-0.66	0.82	0.89	0.15	0.36	-0.08	-0.51	-0.07	0.88	-0.47	0.09	0.15	0.07	0.58	0.47	0.94	-0.19	0.27	0.79	0.24	-0.16	-0.08	0.95	1.00		
Sr	0.18	-0.30	-0.33	0.55	-0.65	-0.28	0.03	-0.17	-0.32	-0.06	0.47	0.50	-0.22	0.45	0.38	0.07	-0.01	0.27	0.14	0.26	0.67	0.59	-0.13	0.02	1.00	

CHAPTER 6

DISCUSSION

The Sabraoli uranium mineralization has been located at the hinge zone of regional syncline defined by folding of Raialo, Alwar and Ajabgarh Group of rocks overlying the granite-gneiss of Mangalwar Complex. Basement granite-gneiss, litho-units of Raialo Group and quartzite of Rajgarh Formation (Alwar Group) are only covered under the study area. The area is characterized by two prominent unconformity surfaces. The basement granite gneiss is non-conformably overlain by quartzite, schist and meta-basic rocks of Raialo Group which are successively overlain by quartzite of Rajgarh Formation (Alwar Group) having a disconformable relationship.

The area has undergone several phases of deformation as defined by various planar, linear fabrics and disturbed contact between litho-units. The litho-units are strongly foliated which corresponds to axial planar cleavage of the regional fold. Foliation plane within quartzite of Serrate Formation (Raialo Group) has an average strike of N46°E with dip of 83° towards N44°W, whereas gritty quartzite of Rajgarh Formation (Alwar Group) has an average strike of N46°E with dip of 77° towards N44°W. Stereonet plot of joint planes in the area suggest an average strike of NW-SE with moderate to high dip either towards NE or SW. Shearing is prominent as defined by highly stretched, elongated clasts parallel to foliation near the Sabraoli uranium mineralization. The rocks of the study area have undergone metamorphism up to amphibolite facies. Development of minerals like chlorite, epidote with depth within quartz-biotite-sericite schist represents low grade metamorphism in the area. Development of amphibole with depth in quartz-biotite-sericite schist may be due to the association of meta-basic rock with schist of Tehla Formation as reported from other parts of the Alwar sub-basin. Regional geological cross sections show co-folding of both Raialo and Alwar Group of rocks. Satellite imagery also shows NE-SW trending fold axis in the area

and M/W pattern near Sabraoli uranium mineralization indicative of hinge zone of regional fold.

Uranium mineralisation is found within gritty quartzite/conglomerate at the basal part of the Rajgarh Formation (Alwar Group) overlying the quartz-biotite-sericite schist of Raialo Group, although a part of the quartz-biotite-sericite schist is also radioactive. Few radioactive quartz-feldspathic veins are also observed in the field. However, litho-units hosting the mineralisation are highly sheared. Uraniferous radioactivity has also been recorded at one of the borehole within gritty quartzite/conglomerate of basal Rajgarh Formation. The matrix content in both surface and borehole radioactive unit is different from the overlying litho-unit by having higher content of magnetite, biotite, and sericite.

The basement granite gneiss is composed of quartz, feldspar (dominantly microcline), biotite, muscovite, sericite with magnetite and apatite occurring as accessory minerals. Development of gneissosity is defined by alignment of micaceous minerals. Alteration of feldspar to sericite and hematitization of magnetite are prominent. Xenoliths of some earlier litho-units within basement granite-gneiss occur as dark coloured patches and are comprised of quartz, biotite, muscovite, plagioclase, sericite with apatite, zircon, and magnetite as accessory minerals.

The quartz muscovite/sericite schist occurring in between the basement granite-gneiss and quartzite of Serrate Formation is composed of mainly quartz, and muscovite/sericite. Flakes of sericite occur along bedding parallel schistosity. Magnetite occurs as accessory mineral. The litho-unit is highly sheared as indicated by presence of S-C fabric and elongated quartz grains. Tourmaline and zircon occur as accessory minerals. Highly stretched quartz along foliation plane and undulose extinction is prominent. These features represent high strain conditions in the area. Quartz and prismatic hornblende dominate within the meta-basic unit of Tehla Formation with occasional presence of plagioclase and biotite. Quartzite of

Tehla Formation is comprised mainly of quartz with tourmaline in heavy mineral fraction. The quartz-biotite-sericite schist underlying the quartzite of Rajgarh Formation is composed of quartz, biotite, sericite, and magnetite. Shearing is prominent indicated by highly stretched quartz, magnetite and alignment of biotite, sericite.

The quartzite of Rajgarh Formation is sub-mature, poorly sorted, sub-arkosic and is comprised of quartz, feldspar (mostly microcline), sericite aligned along foliation plane and tourmaline in heavy mineral fraction. Presence of stretched clasts, undulating quartz and development of S-C fabric represent high strain conditions.

Radioactivity is confined to the basal part of the Rajgarh quartzite. The radioactive gritty quartzite/conglomerate is comprised of quartz, muscovite/sericite, magnetite, apatite, biotite, and tourmaline. Presence of S-C fabric, polycrystalline quartz fish, grain boundary bulging and grain boundary migration represent high strain conditions. Apatite is important constituent present as granular aggregate in groundmass. Hematization and goethitization of magnetite are prominent. Medium density and a few high density alpha tracks corresponding to goethitized grains signify presence of some primary radioactive grains. Few suspected grains of uranothorite occurring as inclusions within quartz and biotite have been found. Radioactive quartz-biotite-sericite schist is medium to fine grained comprising quartz, biotite, muscovite/sericite as major constituent and apatite, epidote and allanite minor minerals. Zircon is present in trace amount. Allanite is the main radioactive mineral present as fine sized irregularly dispersed grains except rare presence of suspected uranothorite grains.

Metanatroautunite $((\text{NaUO}_2\text{PO}_4)_3\text{H}_2\text{O})$ within quartz-muscovite-sericite schist and rutile within meta-conglomerate has been identified as atomic minerals under X-ray diffraction studies. Hematite and magnetite occur as other ore minerals. Rock forming minerals of biotite, fluorapatite, muscovite, and quartz are identified. However, presence of

primary uranium mineral couldn't be ascertained. This may be due to occurrence of fine grained primary uranium minerals as inclusions.

Radiometric assay of radioactive samples shows uraniferous nature with 0.014-0.096 % eU_3O_8 , 0.012-0.11% U_3O_8 , <0.010% ThO_2 , 0.013-0.095% Ra (eU_3O_8). All the non-radioactive litho-units are either thoriferous in nature or have negligible radio-elements except few samples of quartz-biotite-sericite schist and quartzo-feldspathic veins having comparatively higher uranium content.

The basement granite-gneiss is of monzogranite type and define calc-alkaline trend in AFM diagram. It is having high alumina saturation index indicating peraluminous nature. The granite-gneiss is mostly of magnesian type and is alkali-calcic to calc-alkalic. The overall pattern of decreasing Fe_2O_3 (t), MgO, CaO with increasing SiO_2 characterizes fractionating granitic systems. REE plots show depleted HREE compared to LREE with negative Eu anomaly. Xenoliths within basement granite show bimodal distribution of geochemical data. The major oxides composition of quartz-muscovite/sericite schist represent overall granitic composition indicating that it may be sheared equivalent of basement granite. The quartzite of Serrate Formation is of sub-litharenite and litharenite type whereas quartzite of Tehla Formation is of sub-litharenite as indicated by geochemical classification diagram by Pettijohn et al. (1987). The quartzite of Rajgarh Formation is of arkose to sub-arkose, sub-litharenite to litharenite. The sub-arkosic to arkosic nature of Rajgarh quartzite is also observed during petrographic studies. Higher content of MgO, Fe_2O_3 (t), Al_2O_3 in quartz-hornblende schist is reflected by the presence of hornblende. Relatively higher content of CaO represent presence of calcite. Variable percentage of SiO_2 within quartz-biotite-sericite schist represents variation in quartz content. High Fe_2O_3 (t) represents presence of magnetite/hematite. Higher content of Al_2O_3 , MgO, K_2O indicate biotite, muscovite/sericite which is also observable under microscopic studies.

TiO₂ and Zr concentrations in siliciclastic rocks are good indicators of source rock. Hayashi et al. (1997) have devised a scheme for discriminating the source of sedimentary rocks on the basis of TiO₂/Zr weight ratios. As per that scheme of discrimination, the TiO₂/Zr weight ratios indicate derivation of quartzites of both Serrate and Tehla Formations dominantly from felsic and that of quartz-biotite-sericite schist from intermediate igneous rocks (fig.6.1). Similarly, TiO₂/Zr weight ratios for quartzite of Rajgarh Formation indicate derivation mostly from felsic and to some extent intermediate igneous rocks whereas that of radioactive samples from the basal part represent derivation mostly from intermediate and to some extent felsic and mafic igneous rocks (fig. 6.2).

The influence of climatic conditions on the chemical maturity of sandstone can be studied, and thereby the prevalent palaeoclimatic conditions during provenance weathering can be deciphered, using SiO₂ vs. (Al₂O₃+K₂O+Na₂O) bivariate plot (Suttner and Dutta, 1986). The plots of quartzites from the Serrate and Tehla Formations in SiO₂ vs. (Al₂O₃+K₂O+Na₂O) binary space apparently (ignoring the effect of reworking/recycling) indicate derivation of the precursor sediments dominantly under a semi-humid palaeoclimatic condition (fig.6.3). Similarly, that of Rajgarh Formation indicates derivation under semi-humid to semiarid condition. However, the samples from basal part of Rajgarh Formation (radioactive) represent derivation under humid to semi-humid conditions (fig. 6.4).

Invariably high P₂O₅ is recorded along with high CaO in all radioactive samples indicating the presence of apatite mineral phase which is also observable under microscope. High Fe₂O₃ (t) represents presence of magnetite and hematite. Relatively high Cu values indicate the presence of secondary Cu as observed presence of malachite stains in the field. Relatively low Na₂O represent absence of plagioclase feldspar in the matrix. The samples exhibit higher content of V, Cr. Moderate to very strong positive correlation of U(T) with Fe₂O₃, Cu, Zn, V and dominance of Fe₂O₃ over FeO indicate mobilization of uranium during

ferruginization. Very strong negative correlation of Th with Fe_2O_3 and moderate negative correlation of Th with U(T) indicates relatively immobile nature of Th during ferruginization.

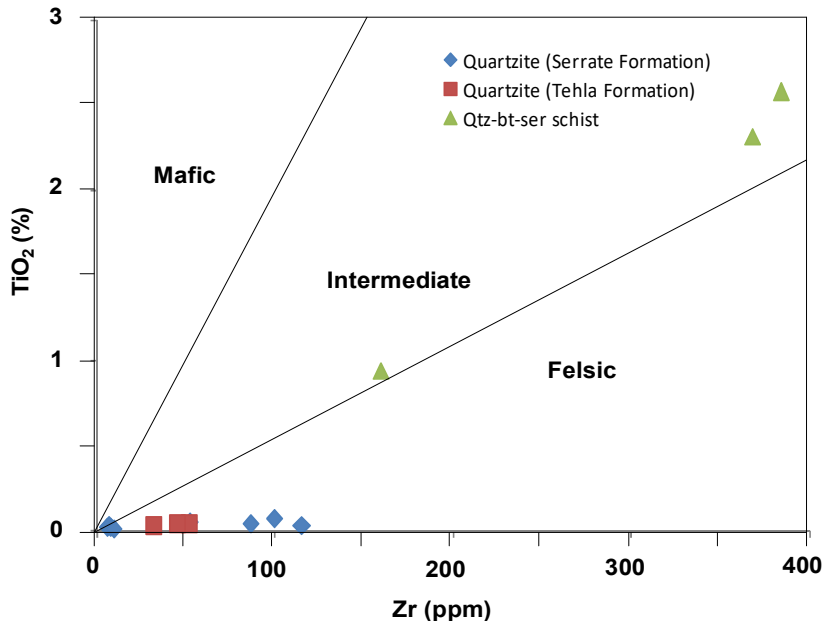


Figure 6.1 Inferred source rocks for quartzites and quartz-biotite-sericite schist of Raialo Group as revealed in Zr vs. TiO_2 plot (after Hayashi et al., 1997).

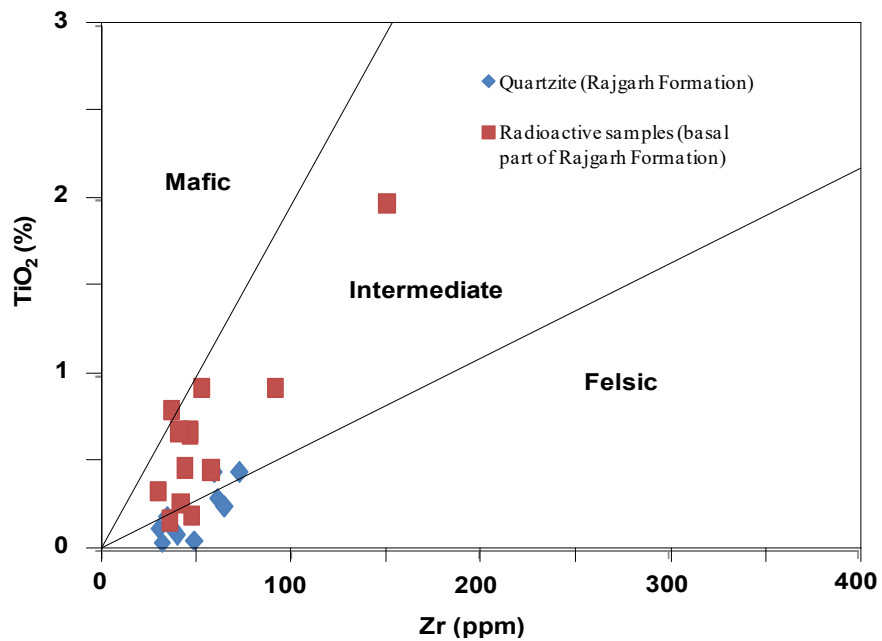


Figure 6.2 Inferred source rocks for quartzites/conglomerates (Rajgarh Formation) of Alwar Group as revealed in Zr vs. TiO_2 plot (after Hayashi et al., 1997).

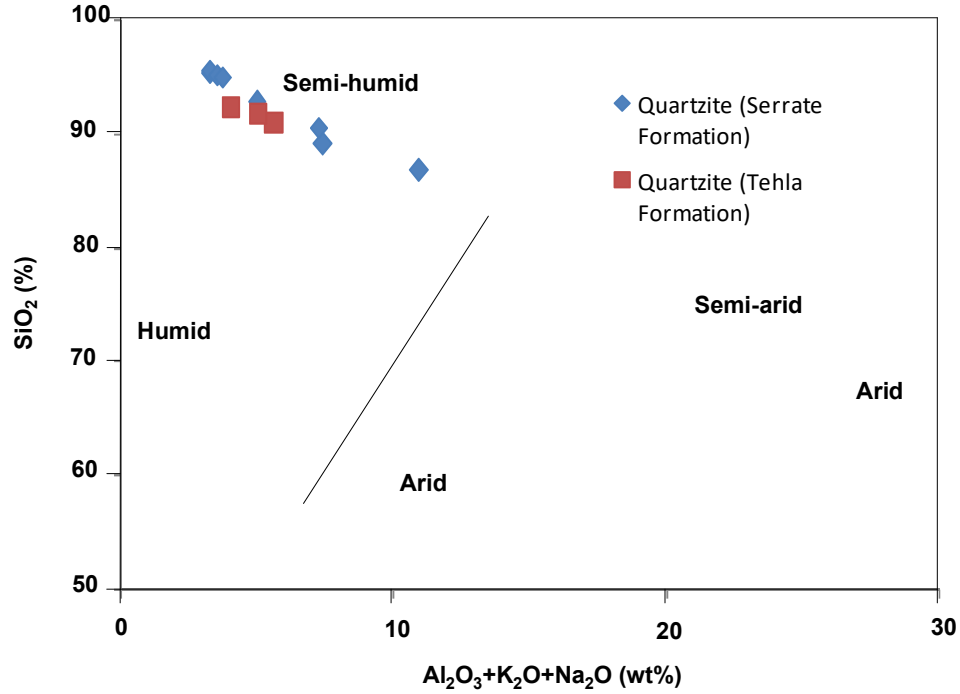


Figure 6.3 Influence of climatic conditions on the chemical maturity of quartzites of Serrate, Tehla Formations expressed as a function of SiO_2 and $(\text{Al}_2\text{O}_3 + \text{K}_2\text{O} + \text{Na}_2\text{O})$ (after Suttner and Dutta, 1986).

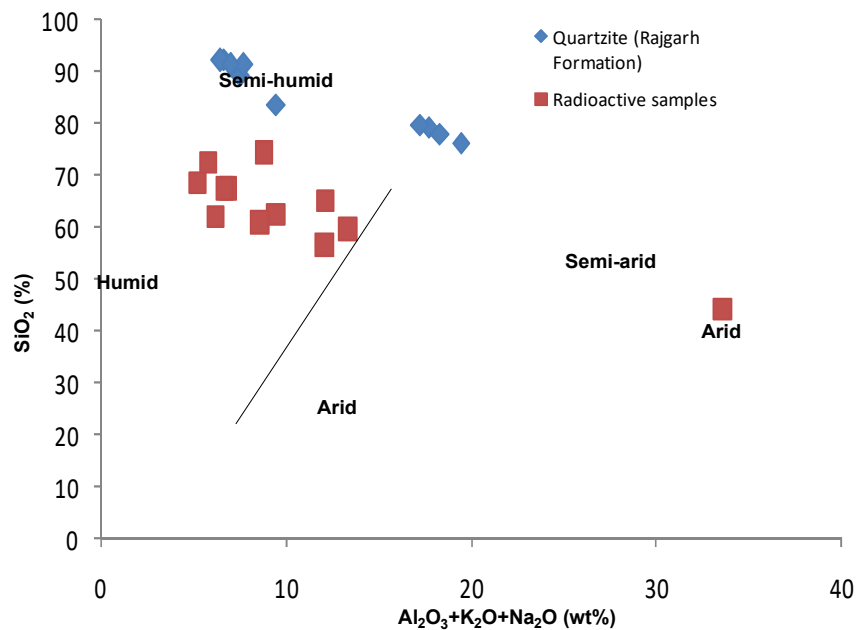


Figure 6.4 Influence of climatic conditions on the chemical maturity of quartzite of Rajgarh Formation expressed as a function of SiO_2 and $(\text{Al}_2\text{O}_3 + \text{K}_2\text{O} + \text{Na}_2\text{O})$ (after Suttner and Dutta, 1986).

6.1 Proposed Genetic Model

The Alwar sub-basin is well known for its significant base metal mineralization and forms a potential uranium province because of suitable geo-tectonic set up and comprise of basement Mangalwar Complex overlain by meta volcano-sedimentary sequences of Delhi Supergroup and has undergone three phases of deformation. The N-S to NE-SW folds are the prominent second generation folds. Besides, N-S to NE-SW striking map scale fractures are common within the basin. Exploration by Atomic Minerals Directorate for Exploration and Research (AMD) over several decades has located uranium mineralization associated with fracture/shear zones, and also related to granitic and pegmatitic activities. However, occurrence of radioactive basal conglomerate (Alwar Group) at the unconformity between the Raialo and Alwar Groups has provided new avenues for unconformity proximal related uranium mineralization.

An area around Sabraoli exposes gritty feldspathic quartzite with intraformational conglomerates of Alwar Group having coarse grained, poorly sorted, sub-rounded to angular clasts. At the basal part of the quartzite, the clast size increases to cobble size even to boulder forming 5-10m thick meta-conglomerate horizon. The quartzite is underlain by schistose litho-unit of Raialo Group composed of quartz, biotite, sericite/muscovite, and disseminated magnetite. Numbers of quartzo-feldspathic veins have been intruded into the meta-sediments.

The Raialo and Alwar Group of meta-sediments have been co-folded having NE-SW striking axial plane in the study area. The meta-conglomerate horizon has an average dip of 30° near hinge zone of regional fold and the dip amount increases gradually towards the limb of the fold. The litho-units have been pervaded by NE-SW striking foliation with steep dip towards NW corresponding to axial planar cleavage of the regional fold. Sub-surface repetition of meta-conglomerate is observed due to development of M or W fold patterns near the hinge zone. Highly stretched and elongated pebbles within the meta-conglomerate

represent high strain conditions in the area. Shear fabrics are also prominently observed under microscope. Presence of quartzo-feldspathic veins and secondary copper depicts hydrothermal activity in the area.

Uranium mineralization at Sabraoli has been located at the basal part of Rajgarh Formation (Alwar Group) in the Alwar sub-basin. The mineralization is spatially related to meta-conglomerates representing unconformity between meta-sediments of Alwar and Raialo Groups and depicts unconformity proximal type of uranium mineralization. Besides, underlying quartz-biotite-sericite schist and few quartzo-feldspathic veins (Raialo Group) have recorded radioactivity. The quartzo-feldspathic veins might have contained intrinsic uranium and facilitated in enrichment of uranium.

Uranothorite inclusions, allanite were identified as the prominent radioactive phases and development of chloritic rim around uranothorite represents marginal alteration. Radioactive minerals including uranothorite, U-Ti-Si-Fe complex, allanite, uraninite inclusions within sphene has also been reported in EMP studies (Saxena, 2020). Uranothorite occurred as inclusions within quartz, biotite, and magnetite as well as in interstitial spaces of matrix of meta-conglomerate. Uranothorite was surrounded by thin chloritic and goethitised rim indicating marginal alteration (fig.6.5a). U-Ti-Si-Fe complex occurred as irregular patches within sphene, having distinct alteration rim. Uraninite (2-5 μ m) has been reported as inclusions within sphene which occurred as sporadic irregular grains and roughly follows foliations (fig. 6.5b). Allanite was found replacing sphene, biotite (pseudomorphic replacement) and occupying microfractures within sphene, which shows later formation of allanite in the paragenetic sequence.

From the above observations, it may be inferred that uranothorite at the basal part of Rajgarh Formation may be the primary or proto-ore for uranium mineralization derived from

granitic source. Uranium and REE might have been released by remobilization/alteration of uranothorite.

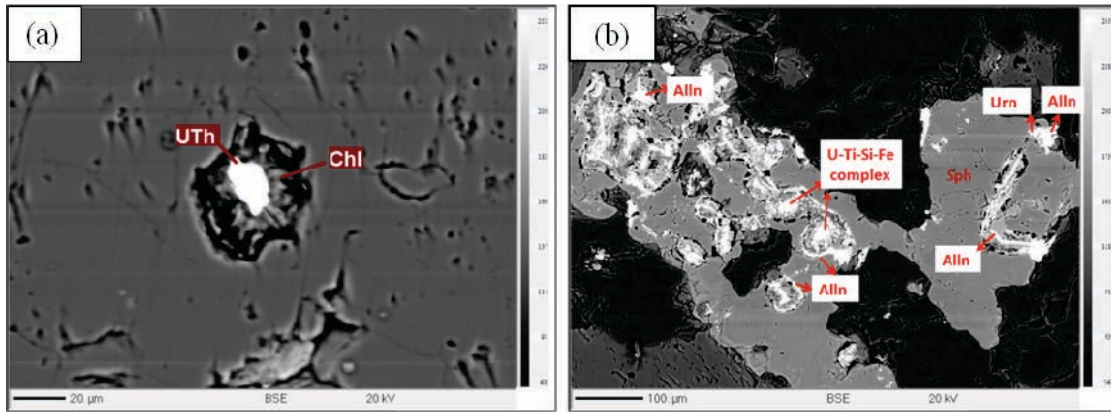


Figure 6.5 (a) Back scattered image of uranothorite surrounded by chloritic rim (b) Back scattered image of patches of U-Ti-Si-Fe complex rimmed by allanite. Note fine inclusion of uraninite within sphene (after Saxena, 2020).

Uraninite, U-Ti-Si-Fe complexes and allanite are the second phase of uranium minerals associated with sphene. Hydrothermal solution might have scavenged uranium (from uranothorite) and other elements and precipitated as uraninite and U-Ti-Si-Fe complexes within sphene.

CHAPTER 7

CONCLUSION

From the integrated results of detailed geological mapping, petro-mineralogical, radiometric and geochemical studies around Sabraoli area, following conclusions are drawn.

- The Sabraoli uranium mineralisation is located at the hinge zone of regional syncline having NE-SW trending fold axis defined by folding of Delhi meta-sediments overlying the granite-gneiss of Mangalwar Complex.
- Foliation planes representing axial planar cleavage in the area have an average strike of NE-SW with steep dip towards NW. Joint planes in the area have an average strike of NW-SE with moderate to high dip either towards NE or SW
- The area presents high strain conditions inferred from development of highly sheared, elongated clasts, S-C fabric, polycrystalline quartz fish, grain boundary bulging or migration. Foliation parallel shear planes have provided pathways for circulation of hydrothermal fluid.
- The basement granite-gneiss is monzogranite type, peraluminous nature, magnesian type, alkali-calcic to calc-alkalic and is characterized by calc-alkaline trend in AFM diagram. It has depleted HREE compared to LREE with negative Eu anomaly.
- The quartzite of Serrate Formation is of sub-litharenite and litharenite type whereas quartzite of Tehla Formation is of sub-litharenite. The quartzite of Rajgarh Formation is of arkose to sub-arkose, sub-litharenite to litharenite.
- Quartzites of both Serrate and Tehla Formations are derived dominantly from felsic and quartz-biotite-sericite schist from intermediate igneous rocks. Quartzite of Rajgarh Formation indicate derivation mostly from felsic and to some extent intermediate igneous rocks whereas that of radioactive samples from the basal part

represent derivation mostly from intermediate and to some extent felsic and mafic igneous rocks.

- Quartzites of Serrate and Tehla Formations are formed of the precursor sediments dominantly under a semi-humid palaeoclimatic condition whereas that of Rajgarh Formation is derived under semi-humid to semi-arid conditions. However, radioactive litho-unit from basal part of Rajgarh Formation is derived under humid to semi-humid conditions.
- Uranothorite, allanite, and metanatroautunite (traces) are the major radioactive phases. Uranothorite is the primary/proto-ore for uranium mineralization and uraninite might have been formed as inclusions within sphene during hydrothermal alteration of uranothorite.
- The Sabraoli uranium occurrence depicts unconformity proximal type of mineralization and provides scope for potential target of uranium exploration in the Alwar sub-basin.
- The present study incorporates litho-structural, petro-mineralogical and geochemical data to characterize the uranium mineralization at Sabraoli in the Alwar sub-basin. As the radioactive mineral phases occur in very fine sizes, detailed EPMA analysis is recommended to further understand the mineral phases and their interrelationship. Detailed ground geophysical study is required to delineate the unconformity contact between the quartzite of Rajgarh Formation (Alwar Group) and underlying quartz-biotite-sericite schist of Raialo Group. The current study highlights scope for unconformity type of uranium mineralization in Alwar sub-basin. Thus, further study requires detailed geological understanding in other parts of the sub-basin for uranium mineralization related to unconformity surface between the Raialo and Alwar Group of rocks.

REFERENCES

- Ahmad, S. (2015). Petrography of clastic sedimentary rocks of the Palaeoproterozoic Alwar Basin, North-Eastern Rajasthan. *International Journal of Research in Advent Technology*, 3(2), pp.147-153.
- Banerjee, A. K. and Singh, S. P. (1977). Sedimentary tectonics of Bayana subbasin, northeastern Rajasthan. *J. Indian Assoc. Sedimentol.*, 1, pp.74-85.
- Banerjee, A. K., Datta, A. K. and Ravindra, R. (1980). Geology & mineral resources of Alwar district Rajasthan. *Memoir Geological Survey of India*, 110.
- Banerjee, A. K. and Malhotra, G. (2011). Lithofacies association, petrography and geochemistry of Kankwarhi Formation, Alwar area, Delhi supergroup: Implication for detailed lithostratigraphy and basin tectonics. *Indian Journal of Geosciences*, 65(2), pp.159-170.
- Barman, G. (1980). An analysis of the Marwar Basin, Western Rajasthan, in the light of stromatolitic study. *Geological Survey of India, Hyderabad, Miscellaneous Publications*, 44, pp.292–297.
- Biswal, T. K. (1988). Polyphase deformation in Delhi rocks, south-east Amirgarh, Banaskantha district, Gujarat, in Precambrian of the Aravalli Mountain, Rajasthan, India. *Memoir Geological Survey of India*, 7, pp.267–277.
- Biswal, T. K., Gyani, K.C., Parthasarathy, R. and Pant, D.R. (1998B). Tectonic implication of geochemistry of gabbro-norite-basic granulite suite in the Proterozoic Delhi Supergroup, Rajasthan, India. *Journal of Geological Society of India*, 52, pp.721–732.
- Biswal, T. K., Gyani, K. C., Parthasarathy, R. and Pant, D.R. (1998b). Implications of the geochemistry of the pelitic granulites of the Delhi Supergroup, Aravalli Mountain Belt, Northwestern India. *Precambrian Research*, 87, pp.75–85.

- Bose, U. and Sharma, A. K. (1992). The volcano sedimentary association of the Precambrian Hindoli Supracrustals in the Southeast Rajasthan. *Journal of Geological Society of India*, 40, pp.359–369.
- Boynton, W.V. (1984). Rare Earth Element Geochemistry. pp. 63-114.
- Chopra R., Jain R. C. and Panchal P. K. (2001). Unpublished annual report, F.S. 2000-01. Atomic Minerals Directorate for Exploration and Research, WR, Jaipur.
- Choudhary, A. K., Gopalan, K. and Sastry, C. A. (1984). Present status of the geochronology of the Precambrian rocks of Rajasthan. *Tectonophysics*, 105, pp.131–140.
- Das, A.R. (1988). Geometry of the superposed deformation in the Delhi Supergroup of rocks, north of Jaipur, Rajasthan. In: A. B. Roy (ed.), *Precambrian of the Aravalli Mountain, Rajasthan, India*. Geological Society of India, 7, pp.247-266.
- Deb, M. and Thorpe, R. I. (2001). Geochronological constraints in the Precambrian Geology of Northwestern India and their Metallogenic Implication. In: Deb, M., Goodfellow, W.D. (Eds.), *Pre-Seminar volume on International Workshop on Sediment-hosted Lead-Zinc Sulfide Deposit in the Northwestern Indian Shield, Delhi-Udaipur, India*, Prepared at Dept of Geology, Delhi University, New Delhi, pp.137–152.
- Duggal, N.K. (1954). Unpublished annual report, F.S. 1953-54. Atomic Minerals Directorate for Exploration and Research, WR, Jaipur.
- Frost, B. R., Barnes, C. G., Collins, W. J., Arculus, R. J., Ellis, D. J. and Frost, C. D. (2001). A geochemical classification for granitic rocks. *Journal of Petrology*, 42, pp.2033-48.
- Gangopadhyay, P. K. and Sen, R. (1972). Trends of regional metamorphism: an example from “Delhi System” of rocks occurring around Bairawas, northeastern Rajasthan. *Geol. Rundschau*, 61, pp.270-281.

- Ghosh, D. B. and Saraswat, A. C. (1956). Unpublished annual report, F.S. 1955-56. Atomic Minerals Directorate for Exploration and Research, WR, Jaipur.
- GSI (2011). Geology and mineral resources of Rajasthan. GSI Miscellaneous Publication, 3rd Revised Edition, 30(12), pp.18-19.
- Gupta, B.C. (1934). The geology of the central Mewar. Memoir Geological Survey of India, 65, pp.107–169.
- Gupta, S. N., Arora, Y. K., Mathur, R. K., Iqballuddin, Prasad, B., Sahai, T. N. and Sharma, S. B. (1980). Lithostratigraphic Map of the Aravalli Region. Geological Survey of India Publication, Hyderabad.
- Hacket, C. A., (1877). Aravalli Series in northeastern Rajputana. *Rec. Geol. Surv. Ind.*, 10(2).
- Hacket, C. A., (1881). On the geology or Aravalli region, Central and Eastern. *Rec. Geol. Surv. Ind.*, 14(4).
- Harker, A. (1909). The natural history of igneous rocks. Macmillan, New York.
- Hayashi, K. L., Fujisama, H, Holland, H. D. and Ohmoto, H. (1997). Geochemistry of ~1.9 Ga sedimentary rocks from northeastern Labrador, Canada. *Geochim. Cosmochim. Acta*, 61(19), pp.4115-4137.
- Heron, A.M. (1923). Geology of western Jaipur. Records of the Geological Survey of India, 54, pp.345–397.
- Heron, A.M. (1953). The geology of central Rajputana. Memoir Geological Survey of India, 79, pp.492.
- Kaul, R. (1961). Unpublished annual report, F.S. 1960-61. Atomic Minerals Directorate for Exploration and Research, WR, Jaipur.

- Kaur, P., Chaudhri, N., Raczek, I., Kroner, A. and Hofmann, A. W. (2009). Record of 1.82 Ga Andean-type continental arc magmatism in NE Rajasthan, India: insights from zircon and Sm–Nd ages, combined with Nd–Sr isotope geochemistry. *Gondwana Research*, 16, pp.56–71.
- Khanam, S., Quasim, M. A., Ahmad, A. H. M. and GHOSH, S.K. (2020). Sedimentation in a Rifted Basin: Insights from the Proterozoic Rajgarh Siliciclastics, Delhi Supergroup, Northeastern Rajasthan. *Journal Geological Society of India*, 95, pp.117-130.
- Khandelwal, M. K., Chopra, R. and Pathak, A.K. (2002). Unpublished annual report, F.S. 2001-02. Atomic Minerals Directorate for Exploration and Research, WR, Jaipur.
- Khan, I., Rai, D. K. and Sahoo, P.R. (2013). A note on new find of thick copper and associated precious metal mineralisation from Alwar basin of North Delhi Fold Belt, Rajasthan. *Journal of the Geological Society of India*, 82(5), pp.495–498.
- Khan, M. S., Smith, T. E., Raza, M. and Huang, J. (2005). Geology, geochemistry and tectonic significance of mafic-ultramafic rocks of mesoproterozoic phulad ophiolite suite of South Delhi Fold Belt, NW Indian Shield. *Gondwana Research*, 8, pp.553–566.
- Khazanchi, B. N. (1984). Unpublished annual report, F.S. 1983-84. Atomic Minerals Directorate for Exploration and Research, WR, Jaipur.
- Le Maitre, R. W. (1989). *A classification of igneous rocks and glossary of terms*. Blackwell Scientific Publications, Oxford, pp.193.
- Maddougall, J. D., Gopalan, K., Lugmair, G. W. and Roy, A. B. (1983). The Banded Gneissic Complex of Rajasthan, India: Early Crust from Depleted Mantle at ~3.5 Ga? *Eos, Transactions. American Geophysical Union*, 64, pp.351.

- Middlemost E. A. K. (1994). Naming materials in magma/igneous rock system. *Earth Sci Rev*, 37, pp.215–224
- Misra, P. (2019). Unpublished annual report, F.S. 2018-19. Atomic Minerals Directorate for Exploration and Research, WR, Jaipur.
- Mukhopadhyay, S., Ghosh, S., Das, S. and Rastogi, S. (2018). Copper and associated precious metal mineralization in Kaled–Jaisinghpura area, Dogeta Formation, Delhi Supergroup, North Delhi Fold Belt, Rajasthan. *Indian Journal of Geosciences*, 72, pp.187-202.
- Padhi, A. K., Aravind, S. L., Saxena, A., Kumar, K., Choudhury, D. K., Purohit, R.K., Nanda, L. K. and Rai, A. K. (2016). Uranium potential of Mesoproterozoic North Delhi Fold Belt Rajasthan, India: an overview. *Exploration and Research for Atomic Minerals*, 26, pp.53-70.
- Panchal, P. K. and Kumar, S. N. (2002). Unpublished annual report, F.S. 2001-02. Atomic Minerals Directorate for Exploration and Research, WR, Jaipur.
- Pettijohn, F. J., Potter, P. E. and Siever, R. (1987). *Sand and Sandstones*; Springer, New York, pp.553.
- Porwal, A., Carranza, E. J. M. and Hale, M. (2006). Tectonostratigraphy and base-metal mineralization controls, Aravalli province (western India): new interpretations from geophysical data analysis. *Reviews in Ore Geology*, 29, pp.287–306.
- Ramakrishnan, M. and Vaidyanadhan, R. (2008). *Geology of India*. Geological Society of India, Bangalore, 1, pp.303-304.
- Rode, V. P. (1961). Unpublished annual report, F.S. 1960-61. Atomic Minerals Directorate for Exploration and Research, WR, Jaipur.

- Roy, A. B. and Jakhar, S. R. (2002). Geology of Rajasthan (Northwest India) Precambrian to recent. Scientific Publishers, Jodhpur, India, pp.205.
- Roy, A. B. and Kröner, A. (1996). Single zircon evaporation ages constraining the growth of the Archaean Aravalli craton, northwestern India shield. Geological Magazine, 133, pp.333–342.
- Roy, A. B. and Sharma, K. K. (1999). Geology of the region around Sirohi Town, western Rajasthan-a story of Neoproterozoic evolution of the Aravalli crust. In: Paliwal, B.S. (Ed.), Geological Evolution of the Northwestern India. Scientific Publishers, Jodhpur, India, pp.19–33.
- Sant, V. N. and Sharma, S. B. (1973). Precambrian metasediments of Alwar and Jaipur districts, Rajasthan and their stratigraphic sequences. Abstract, Symp. Recent Advances in Geology of Rajasthan and Gujarat, Jaipur, Nov. 1973.
- Saxena, A. (2020). Unpublished brief annual report, F.S. 2019-20. Atomic Minerals Directorate for Exploration and Research, WR, Jaipur.
- Sharma, G.V.G. (1983). Unpublished annual report, F.S. 1982-83. Atomic Minerals Directorate for Exploration and Research, WR, Jaipur.
- Sharma, G.V.G. (1985). Unpublished annual report, F.S. 1984-85. Atomic Minerals Directorate for Exploration and Research, WR, Jaipur.
- Shaji, T. S. and Panigrahi, B. (2008). Unpublished annual report, F.S. 2007-08. Atomic Minerals Directorate for Exploration and Research, WR, Jaipur.
- Shaji, T. S., Panigrahi, B., Yadav, O. P., Nanda, L. K., Maithani, P. B. and Chaki, A. (2009). Shear controlled uranium mineralization in Kho-Dariba area of Alwar sub-basin, District Alwar, Rajasthan. Current science, 97(3), pp.311-313.

- Sharma, R. S. (1988). Patterns of metamorphism in the Precambrian rocks of the Aravalli mountain belt. In: A.B.Roy (Eds). Precambrians of Aravalli Mountain, Rajasthan, India, Mem. Geological survey of India, 7, pp.33-76.
- Singh, S.P. (1982a) Palaeotectonics and sedimentation trend of the Delhi Supergroup around Rajgarh, northeastern Rajasthan. Journal Indian Asso. Sedimentol., 3, pp.29-44.
- Singh, S. P. (1984). Fluvial sedimentation of the Proterozoic Alwar Group in the Lalgargh graben, northwestern India, Sedimen. Geol., 39, pp.95-119.
- Singh, S. P. (1988A). Sedimentation patterns of the Proterozoic Delhi Supergroup, northeastern Rajasthan, India and their tectonic implications. Sedimentary Geology, 58, pp.79-94.
- Singh, S. P. (1988b). Stratigraphy and sedimentation pattern in the Proterozoic Delhi Supergroup, northwestern India. In: A. B. Roy (Eds) Precambrians of Aravalli Mountain, Rajasthan, India. Memoir Geological Society of India, pp.193-205.
- Singh, S. P., Ravindra, R. and Bakliwal, P. C. (1978). The Raialo-Alwar Unconformity-A reinterpretation. Indian Minerals, 32(1), pp.69-80.
- Singh, Y. K., De Waele, B., Karmarkar, S., Sarkar, S. and Biswal, T. K. (2010). Tectonic setting of the Balaream-Kui-Surpagla-Kengora granulites of the South Delhi Terrane of the Aravalli Mobile Belt, NW India and its implication on correlation with the East African Orogen in the Gondwana assembly. Precambrian Research, 183, pp.669–688.
- Sinha-Roy, S., Malhotra, G. and Mohanty, M. (2013). Geology of Rajasthan. Geological Society of India, First Edition, pp.278.
- Sivaraman, T. V. and Odom, A. L. (1982). Zircon chronology of the Berach granite of Chittorgarh, Rajasthan. Journal of Geological Society of India, pp.575–577.

Suttner, L. J. and Dutta, P.K. (1986). Alluvial Sandstone Composition and Paleoclimate, I. Framework Mineralogy. *Jour. Sed. Petrol.*, 56(3), pp.329- 345.

Wiedenbeck, M. and Goswami, J. N. (1994). High precision $^{207}\text{Pb}/^{206}\text{Pb}$ zircon geochronology using a small ion microprobe. *Geochimica Cosmochimica Acta*, pp.2135–21.

